



2017

Factors Regulating Features of Metabolic Syndrome

Sonja S. Pijut

University of Kentucky, srhee2@uky.edu

Digital Object Identifier: <https://doi.org/10.13023/ETD.2017.044>

[Click here to let us know how access to this document benefits you.](#)

Recommended Citation

Pijut, Sonja S., "Factors Regulating Features of Metabolic Syndrome" (2017). *Theses and Dissertations--Pharmacy*. 70.
https://uknowledge.uky.edu/pharmacy_etds/70

This Doctoral Dissertation is brought to you for free and open access by the College of Pharmacy at UKnowledge. It has been accepted for inclusion in Theses and Dissertations--Pharmacy by an authorized administrator of UKnowledge. For more information, please contact UKnowledge@lsv.uky.edu.

STUDENT AGREEMENT:

I represent that my thesis or dissertation and abstract are my original work. Proper attribution has been given to all outside sources. I understand that I am solely responsible for obtaining any needed copyright permissions. I have obtained needed written permission statement(s) from the owner(s) of each third-party copyrighted matter to be included in my work, allowing electronic distribution (if such use is not permitted by the fair use doctrine) which will be submitted to UKnowledge as Additional File.

I hereby grant to The University of Kentucky and its agents the irrevocable, non-exclusive, and royalty-free license to archive and make accessible my work in whole or in part in all forms of media, now or hereafter known. I agree that the document mentioned above may be made available immediately for worldwide access unless an embargo applies.

I retain all other ownership rights to the copyright of my work. I also retain the right to use in future works (such as articles or books) all or part of my work. I understand that I am free to register the copyright to my work.

REVIEW, APPROVAL AND ACCEPTANCE

The document mentioned above has been reviewed and accepted by the student's advisor, on behalf of the advisory committee, and by the Director of Graduate Studies (DGS), on behalf of the program; we verify that this is the final, approved version of the student's thesis including all changes required by the advisory committee. The undersigned agree to abide by the statements above.

Sonja S. Pijut, Student

Dr. Gregory A. Graf, Major Professor

Dr. David J. Feola, Director of Graduate Studies

FACTORS REGULATING FEATURES OF METABOLIC SYNDROME

DISSERTATION

A dissertation submitted in partial fulfillment of the
requirements for the degree of Doctor of Philosophy in the
Graduate School at the University of Kentucky

By

Sonja Sheena Pijut

Lexington, Kentucky

Director: Dr. Gregory A. Graf, Professor of Pharmaceutical Sciences

Lexington, Kentucky

2017

Copyright © Sonja Sheena Pijut 2017

ABSTRACT OF DISSERTATION

FACTORS REGULATING FEATURES OF METABOLIC SYNDROME

The collective presence of central obesity, low HDL-cholesterol, and elevated triglycerides, blood pressure, and fasting blood glucose constitutes Metabolic Syndrome (MetS), a disease state that increases the risk of cardiovascular disease (CVD) and Type 2 Diabetes Mellitus (T2DM). Nonalcoholic fatty liver disease (NAFLD), present in up to 90% of obese adults, is also linked to MetS. As in CVD, disruptions in cholesterol metabolism play a contributing role in the development of T2DM and NAFLD. Genes involved in cholesterol synthesis, secretion, and catabolism are diurnally regulated in the liver and adipose. Disruptions in the sleep-wake cycle are thought to potentiate metabolic disorders associated with CVD, thus revealing a potential role of disrupted circadian rhythms in the development of MetS phenotypes.

We initially observed that a group of clock-controlled genes in the Par bZip family were downregulated in adipose tissue of obese mice and humans. Further studies revealed that deletion of the core clock gene, *Bmal1*, from adipose tissue alone (ABKO mice) or in combination with the liver (LABKO mice) altered feeding behavior and locomotor activity. Obesity was increased in LABKO mice but there were no further detrimental effects in either ABKO or LABKO mice. Interestingly, high-fat diet suppressed *Bmal1* transcript levels in adipose tissue suggesting that the muted effects observed with genetic *Bmal1* deletion were likely due to the overpowering effects of a high-fat diet.

Cholesterol metabolizing and bile acid synthesizing enzymes oscillate diurnally at the transcriptional level. Promoting cholesterol elimination through bile acid synthesis and biliary secretion is essential for reducing hepatic cholesterol, a perpetrating factor in the progression of NAFLD. Previous studies in animal models demonstrated that deletion of the hepatic cholesterol transporters, *Abcg5* and *Abcg8* (G5G8), decreased biliary cholesterol secretion and increased obesity and hepatic steatosis. Ursodiol (Urso) increased G5G8 protein expression and in combination with ezetimibe, a cholesterol-lowering agent, showed promise as a therapeutic for NAFLD. However, bile acid synthesis was suppressed in the presence of Urso and ezetimibe, suggesting that the overall effect on cholesterol elimination was minimized. The increase in G5G8 and decrease in bile acid synthesis was associated with an increase in *Fgf15/19*, a suppressor of bile acid synthesis. In order to determine if and how FGF15/19 regulates G5G8, mice were injected with FGF19. G5G8 protein expression and biliary total cholesterol were increased. Additionally, G5G8 localized to the canalicular surface of hepatocytes. Urso caused a similar localization of G5G8 that appeared to be dependent of the FGF15/19-FGFR4 signaling

pathway. Interestingly, G5G8 was not required for maintaining cholesterol homeostasis in the presence of FGF15/19.

Data from murine models suggest Urso and ezetimibe promote cholesterol elimination, though the effects may be limited by the suppression of bile acid synthesis. Nonetheless, there may be a therapeutic window in which optimal cholesterol elimination can be reached. Additionally, the effects of Urso and ezetimibe are variable between mice and humans. Given the clinical availability of the two drugs, the translatability into humans and the potential to address whether Urso and ezetimibe can minimize NAFLD is great.

KEYWORDS: Obesity, Insulin Resistance, NAFLD, Circadian rhythm, G5G8, FGF15/19

Sonja Sheena Pijut

February 22, 2017

Date

FACTORS REGULATING FEATURES OF METABOLIC SYNDROME

By

Sonja Sheena Pijut

Gregory A. Graf

Director of Dissertation

David J. Feola

Director of Graduate Studies

February 22, 2017

Date

ACKNOWLEDGEMENTS

The following dissertation was written with the invaluable insights and support of my dissertation chair, dissertation committee, friends, and family. First, my dissertation chair, Dr. Gregory A. Graf, has provided me with experiences and opportunities that have been instrumental in expanding my knowledge and skillset as a scientist. His dedication to research and educating students has been a source of inspiration throughout my training. The qualities of enthusiasm and perseverance he has instilled in me will continue to motivate me as I progress through my professional journey.

Thank you to my dissertation committee, Dr. David J. Feola, Dr. Charles D. Loftin, and Dr. Ming C. Gong, for your expertise and advice. The support and guidance you have provided have facilitated my growth and progression through this doctoral program.

Finally, thank you to my friends and family for their unconditional love and support. To my parents who have sacrificed so much to provide me with the best life possible, to my sister who is my role model in every aspect, to my husband who encourages me to pursue my dreams, and to my daughter who brings so much joy and happiness, I am indebted to you.

TABLE OF CONTENTS

Acknowledgments.....	iii
List of Tables	vii
List of Figures.....	viii
Chapter 1: Introduction.....	1
Overview of Metabolic Syndrome	1
History	1
Etiology and Pathophysiology	2
Clinical Significance and Treatment.....	3
Obesity	3
Adipose Tissue and Obesity.....	3
Adipose Tissue Depots	5
Insulin Resistance.....	5
Mechanisms of Obesity-Induced Insulin Resistance	5
Nonalcoholic Fatty Liver Disease	6
The Hypothesis of the Two-Hit Model.....	7
Dyslipidemia in NAFLD	8
Hepatic Free Cholesterol in NAFLD.....	8
Overview of Circadian Rhythms.....	9
Molecular Components of the Circadian Clock.....	10
The Network of Central and Peripheral Clocks.....	11
Circadian Dysfunction: A Contributing Factor in Features of Metabolic Syndrome	12
Overview of Cholesterol Metabolism	14
Cholesterol Synthesis, Transport, and Regulation.....	14
ABCG5 ABCG8: A Regulator of Sterol Homeostasis	16
Bile Acid Synthesis and Signaling.....	17
Circadian Regulation of Cholesterol and Bile Acid Metabolism.....	19
Chapter 2: Role of Clock-controlled Par bZip Genes in Obesity and Insulin Resistance.....	21
Introduction	21
Methods.....	22

Animals	22
Real Time-PCR.....	22
Statistical Analyses	22
Results	23
Circadian genes are differentially deregulated in white adipose tissue of obese, ABCD2-deficient mice fed erucic acid	23
<i>Dbp</i> , <i>Hlf</i> , and <i>Tef</i> are decreased in white adipose tissue of obese mice.....	25
<i>Dbp</i> and <i>Hlf</i> are decreased in white adipose tissue of obese, insulin-resistant humans....	25
Discussion	27
Chapter 3: Effect of Peripheral Circadian Dysfunction on Metabolic Disease in Response to a Diabetogenic Diet	29
Introduction	29
Methods.....	29
Animals.....	29
Indirect Calorimetry.....	30
Diet and Physiological Measurements.....	30
Histology.....	31
Hepatic Lipid Extraction and Lipid Measurements	31
Real Time-PCR.....	31
Immunoblot Analysis.....	33
Statistical Analyses	33
Results	33
Liver and adipose peripheral clocks mediate centrally-regulated functions	33
Disruptions in liver and adipose peripheral clocks lead to increased body weight and adiposity.....	38
Loss of glycemic control does not correspond with increased body weight and adiposity.....	43
Disruptions in liver and adipose peripheral clocks increase hepatic cholesterol in LABKO mice.....	45
Discussion	47
Chapter 4: Role of the Bile Acid-FGF15/19 Axis in the Regulation of ABCG5 and ABCG8.....	50
Introduction	50

Methods.....	51
Animal Husbandry and Procedures	51
Real Time-PCR.....	52
Immunoblot Analysis.....	52
Lipid Analysis.....	52
Immunofluorescence Microscopy.....	52
Statistical Analysis.....	53
Results	53
FGF19 suppresses bile acid synthesis and increases hepatic G5G8	53
FGF19 increases biliary total lipid concentrations	54
FGF19 localizes G5G8 to the canalicular surface of hepatocytes	55
FGF19 does not disrupt cholesterol homeostasis in the absence of G5G8	56
FGF15/19-FGFR4 signaling is required for Urso to localize G5G8 to the canalicular surface of hepatocytes.....	58
Discussion	60
Chapter 5: A Future Direction in Clinical Application: Effect of Ezetimibe-Ursodiol Combination Therapy on Biomarkers of Liver Function and Sterol Balance in Subjects with NAFLD	64
Chapter 6: Summary	67
Appendices.....	71
Appendix 1: Effect of Ezetimibe-Ursodiol Combination Therapy on Biomarkers of Liver Function and Sterol Balance in Subjects with NAFLD Study Protocol.....	71
Appendix 2: Abbreviations	93
References.....	96
Vita.....	110

LIST OF TABLES

Table 1.1. Genetic mouse models of circadian dysfunction and the corresponding metabolic defects	13
Table 2.1. Functional annotation clustering output from DAVID Bioinformatics Database	24
Table 2.2. Gene symbols of the top 20 probes with the lowest p-value	24
Table 2.3. Human subject characteristics.....	26
Table 3.1. Sequences for primers.....	32

LIST OF FIGURES

Figure 1.1. Pictorial representation of circadian rhythms	9
Figure 1.2. Molecular components of the circadian clock network	10
Figure 2.1. Diagram of statistically significant and non-significant probes from a 2x2 factorial microarray study of wild type and ABCD2 KO mice fed standard or eruric acid-enriched diets .	23
Figure 2.2. Gene expression of PAR bZip genes in WAT of 24-week-old male G5G8 knockout mice fed a low-fat diet (lean) or a high-fat diet (obese).....	25
Figure 2.3. Gene expression of PAR bZip genes in WAT of lean/IS and obese/IR female human subjects.....	26
Figure 3.1. Deletion of <i>Bmal1</i> in WAT and liver of 13-24-week-old female mice on standard rodent chow.....	34
Figure 3.2. Food intake, physical activity and energy expenditure changes in 12-week-old female mice on standard rodent chow	36
Figure 3.3. Body weight, body composition and blood glucose of 13-24-week-old female mice fed a standard rodent chow	37
Figure 3.4. Deletion of <i>Bmal1</i> in WAT and liver of 24-week-old male mice on control diet (CD) or diabetogenic diet (DD) for 16 weeks.....	38
Figure 3.5. Body weight and composition of male mice fed a control diet (CD) or a diabetogenic diet (DD) for 16 weeks	40
Figure 3.6. Adipose histology, quantification and measure of adipogenesis and lipolysis in WAT at circadian time 0 in 24-week-old male mice fed a control diet (CD) or a diabetogenic diet (DD) for 16 weeks.....	42
Figure 3.7. Glycemic control in 24-week-old male mice fed a control diet (CD) or a diabetogenic diet (DD) for 16 weeks	44
Figure 3.8. Liver histology, hepatic lipids and gene expression from liver isolated at circadian time 0 in 24-week-old male mice fed a control diet (CD) or a diabetogenic diet (DD) for 16 weeks	46
Figure 4.1. FGF19 suppresses bile acid synthesis and increases hepatic G5G8.....	54
Figure 4.2. FGF19 increases biliary total lipid concentrations	55
Figure 4.3. FGF19 localizes G5G8 to the canalicular surface of hepatocytes	56
Figure 4.4. FGF19 does not disrupt cholesterol homeostasis in the absence of G5G8.....	58
Figure 4.5. FGF19-FGFR4 signaling is required for Urso to localize G5G8 to the canalicular surface of hepatocytes.....	59
Figure 4.6. FGF15/19-FGFR4 signaling is required for Urso to localize G5G8 to the canalicular surface of hepatocytes.....	60

CHAPTER 1: INTRODUCTION

Cardiovascular disease (CVD), the leading cause of death worldwide, is significantly increased with obesity, Type 2 Diabetes Mellitus (T2DM), dyslipidemia, and hypertension. The cumulative presence of these CVD-related risk factors is described as Metabolic Syndrome (MetS).

Emerging as an associated feature of MetS is nonalcoholic fatty liver disease (NAFLD). NAFLD is highly prevalent in obese individuals and is likely an independent risk factor for CVD as well [1]. As in CVD, disruptions in cholesterol metabolism play a causative role in the development and progression of NAFLD.

Glucose and lipid metabolism display diurnal rhythmicity, suggesting the importance of circadian rhythms in maintaining energy homeostasis. Studies reveal that altered sleep-wake cycles are associated with features of MetS including obesity and dyslipidemia [2, 3]. Additionally, glucose and lipid metabolizing enzymes, including those involved in cholesterol synthesis, secretion, and catabolism, exhibit diurnal regulation. This reveals a potential role of disrupted circadian rhythms in the development of MetS phenotypes.

Overview of Metabolic Syndrome

The group of risk factors that constitute Metabolic Syndrome (MetS) include central obesity, low HDL-cholesterol, and high triglycerides, fasting blood glucose, and blood pressure. These risk factors tend to occur in combination, and the presence of three or more defines MetS. Individuals with MetS have an even greater risk of CVD compared to the sum of the risk associated with each risk factor. As the prevalence of obesity continues to rise, a similar trend is observed with MetS. Approximately 35% of adults in the United States were thought to have MetS between 2011 and 2012, though the prevalence is highly variable between sex, age, and ethnic groups [4]. MetS is more prevalent in females, adults 60 years of age and older, and in Hispanics [4]. Nonetheless, MetS is consistently higher in overweight and obese individuals within each group underscoring the important relation between obesity and MetS [5, 6].

History

Features of MetS were first described in the 1920s by two groups of physicians observing an association between T2DM and hypertension in their patients [7]. Subsequently, a number of researchers made similar observations linking various metabolic disorders. In 1988, it was proposed that the common factor in individuals with impaired glucose tolerance, hyperinsulinemia, elevated very low density lipoprotein (VLDL)-triglycerides, elevated high

density lipoprotein (HDL)-cholesterol, and hypertension was insulin resistance [7, 8]. Central obesity was later included as part of the cluster of risk factors [7]. Though MetS centers around the core disease states of obesity, insulin resistance, dyslipidemia, and hypertension, the criteria for diagnosis by the World Health Organization, the National Cholesterol Education Program Adult Treatment Panel III, the European Group for the Study of Insulin Resistance, the American Association of Clinical Endocrinologists, and the International Diabetes Federation vary slightly [7]. Thus, there is not one well-established definition for MetS.

Etiology and Pathophysiology

The presence of multiple disease states as part of the diagnostic criteria gives an indication of the complex nature of MetS. The phenotypic presentation of MetS may also vary greatly as there are lean individuals who are considered “metabolically-obese” and vice versa. Therefore, the etiology and pathophysiology of MetS are likely explained by various interconnected physiological and biochemical mechanisms involving multiple organs.

It is widely thought that obesity and insulin resistance are the underlying insults that link the features of MetS together. Initial efforts identified the relationship between insulin resistance and metabolic disorders. In a cohort of subjects from the San Antonio Heart Study followed for 8 years, elevations in fasting insulin as a marker of insulin resistance were observed to precede the development of T2DM, decreased HDL-cholesterol, increased triglycerides, and hypertension [9]. In an insulin resistant state, impaired insulin signaling in tissues such as the liver, skeletal muscle, and adipose tissue reduces the glucose uptake capability of these tissues. This necessitates increased insulin secretion from the β -cells of the pancreas in order to maintain normal plasma glucose levels. Persistently increased insulin secretion leading to β -cell failure coupled with decreased insulin sensitivity result in the development of T2DM.

The adipose tissue plays a key role in storing excess free fatty acids (FFAs) as triglycerides in adipocytes. Over-expansion of adipocytes as seen in obesity leads to adipose dysfunction characterized by increased inflammation and impaired insulin sensitivity. Insulin normally inhibits lipolysis. However, in the setting of adipose dysfunction, lipolysis and mobilization of FFAs to peripheral tissues are increased. FFAs are thought to increase hepatic glucose production and inhibit insulin-mediated glucose uptake into cells, further precipitating the insulin resistant state [10]. Additionally, studies reveal that visceral adipose, associated with central obesity, produces more inflammatory cytokines than subcutaneous adipose, leading to ectopic fat accumulation and insulin resistance [11, 12].

Clinical Significance and Treatment

Individuals with MetS are twice as likely to develop CVD over the following 5 to 10 years and five times as likely to develop T2DM [13]. Features of MetS, particularly obesity and insulin resistance, have also been associated with NAFLD. Approximately 90% of obese individuals have NAFLD, though NAFLD is highly prevalent with insulin resistance independent of obesity as well [14].

Treatment for MetS involves management of individual risk factors using both non-pharmacological and pharmacological modalities. Lifestyle modifications through diet and exercise remain an essential component for treatment, particularly during the initial stage. In a systematic review, lifestyle modification programs were found to improve quality of life and have beneficial effects on features of metabolic syndrome [15]. However, adapting and maintaining non-pharmacological, lifestyle modifications is challenging.

Obesity

Over one-third of adults in the United States are considered obese. Obesity, defined as having a body mass index (BMI) of $>30 \text{ kg/m}^2$, precipitates a number of disease states such as T2DM, hypertension, CVD, sleep apnea, osteoarthritis, depression, and cancer [16]. Obesity increases morbidity and mortality, thus complicating all aspects of clinical care.

Adipose Tissue and Obesity

Adipose tissue has traditionally been viewed solely as a storage place for FFAs as triglycerides. While this is an important function for storing excess energy and providing insulation and protection, adipose tissue is now viewed as a highly metabolically active organ responsible for the synthesis of multiple cytokines and hormones involved in energy regulation. Adipose tissue is comprised of adipocytes, the site of energy storage, as well as stromal vascular cells including fibroblasts, endothelial cells, preadipocytes, and macrophages that support its dynamic role [17].

The regulation of energy storage and release in adipose tissue is dependent on a series of pathways that occur in response to feeding and fasting. Following food intake, FFAs are transported through the circulation by VLDLs and chylomicron remnants. Triglycerides are hydrolyzed by lipoprotein lipase (LPL) located on the surface of endothelial cells of capillaries lining tissues such as adipose to facilitate uptake and storage of FFAs as triglycerides. Glucose is converted into FFAs for long term storage as triglycerides in a process called lipogenesis. When energy demand is high during the fasted state, lipolysis occurs. Stored triglycerides are

hydrolyzed to FFAs by adipose triglyceride lipase (ATGL) and hormone sensitive lipase (HSL) for release back into the circulation. Insulin and glucagon are two primary hormones essential for the regulation of these processes. Insulin is released during the fed state to stimulate glucose uptake into adipocytes as well as lipogenesis while inhibiting lipolysis. Glucagon opposes insulin and induces lipolysis during the fasted state.

Adipose tissue plays a role as an endocrine organ by synthesizing and releasing cytokines and hormones referred to as adipocytokines. Adipocytokines are involved in regulating food intake, glucose and lipid metabolism, blood pressure, and immunity. Two of the more well-defined adipocytokines in regulating energy homeostasis include leptin and adiponectin. Leptin is stimulated by insulin and signals to the brain to suppress food intake and increase energy expenditure, mediating between feeding behavior and energy homeostasis. Peripherally, leptin increases hepatic lipid oxidation and lipolysis [18-20]. Accordingly, leptin-deficient (*ob/ob*) and leptin receptor-deficient (*db/db*) mice become morbidly obese [21, 22]. As food intake increases and adipocytes enlarge, leptin production increases in an effort to decrease food intake, increase energy expenditure and regulate fat mass. In obesity, increased leptin is ineffective in implementing these changes; therefore, obese individuals become leptin resistant despite having increased leptin. Unlike leptin, adiponectin is conversely related to fat mass. Adiponectin stimulates glucose uptake and fatty acid oxidation and inhibits hepatic glucose production. Metabolic disorders including MetS, obesity, and T2DM are associated with decreased adiponectin while administration of adiponectin in mouse models of obesity improves insulin sensitivity [23-28].

Adipocyte expansion during the development of obesity is also accompanied by the accumulation of macrophages and the release of inflammatory adipocytokines including tumor necrosis factor alpha (TNF- α) and interleukin 6 (IL-6). Although adipocytes produce and release TNF- α , macrophages within adipose tissue are the major source contributing to the increased inflammatory adipocytokine [29]. TNF- α has been shown to impair insulin signaling and is a proposed mechanism linking obesity and insulin resistance [30]. Similar to TNF- α , IL-6 inhibits insulin signaling and is associated with T2DM. Although doses of IL-6 administered peripherally increases blood glucose in humans, mice deficient of IL-6 develop obesity [31, 32]. These data suggest that IL-6 may induce differing effects centrally versus peripherally [32]. The release of inflammatory adipocytokines during the development of obesity results in a chronic inflammatory state that leads to adipose dysfunction and subsequently insulin resistance.

Adipose Tissue Depots

Adipose tissue depots have anatomical and functional differences that become relevant in metabolic disease states. Subcutaneous adipose tissue is distributed throughout the peripheral, gluteo-femoral region and expands under normal physiological conditions to store excess FFAs. In contrast, visceral adipose tissue is distributed throughout the central, abdominal region and thought to be highly pathogenic. While subcutaneous adipose tissue produces higher levels of leptin and adiponectin, visceral adipose tissue produces more macrophages and inflammatory adipocytokines, IL-6 and fatty acid binding protein 4 (FABP-4) [11, 12]. The anatomical location may also contribute to the pathological tendency of visceral adipose tissue. Close proximity to the portal circulation suggests a greater impact of adipocytokines and FFAs from visceral adipose tissue on glucose and lipid metabolism in the liver. In a study measuring splanchnic FFAs in obese and lean humans, the proportion of hepatic FFA delivery increased with increasing visceral fat indicating a greater exposure of FFAs to the liver in centrally obese individuals [33]. Adipose tissue dysfunction that occurs in obesity can lead to the deposition of fat in tissues that do not normally accumulate large quantities of fat. This process, known as ectopic lipid accumulation, can lead to increased visceral adipose tissue as well as lipid accumulation in the liver, skeletal muscle, and heart. Ectopic lipid accumulation impairs the homeostatic functions of the affected tissues and leads to the metabolic disturbances observed in diseases such as T2DM and NAFLD.

Insulin Resistance

Early studies in humans provided evidence that insulin resistance, rather than insulin deficiency is the initiating abnormality associated with T2DM. This concept was suggested in 1936 when it was observed that diabetic patients had varying responses to insulin [34]. Subsequent studies supporting this notion revealed that insulin levels were increased with T2DM [35, 36]. Insulin resistance is characterized by decreased glucose uptake into tissues and increased hepatic glucose production resulting in hyperglycemia and hyperinsulinemia. Insulin resistance is of great clinical significance because it is now widely accepted that the eventual fate of insulin resistance is the development of T2DM. Additionally, insulin resistance and T2DM are highly associated with obesity, NAFLD, and other metabolic disorders known to increase the risk of CVD.

Mechanisms of Obesity-Induced Insulin Resistance

The mechanisms involved in obesity-induced insulin resistance include a number of alterations (e.g. FFA accumulation, inflammation) that converge to impair insulin signaling in adipose tissue, liver, and skeletal muscle. In obesity, hypertrophic adipocytes release more FFAs and

inflammatory adipocytokines. Accordingly, increased FFAs are observed in obese individuals [37]. Elevated FFAs lead to ectopic lipid accumulation and impair insulin signaling thereby increasing lipolysis, increasing hepatic glucose production, and inhibiting glucose uptake into tissues. FFAs also induce inflammation by activating Toll like receptor 2 (TLR2) and TLR4 [38]. Together with the increased release of adipocytokines, FFA-induced inflammatory cytokines promote recruitment of macrophages and other immune cells to further increase inflammation. Both pro- and anti-inflammatory cytokines have been identified to modulate the insulin signaling pathway. Some examples include TNF- α , IL-1 α , and IL-10. TNF- α and IL-1 α impair insulin by decreasing phosphorylation of insulin receptor substrate 1 (IRS-1) while IL-10 reduces inflammation by inhibiting NF- κ B activity [39-41].

As in adipose tissue, excess glucose neither used for energy nor stored as glycogen are stored in the liver as triglycerides by undergoing lipogenesis and triglyceride synthesis. Glucose and insulin induce lipogenesis by regulating carbohydrate responsive element binding protein (ChREBP) and sterol regulatory element binding protein 1c (SREBP-1c), respectively [42-44]. ChREBP and SREBP-1c activate transcription of lipogenic genes in response to high-carbohydrate diets [44, 45]. In the insulin resistant state, insulin is unable to promote glucose uptake and suppress hepatic glucose production though lipogenesis in the liver persists. This paradox, called selective hepatic insulin resistance, is thought to mediate the phenotypes associated with MetS. Thus, increased hepatic lipogenesis is observed in humans with insulin resistance or NAFLD [46, 47]. Ectopic lipid accumulation in the liver results in increased FFAs and lipid metabolites such as ceramides and DAG that promote mitochondrial dysfunction and ER stress, inducing insulin resistance [48].

Skeletal muscle is the primary site for insulin-mediated glucose uptake and glycogen storage. As a result, impaired insulin signaling in skeletal muscle can have overt effects on whole-body glucose metabolism. Similar to other tissues, FFAs have been implicated in the development of skeletal muscle insulin resistance by inducing inflammation and modulating mitochondrial function [49]. Additionally, lipid metabolites produced as a result of ectopic lipid accumulation have been implicated in skeletal muscle insulin resistance [50, 51]

Nonalcoholic Fatty Liver Disease

NAFLD has become increasingly more prevalent over the past couple of decades and is now the leading cause of chronic liver disease in the United States [52]. NAFLD is the accumulation of $\geq 5\%$ liver fat not caused by known factors of fatty liver such as alcohol consumption, viral

hepatitis, autoimmune disease, and certain drugs. It is characterized by a continuum of disease severity ranging from hepatic steatosis to nonalcoholic steatohepatitis (NASH). While hepatic steatosis is common and relatively benign, NASH involves inflammation, fibrosis, and hepatocyte damage that lead to cirrhosis [53].

The prevalence of NAFLD ranges from 15-40% in the general population and is even greater in disease states that increase CVD risk including obesity, T2DM, dyslipidemia, hypertension, and MetS [54-57]. Indeed, NAFLD is associated with increased carotid-artery intimal medial thickness and carotid atherosclerotic plaques, markers of CVD [58]. Although it is more likely for NAFLD to be present in combination with other metabolic disease states known to increase CVD, NAFLD is also thought to be an independent CVD risk factor [59-61].

Current treatment strategies for NAFLD include lifestyle modifications for weight loss such as diet and exercise. Various studies show that weight loss is effective in reducing aminotransferase levels and hepatic steatosis as well as improving features of MetS that are commonly associated with NAFLD. Accordingly, the American Association for the Study of Liver Diseases recommends a minimum weight loss of 3-5% of body weight in order to improve steatosis [62]. Aside from lifestyle modifications, there are currently no pharmacologic agents approved for the treatment of NAFLD and NASH.

The Hypothesis of the Two-hit Model

Given the close association, it is likely that similar physiological and biochemical alterations are implicated in the pathogenesis of NAFLD and features of MetS. The pathophysiology of NAFLD is often explained by the two-hit model that includes two distinct mechanisms that first induce fatty liver (steatosis) then fatty liver with the presence of inflammation (steatohepatitis). The initial insult is ectopic lipid accumulation in the liver. As in obesity and insulin resistance, excessive FFAs are stored in the liver as triglycerides. FFAs in the liver are derived from 1) the release of FFAs from adipose tissue, 2) lipogenesis in the liver, and 3) the diet. Although hepatic lipogenesis is a minor source of FFAs in healthy individuals, it is significantly increased in NAFLD and insulin resistance [46, 47]. The secondary insult required for the progression of hepatic steatosis to NASH involves the development of inflammation and fibrosis induced by inflammatory cytokines, mitochondrial dysfunction, and oxidative stress. FFAs play a direct role by stimulating the inflammatory cytokine, TNF- α , and promoting oxidative stress [63, 64].

Dyslipidemia in NAFLD

Similar to the plasma lipoprotein profile observed in MetS, NAFLD is often associated with increased triglycerides and decreased HDL-cholesterol [65]. Dyslipidemia in NAFLD can be explained in part by mechanisms involved in insulin resistance [66]. Insulin resistance increases the FFA flux into the liver by inducing lipolysis in adipose tissue. Additionally, upregulation of SREBP-1c and ChREBP increases hepatic lipogenesis. Microsomal triglyceride transfer protein (MTP) and apolipoprotein CIII (apoCIII), required for VLDL synthesis, are increased in insulin resistance through a mechanism involving the disinhibition of forkhead box protein O1 (FOXO1) [67, 68]. Together, these alterations promote VLDL synthesis and secretion. In the plasma, circulating VLDL bind to LPL in tissues for hydrolysis and uptake of triglycerides. LPL activity is decreased in insulin resistance, impairing the clearance of VLDL triglycerides. Decreased HDL-cholesterol is commonly observed in association with increased triglycerides. It is hypothesized that this is mediated by the lipid transfer protein, cholesteryl ester transfer protein (CETP). CETP facilitates the transfer of triglycerides from triglyceride-rich lipoproteins such as VLDL to HDL in exchange for cholesterol, resulting in decreased HDL-cholesterol. This transfer is dependent on the concentration of plasma triglycerides, thus it is plausible that CETP activity is increased in disease states that induce hypertriglyceridemia [66, 69]. Indeed, CETP activity is increased in NAFLD and MetS [70]. Elevated triglycerides and decreased HDL-cholesterol are significant risk factors for CVD and likely to contribute to the increased risk of CVD-related deaths associated with NAFLD.

Hepatic Free Cholesterol in NAFLD

Elevated FFAs in the liver have been established to induce oxidative stress and apoptosis in NAFLD [63]. However, studies suggest that free cholesterol may play a role in the development of NAFLD and progression to NASH. A lipidomic analysis of livers from subjects with suspected NAFLD has revealed a significant increase in free cholesterol with NASH while cholesterol ester levels remain unchanged [71]. Increases in free cholesterol that correspond with *Srebp-2* expression are observed in NASH [72]. Similarly, cholesterol synthesis determined by serum desmosterol to cholesterol ratio as well as transcript levels of HMG-CoA reductase (*Hmgcr*) and *Srebp-2* are increased with NAFLD [73]. In low density lipoprotein (LDL) receptor-deficient mice, the addition of cholesterol to a high-fat, high-carbohydrate diet exacerbates hepatic steatosis while dietary cholesterol in humans is associated with cirrhosis [74, 75]. Free cholesterol can form crystals within hepatocyte lipid droplets, activating Kupffer cells to promote the

progression of steatosis to NASH [76]. Minimizing the accumulation of excess free cholesterol in the liver may be effective in both the treatment and prevention of NAFLD.

Overview of Circadian Rhythms

Virtually all organisms regulate behavior and physiological processes such as glucose and lipid metabolism in synchrony to the environment. When the availability and abundance of resources are variable, coordination to the environment is necessary in order to optimize energy utilization. Modern conveniences allow availability of food and light throughout the day and night, creating an opportunity where rhythmic behaviors and processes become asynchronous to the intrinsic circadian rhythms of organisms. Consequently, waking and eating during typical rest periods are thought to exacerbate metabolic disorders.

Circadian rhythms refer to patterns that occur ‘around the day’ from the Latin word *circa* meaning ‘around’ and *diēm* meaning ‘day.’ Circadian rhythms occur with a periodicity of approximately 24 hours. The period or tau (τ) is defined as the time between two recurring points of a cycle and the amplitude is defined as the degree of difference between the peak or trough and the mean value of the cycle (Figure 1.1). Circadian rhythms have the intrinsic property of maintaining rhythmicity independent of influences by the environment. This can be observed by measuring wheel running activity in mice housed in either constant dark or constant light ‘free-running’ conditions. However, external cues (zeitgebers) have the capability to entrain the clock to align with the environment and play an important role in maintaining synchrony of clocks in varying tissues.

Figure 1.1

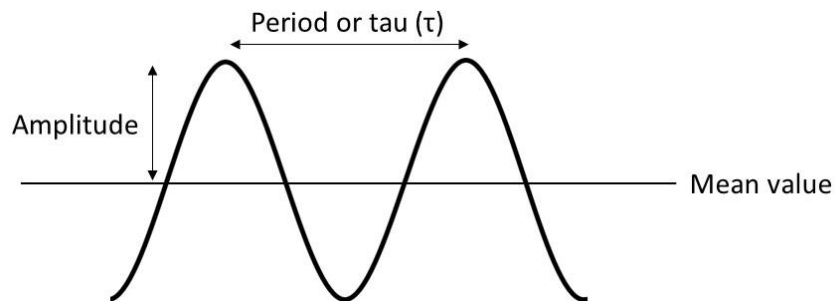


Figure 1.1. Pictorial representation of circadian rhythms. The mean value is the average of all oscillating values within a circadian cycle. The period or tau (τ) is the time between two consecutive peaks, troughs, or recurring point of a cycle. The amplitude is the difference between the peak or trough and the mean value of the cycle.

Molecular Components of the Circadian Clock

The circadian clock network is comprised of transcription factors that oscillate through a transcriptional/translational feedback loop (Figure 1.2). BMAL1 and CLOCK, components of the positive arm of the loop, heterodimerize and bind to E-box sequences in the promoters of target genes to activate transcription. The *period* (*Per*) and *cryptochrome* (*Cry*) families are such genes that are upregulated by BMAL1 and CLOCK. The PER and CRY proteins in turn inhibit BMAL1 and CLOCK, serving as the negative arm of the loop. Through this cyclic manner, the core clock genes—*Bmal1*, *Clock*, *Per1/2*, and *Cry1/2*—auto-regulate their own expression. Genetically engineered mice either lacking or with mutated forms of core clock genes exhibit varying degrees of impaired gene expression of core clock and clock-controlled genes as well as arrhythmic behavior [77-79]. Interestingly, detrimental phenotypes such as premature aging, infertility, and altered glucose regulation are also observed, signifying the importance of clock genes in whole body physiology [80-82].

Figure 1.2

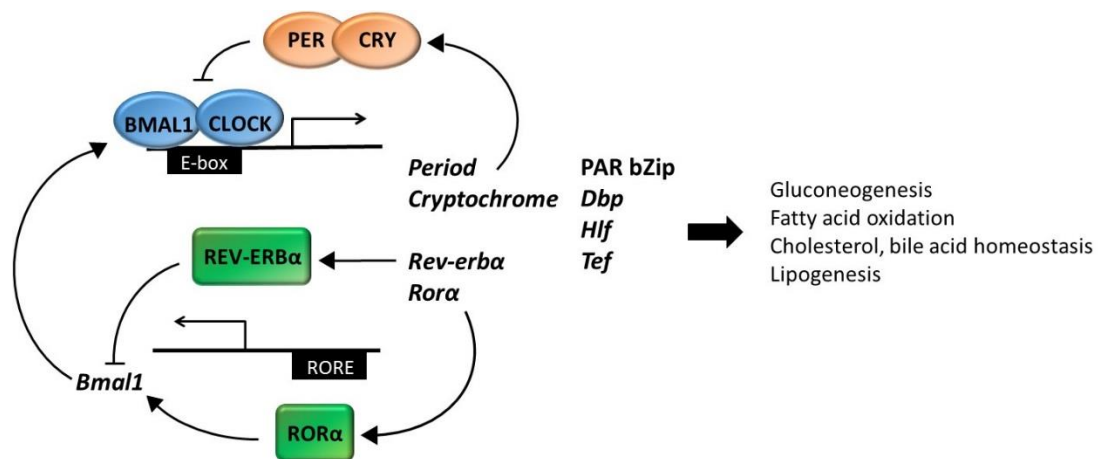


Figure 1.2. Molecular components of the circadian clock network. BMAL1 and CLOCK heterodimerize and bind to E-box sequences to activate transcription of *period*, *cryptochrome*, *Rev-erba*, *Rora*, and the PAR bZip family. PER and CRY heterodimerize and inhibit BMAL and CLOCK, suppressing their own transcription. REV-ERB α and ROR α bind to the retinoic acid-related orphan receptor response element (RORE) sequence of *Bmal1* to inhibit and activate *Bmal1* transcription, respectively. Core clock and clock-controlled genes in peripheral tissues regulate metabolic processes.

Downstream of the core clock genes are clock-controlled genes including nuclear receptor subfamily 1, group D, member 1 (*Rev-erba*), retinoic acid receptor-related orphan receptor alpha (*Rora*), and the proline- and acid-rich basic region leucine zipper (PAR bZip) family (Figure 2). *Rev-erba* and *Rora* are of particular significance as they are involved in creating an accessory

loop that further regulates the circadian cycle. The *Rev-erba* promoter contains an E-box sequence recognized by BMAL1 and CLOCK. Consequently, *Clock* mutant mice have decreased *Rev-erba* gene expression. REV-ERB α inhibits the transcription of *Bmal1* through the recognition of retinoic acid-related orphan receptor response elements (ROREs). Mice deficient of *Rev-erba* have decreased amplitude of *Bmal1* mRNA and protein oscillations. ROR α and REV-ERB α are coordinately regulated yet have opposing functions. While REV-ERB α inhibits *Bmal1*, ROR α activates *Bmal1* transcription. Cells deficient of *Rora* have dampened oscillations of *Bmal1* and *Rora*-deficient mice have altered locomotor activity and rhythm.

The expression of PAR bZip genes, *Dbp*, *Hlf*, and *Tef*, exhibit robust diurnal patterns and is dependent on BMAL1 and CLOCK activity. The PAR bZip proteins act as functionally redundant homo- and heterodimers. While phenotypes observed with the deletion of one or two PAR bZip genes are relatively modest, deletion of all three genes elicits epileptic seizures and impaired xenobiotic metabolism resulting in premature aging and mortality [83-86].

The Network of Central and Peripheral Clocks

The suprachiasmatic nucleus (SCN) houses the central clock, also known as the master regulator. Early studies in rats with SCN lesions have linked this region of the brain to rhythmic locomotor activity, drinking behavior, and corticosterone secretion [87, 88]. The SCN is located in the hypothalamus and receives entrainment signals from the environment to cue the circadian cycle. While both photic and non-photoc signals are received by the SCN, light is the predominant zeitgeber for the central clock. Light enters the retina of the eye and signals to the SCN through the retinohypothalamic tract [89, 90]. Neurons within the SCN undergo synchronized depolarization to maintain the transcriptional/translational feedback loop of the circadian cycle. The central clock is the pacemaker for clocks located outside of the SCN both within the brain and in other peripheral tissues. Neuronal and humoral signals are sent from the central clock to downstream peripheral clocks in order to synchronize oscillations. Transplantation of a functional SCN can establish rhythmicity in a mouse with disrupted circadian rhythms, demonstrating the hierarchical organization of circadian clocks [91].

As mentioned previously, peripheral clocks are regulated by signals from the central clock. However, circadian rhythms in peripheral tissues can oscillate independent of the central clock. This uncoupling of the central clock from peripheral clocks is observed in food restriction studies. In nocturnal mice, restricting food to the daytime under both light-dark and constant dark conditions reverses the rhythmic pattern of core clock and clock-controlled genes in the liver but

not the SCN [92]. As this study suggests, food is the main zeitgeber for peripheral clocks but not the central clock. Although rhythmicity in the central and peripheral clocks is coordinated in part through distinct mechanisms, the convergence of behavior regulated by the central clock and metabolism regulated by peripheral clocks in maintaining energy homeostasis necessitates communication between the brain and the periphery. Hormones released diurnally from the periphery signal to the brain to facilitate the regulation of the feeding/fasting cycle. Ghrelin is released from the stomach and binds to its receptor in the brain during the fasted state to stimulate appetite while leptin, released from adipose tissue, has an opposite effect. Insulin and leptin regulate neurotransmitters in the hypothalamus essential for modulating food consumption and energy expenditure [93]. Food consumption, regulated by the feeding/fasting cycle via the central clock, is associated with food anticipatory activity (FAA) that occurs immediately prior to food availability. FAA is observed in SCN-lesioned rats as well as mice with global disruptions in circadian rhythms, suggesting the role of clock-independent modalities in FAA [94, 95]. The integrated relationship between circadian rhythms and metabolic processes foretell the importance of rhythmicity in maintaining energy homeostasis.

Circadian Dysfunction: A Contributing Factor in Features of MetS

A relationship between impaired circadian rhythms and the development of features of MetS has been observed in a number of epidemiological studies. Shift workers are particularly susceptible to disruptions in sleep and eating cycles that contribute to misalignments between behavioral and physiological rhythms [96]. Increased risk of CVD has been associated with shift work, suggesting that maintaining synchrony between daily activities and environmental cues is essential for metabolic homeostasis [97]. In a cross sectional, population-based study of 27,485 participants, obesity, high triglycerides, and low HDL-cholesterol were more common in shift workers compared to day workers [2]. In another study of 7,839 participants followed from birth to age 45, BMI, abdominal circumference, and C-reactive protein were higher in shift workers after adjusting for confounders [98]. The relative risk of T2DM in women was found to be higher with shift work in a study comparing day workers to rotating night shift workers [99]. Night eating syndrome is another condition that has been associated with T2DM. Although it has been reported that sleep onset, offset, and duration are not impaired, individuals with night eating syndrome have an altered feeding pattern and significantly increased caloric consumption during the night [100, 101].

In an effort to explore the cause and effect relationship between disrupted circadian rhythms and various aspects of metabolic disease, several genetic models targeting core clock or clock-

controlled genes have been generated (Table 1.1). Studies from these models demonstrate the physiological significance of clock components on regulating energy homeostasis. While whole body knockout (KO) models reveal significant defects in circadian behavior regulated by the central clock, much interest has been gained in elucidating the importance of peripheral clocks with respect to metabolism.

Table 1.1

Gene Mutation	Metabolic Defects	Reference
<i>Bmal1</i> whole body KO	Ectopic lipid accumulation; Elevated triglycerides, FFAs, and cholesterol; impaired gluconeogenesis	[82, 102]
<i>Bmal1</i> liver KO	Fasting hypoglycemia	[103]
<i>Bmal1</i> adipose KO	Increased adiposity; decreased polyunsaturated FAs	[104]
<i>Clock</i> whole body loss of function	Obesity; hyperphagia; hyperleptinemia; hyperglycemia; hypoinsulinemia; hyperlipidemia; hepatic steatosis	[105]
<i>Per2</i> whole body KO	Altered lipid metabolism; Reduced epididymal fat pad; impaired glucocorticoid rhythm	[106, 107]
<i>Cry1/Cry2</i> whole body, double KO	Hyperglycemia; glucose intolerance; elevated corticosterone levels; decreased body weight;	[108, 109]
<i>Rev-erba</i> whole body KO	Increased adiposity; hyperglycemia	[110]
<i>Rora</i> whole body KO	Atherosclerosis; hypoalphalipoproteinemia; decreased HDL-cholesterol	[111]

Table 1.1. Genetic mouse models of circadian dysfunction and the corresponding metabolic defects. Deletion or mutation of core clock and clock-controlled genes leads to alterations in glucose and lipid metabolism.

The liver and adipose tissue are essential for the signaling of substances involved in glucose and lipid metabolism. These substances including glucose, insulin, leptin, glucocorticoids, and lipids, exhibit diurnal oscillations in the plasma that occur in coordination with nutrient availability, thus allowing energy utilization to be optimized [82, 112-118]. Additionally, transcriptome and metabolome profiling studies in the liver have revealed a large portion of diurnally expressed transcripts and metabolites, respectively [119-121]. Approximately 10% of transcripts in the liver, many of which are involved in glucose, lipid, bile acid and xenobiotic metabolism, are rhythmically expressed [119, 121]. Liver-specific *Bmal1* KO mice become hypoglycemic during fasting due to defects in hepatic glucose export and gluconeogenesis [103]. Liver-specific deletion of *Bmal1* in the setting of apolipoprotein E (*ApoE*) whole body deletion induces hyperlipidemia and atherosclerosis while suppressing gene expression of the sterol half transporters, ATP binding cassette subfamily G, member 5 (*Abcg5*) and ATP binding cassette subfamily G, family 8 (*Abcg8*) (*G5G8*), and biliary cholesterol secretion [122]. Additionally,

REV-ERB α has been shown to be a regulator of bile acid synthesis [123]. The PAR bZip transcription factor, d site albumin promoter binding protein (DBP), is thought to regulate the circadian expression of cholesterol 7 α -hydroxylase (*Cyp7a1*) in rats and has been demonstrated to activate phosphoenolpyruvate carboxykinase (PEPCK) in hepatoma cells [124, 125]. Together, these data demonstrate the role of core clock and clock-controlled genes in mediating metabolic processes in the liver.

In adipose tissue, deletion of *Bmal1* leads to alterations in circulating polyunsaturated FAs and feeding behavior, resulting in obesity [104]. Food is a potent zeitgeber for peripheral clocks and the timing of food intake can have significant impacts on metabolic homeostasis. Food intake during the rest phase induces obesity while food intake during the active phase has protective effects [126-130]. Furthermore, in a clinical trial assessing the influence of food timing on weight loss, participants consuming more calories during the early part of the day lost more weight than those consuming more later in the day despite similar overall caloric intake [131]. Current data from animal models and humans provide convincing evidence of a direct role of peripheral clocks in regulating energy homeostasis.

Overview of Cholesterol Metabolism

Cholesterol is essential for many biological functions as a component of the cell membrane and as a precursor for vitamin D, steroid hormones, and bile acids. Cholesterol can either be derived from dietary sources or endogenous cholesterol synthesis. The majority of cholesterol in the body comes from cholesterol synthesis, making this pathway a favorable target for regulating plasma cholesterol levels. Too much cholesterol can be detrimental as observed in the development of atherosclerosis. A physiological level is dependent on the coordinated regulation between cholesterol absorption, synthesis, and elimination.

Cholesterol Synthesis, Transport, and Regulation

Sterol homeostasis in the liver is largely maintained by processes regulating cholesterol synthesis, plasma lipoprotein uptake, VLDL secretion, biliary cholesterol secretion, and bile acid synthesis. Cholesterol synthesis is transcriptionally regulated by SREBP-2. In the setting of sufficient cellular sterol content, SREBP cleavage-activating protein (SCAP) binds cholesterol and forms a complex with insulin-induced protein 1 and 2 (INSIG1 and 2) to retain SREBP-2 in the endoplasmic reticulum (ER). SCAP does not interact with INSIG1 and 2 when cellular sterol content is low, allowing SCAP to facilitate SREBP-2 mobilization from the ER to the Golgi. Proteolysis of SREBP-2 in the Golgi results in transcriptional activation of cholesterol

synthesizing genes such as *Hmgcr*. *Hmgcr*, the rate-limiting enzyme of the cholesterol synthesis pathway, is a key step for regulation and the target for the cholesterol-lowering agents referred to as statins. Statins modulate plasma cholesterol levels by inhibiting HMGCR in hepatocytes. Decreases in HMGCR activity leads to a reduction in intracellular cholesterol, creating an environment favorable for SREBP-2 mobilization. In addition to inducing *Hmgcr*, SREBP-2 increases the expression of LDL receptor (*Ldlr*). Upregulation of LDLR promotes the clearance of apo-B-containing lipoproteins thus lowering plasma cholesterol. Statins are effective in lowering LDL-cholesterol by as much as 60%, has been demonstrated to decrease CVD-related morbidity and mortality, and is the recommended treatment for primary and secondary prevention of atherosclerotic CVD [132].

Intestinal absorption of cholesterol is also a therapeutic target for dyslipidemia. Ezetimibe (EZ) inhibits the sterol transporter Niemann-Pick C1-like 1 (NPC1L1) to decrease plasma LDL-cholesterol by approximately 18% [133, 134]. Interestingly, a counter-relationship between cholesterol absorption and synthesis has been demonstrated, suggesting a regulatory interplay between the two sources of cholesterol. Several studies have found that statins increase cholesterol absorption while EZ increases synthesis [135-138]. In the Scandinavian simvastatin survival study (4S), a subgroup of patients with low baseline cholesterol absorption benefited from simvastatin treatment by experiencing less coronary events compared to those with high cholesterol absorption [137, 139]. A subsequent study in the 4S subgroup revealed that simvastatin is more effective in suppressing cholesterol synthesis in those with higher baseline cholesterol synthesis [137]. Together, these data suggest that the addition of EZ to offset the increase in cholesterol synthesis by a statin may be more beneficial. While the clinical significance of a statin combined with other non-statin therapies has been conflicting, the recent findings from the Improved Reduction of Outcomes: Vytorin Efficacy International Trial (IMPROVE-IT) have demonstrated that the addition of EZ to simvastatin not only further reduces LDL-cholesterol but also reduces the risk of cardiovascular events [140].

Endogenously-derived cholesterol along with dietary cholesterol within the liver are packaged into VLDL and transported into the circulation. VLDL interacts with LPL in the periphery resulting in the depletion of triglycerides and the conversion of VLDL to remnant particles. The remnant particles bind to receptors in the liver (e.g. LDLR) for removal from the circulation while a portion of the remnant particles are repackaged into other lipoproteins. The majority of plasma cholesterol is carried within LDL and is removed from the circulation via LDLR. LDL and other apoB-containing lipoproteins in the plasma can undergo oxidation and accumulate

within endothelial cells of arteries, leading to the development of atherosclerosis and increased CVD risk. In contrast, HDL mediates reverse cholesterol transport (RCT), a multi-step process that promotes the transport of cholesterol from peripheral tissues through the circulation to the liver for elimination. Pre- β HDL particles containing apoA1 acquire free cholesterol from peripheral tissues via ATP binding cassette subfamily A, member 1 (ABCA1). Upon activation by apoA1, lecithin:cholesterol acyltransferase (LCAT) esterifies free cholesterol associated with pre- β HDL resulting in the formation of mature HDL. Scavenger receptor B1 (SR-B1) mediates the selective uptake of cholesteryl ester from HDL into the liver. HDL can also interact with CETP to transfer cholesteryl ester to apoB-containing lipoproteins in exchange for triglycerides. Through this process, cholesterol is transported to the liver via LDLR. Cholesterol within the liver can then be secreted into the bile by G5G8 as free cholesterol or converted into bile acids.

ABCG5 ABCG8: A Regulator of Sterol Homeostasis

The ABC half transporters, G5G8, promote sterol efflux from hepatocytes and enterocytes. G5G8 in the liver is responsible for the secretion of up to 90% of the free cholesterol entering the bile and involved in the final step of RCT. In the intestine, G5G8 promotes the efflux of plant sterols (phytosterols) and cholesterol absorbed via NPC1L1. Studies have revealed G5G8 to be direct targets of liver X receptor alpha (LXR α), a nuclear receptor that is activated by oxysterols and regulates the expression of genes involved in lipid metabolism [141, 142]. Upon transport into the enterocytes, cholesterol is esterified with FAs by acetyl-CoA acetyltransferase 2 (ACAT2), packaged into chylomicrons, and secreted through the basolateral side to be transported into the circulation. Phytosterols are poor substrates for ACAT2 and therefore, the majority are secreted from enterocytes into the intestinal lumen by G5G8. Defects in G5G8 result in a rare autosomal recessive disease called sitosterolemia. Characteristics of sitosterolemia include tendon xanthomas, arthralgias, and premature coronary artery disease that occur as a result of increased plasma phytosterol levels. Normally, only about 5% of ingested phytosterols are absorbed and retained compared to 15-60% with sitosterolemia. Plasma cholesterol levels are also increased due to increased intestinal absorption and decreased biliary secretion rates. Similarly in mice, disruptions in G5G8 leads to increased fractional absorption and plasma levels of phytosterols while biliary cholesterol is decreased [143]. In transgenic mice, overexpression of G5G8 yields an opposite effect, decreasing plasma phytosterol levels and increasing biliary cholesterol [144].

The role of G5G8 in governing sterol homeostasis has attracted interest as a potential therapeutic target for CVD-related disease states such as atherosclerosis, NAFLD, and MetS. Indeed, overexpression of both intestinal and hepatic G5G8 in *Ldlr*^{-/-} mice placed on a high-fat, high-

cholesterol diet increases biliary cholesterol and fecal neutral sterols and decreases fractional absorption of cholesterol [145]. Hepatic cholesterol as well as LDL-cholesterol and VLDL-cholesterol fractions of plasma cholesterol are reduced and correlated with a decrease in atherosclerotic lesion area [145]. Liver-specific overexpression of G5G8 in *Ldl^{-/-}* mice increases biliary cholesterol secretion but decreases fractional absorption, lesion area, LDL-cholesterol and VLDL-cholesterol only when intestinal absorption is inhibited by EZ [146]. Similarly, increasing biliary cholesterol secretion through adenoviral vectors encoding G5G8 in *db/db* mice leads to a paradoxical increase rather than a decrease in plasma cholesterol, an effect alleviated by the addition of EZ [147]. Together, these studies suggest that biliary secretion and intestinal absorption of cholesterol act cooperatively to regulate cholesterol elimination.

Hepatic free cholesterol is thought to promote the development of NAFLD and progression to NASH [71-76]. Studies in mice suggest that G5G8 may play a role in modulating NAFLD and features of MetS [147-149]. Mice deficient of G5G8 become obese, insulin resistant, and have decreased biliary cholesterol secretion and increased hepatic free cholesterol when fed a high-fat diet [149]. In obese, insulin resistant *ob/ob* and *db/db* mice, G5G8 is decreased [148]. Overexpression of G5G8 in *db/db* mice decreases plasma triglycerides, insulin resistance, and ER stress [147]. Therefore, promoting G5G8 and biliary cholesterol secretion may be effective in alleviating features of MetS.

The pharmacologic bile acid, ursodiol (Urso), has been shown to increase G5G8, biliary cholesterol secretion, and fecal neutral sterols [150]. Urso has anti-apoptotic and anti-inflammatory properties among a number of other effects [151]. However, it is not entirely known what the mechanisms are for G5G8 regulation. Tauroursodeoxycholic acid (TUDCA) is the taurine-conjugated metabolite of Urso that acts as a molecular chaperone and also increases G5G8. Thus, Urso may similarly regulate G5G8 post-transcriptionally by acting as a chaperone to alleviate ER stress. Proper formation of G5G8 is dependent on N-linked glycosylation facilitated by the lectin chaperones, calnexin and calreticulin within the ER [152-154]. G5G8 is then transported to the canalicular surface of hepatocytes to facilitate sterol efflux [152-154].

Bile Acid Synthesis and Signaling

Bile acid synthesis is essential for facilitating solubilization of dietary cholesterol, lipids, and fat-soluble vitamins and nutrients in micelles for absorption. An equally important role of bile acid synthesis is cholesterol catabolism. Bile acid synthesis is the major route by which excess cholesterol is eliminated from the body [155]. Cholesterol is converted to bile acids by a series of

enzymes in the neutral or acidic pathways. Bile acids are predominantly synthesized via the neutral pathway involving CYP7A1. CYP7A1 catalyzes the formation of 7- α -hydroxycholesterol and is the rate-limiting step of bile acid synthesis [155, 156]. The two primary bile acids that are synthesized within the neutral pathway are cholic acid (CA) and chenodeoxycholic acid (CDCA) [155, 156]. CA and CDCA have differing signaling properties and the relative abundance is determined by sterol 12 α -hydroxylase (CYP8B1) [156]. Sterol 27-hydroxylase (CYP27A1) and 25-hydroxycholesterol 7 α -hydroxylase (CYP7B1) are involved in the synthesis of bile acids through the acidic pathway [155, 156]. Bile acids synthesized in the liver are secreted into the bile canaliculi by ATP binding cassette, subfamily B, member 11 (ABCB11). Bile acids, along with phospholipids transported by ATP binding cassette, subfamily B, member 4 (ABCB4) and free cholesterol transported by G5G8, are stored in the gallbladder and released into the duodenal lumen in response to hormones secreted upon food consumption. Approximately 95% of bile acids are reabsorbed in the ileum, cycling through the enterohepatic circulation [157]. Bile acid absorption occurs in the ileum, mediated by the apical sodium-dependent bile acid transporter (ASBT) and the organic solute transporter alpha/beta (OST α/β) located on the apical and basolateral surfaces, respectively [158-161].

With the discovery of the nuclear receptor, farnesoid X receptor (FXR), much has been revealed about the signaling properties of bile acids. Bile acids are ligands for FXR in the intestine and liver, participating in the feedback mechanism for regulating the bile acid pool [162]. FXR forms a heterodimer with retinoid X receptor (RXR) and binds to target genes with FXR response elements (FXREs) including *small heterodimer partner (Shp)* and *fibroblast growth factor 15 (Fgf15)* [156]. SHP is a transcriptional co-repressor that indirectly binds and suppresses *Cyp7a1*, thus decreasing bile acid synthesis [163]. Mouse FGF15 and human FGF19 (FGF15/19) are orthologous proteins that only share about 50% amino acid sequence yet are functionally similar [164]. FGF15/19, stimulated in the intestine in response to FXR activation, travels to the liver via the enterohepatic circulation where it binds to the fibroblast growth factor receptor 4 (FGFR4) and β -Klotho complex. The role of FGF15/19 in regulating bile acid homeostasis via the gut-liver axis was evaluated in a series of experiments demonstrating that 1) FXR activation stimulates FGF15 in the intestine but not the liver, 2) FGF15 suppresses *Cyp7a1*, and 3) mice deficient of FGF15 have increased *Cyp7a1* [163].

Research in the field of FXR as a regulator of lipid and glucose metabolism shows promise of FXR as a therapeutic target for disease states associated with MetS. Initial evidence was established by the role of bile acid sequestrants in lowering plasma cholesterol levels. Bile acid

sequestrants prevent intestinal absorption of bile acids, disrupting the enterohepatic circulation of bile acids as well as cholesterol to the liver. CYP7A1 is stimulated to increase bile acid synthesis and as a result, hepatic cholesterol decreases. Decreased hepatic cholesterol leads to the activation of SREBP-2 to increase cholesterol synthesis and LDLR expression. Consequently, bile acid sequestrants are effective for reducing total cholesterol and LDL-cholesterol [165, 166]. Modulation of FXR is associated with changes in glucose metabolism in the liver, adipose tissue, and skeletal muscle [167-169]. FXR-deficient mice are hyperglycemic and exhibit impaired peripheral insulin sensitivity [167-169]. Activation of FXR in *db/db* mice suppresses hepatic gluconeogenesis and increases glycogen synthesis, improving insulin sensitivity [169]. In mouse embryonic fibroblasts, FXR deficiency impairs adipocyte differentiation, linking FXR to adipocyte function [167]. Interestingly, insulin signaling is impaired in skeletal muscle of FXR-deficient mice despite the lack of FXR expression in skeletal muscle of wildtype mice [168]. While the effect of FXR deficiency on skeletal muscle is attributed to the increase in triglycerides and FFAs, the possible role of FGF15 cannot be ruled out [168]. Recently, promising results were demonstrated from clinical trials assessing the safety and efficacy of a synthetic, potent FXR agonist, obeticholic acid (OCA), in the treatment of NAFLD and NASH [170, 171]. OCA increases FGF19, a direct target of FXR [170]. In addition to regulating bile acid synthesis and stimulating gallbladder filling, FGF15/19 is involved in regulating energy homeostasis [172-174]. FGF19 transgenic mice have decreased fat mass and hepatic steatosis, increased energy expenditure, and are protected from diet-induced obesity [174]. In obese mice, FGF19 treatment increases metabolic rate, reducing weight gain [173]. FGF15/19 has also been shown to decrease hepatic gluconeogenesis and increase protein and glycogen synthesis [175, 176]. Thus, the role of FGF15/19 in the gut-liver axis is not limited to the regulation of bile acid synthesis but includes governing glucose and lipid metabolism.

Circadian Regulation of Cholesterol and Bile Acid Metabolism

Aspects of cholesterol and bile acid metabolism are governed by circadian rhythms. It has been shown in rodents that cholesterol synthesis, mediated by HMGCR, exhibits a diurnal pattern in the liver and intestine and appears to be highly dependent on food intake [177-179]. Similarly, bile acid synthesis is variable throughout a 24-hour period [180, 181]. Additional evidence of circadian regulation is demonstrated by the diurnal oscillations of *Abcg5*, *Abcg8*, *Ldlr*, *Abcb4*, *Abcb11*, and *Cyp8b1* transcript levels in mouse liver that have been identified in the open access bioinformatics database, CircaDB.

It appears that the core clock gene, *Clock*, plays an essential role in the liver expression of several genes related to cholesterol and bile acid metabolism. In *Clock* mutant mice, *Hmgcr*, *Ldlr*, and *Cyp7a1* expression are muted [182]. Furthermore, *Clock* mutant mice fed a diet supplemented with cholesterol and cholic acid accumulate more hepatic cholesterol than wildtype mice suggesting that cholesterol homeostasis requires functional circadian clocks [182]. Indeed, it has previously been reported that *Clock* mutant mice exhibit features of MetS including obesity, hyperglycemia, and hyperlipidemia [105].

Diurnal regulation of genes involved in cholesterol and bile acid metabolism allows for coordination with nutrient availability that is necessary for efficient maintenance of energy homeostasis. In addition to modulating the cholesterol-bile acid axis for the regulation of glucose and lipid metabolism, targeting core clock genes to maintain rhythmicity is a potential therapeutic strategy for MetS and other related disease states such as NAFLD. This dissertation will explore the effects of peripheral circadian dysfunction particularly in the adipose and liver on the development of features of MetS [183]. Additionally, the role of the bile acid-FGF15/19 axis in sterol metabolism will be studied in order to identify a therapeutic regimen that may be effective in the treatment of NAFLD.

CHAPTER 2: ROLE OF CLOCK-CONTROLLED PAR BZIP GENES IN OBESITY AND INSULIN RESISTANCE

Introduction

Obesity is observed at higher rates in individuals with altered sleep-wake cycles, suggesting a causal relationship between disrupted circadian rhythms and metabolic disease. As a result, much attention has been focused on understanding the role of circadian clocks in energy homeostasis, particularly in highly metabolic tissues such as the adipose. Adipose tissue has a wide array of functions critical for energy regulation. Adipocytes expand to store excess FFAs as well as secrete hormones involved in regulating appetite, body weight, and glucose and lipid metabolism. These processes occur in coordination with the diurnal pattern of the feeding/fasting cycle. Thus, the regulation of energy homeostasis is tightly coupled to circadian rhythms.

The circadian clock is regulated by transcriptional/translational feedback loops involving the core clock components, BMAL1, CLOCK, PER, and CRY. BMAL1 and CLOCK bind to E-box sequences of *Per* and *Cry* to stimulate transcription. In turn, PER and CRY auto-suppress transcription by inhibiting BMAL1 and CLOCK. When PER and CRY concentrations decrease below the threshold for auto-suppression, BMAL1 and CLOCK activity resumes. *D-site binding protein (Dbp)*, *hepatic leukemia factor (Hlf)*, and *thyrotroph embryonic factor (Tef)*, members of the proline- and acid-rich basic region leucine zipper (PAR bZip) family, are direct downstream targets of the circadian clock network. The role of PAR bZip genes have been revealed in pathways involved in xenobiotic metabolism, gluconeogenesis, bile acid synthesis, and lipid metabolism [86, 124, 125, 184, 185]. PAR bZip triple knockout mice are prone to epilepsy and accelerated aging partly due to altered expression of detoxification enzymes such as constitutive androstane receptor (CAR) [86]. In adipose tissue, *Dbp* was found to regulate oscillations of peroxisome proliferator activated receptor gamma (PPAR γ), a nuclear receptor essential for adipocyte differentiation and glucose metabolism [185]. Additionally, gene expression of *Dbp* in subcutaneous adipose tissue was either negatively or positively correlated to BMI depending on the degree of obesity [186].

In the current study, transcriptome profiling of white adipose tissue (WAT) from wildtype and ATP binding cassette, subfamily D, member 2 (ABCD2)-deficient mice fed control or erucic acid-supplemented diets was conducted in an effort to identify potential genes implicated in the development of obesity. ABCD2 is a lipid transporter involved in the transport of long chain monounsaturated fatty acids into the peroxisome for β -oxidation [187-189]. Mice deficient of

ABCD2 exhibit obesity and insulin resistance only in the presence of erucic acid [187]. In this unique model of obesity, there was an overrepresentation of circadian-regulated genes, including the PAR bZip family, that were significantly deregulated in WAT of ABCD2-deficient mice fed erucic acid. Further analyses in other models of obesity confirmed the observation that PAR bZip genes are altered in WAT during obesity.

Methods

Animals

Mice (n=2-6) used for the microarray study came from a previously reported study [187]. Briefly, 8-week-old wild type and *Abcd2* knockout mice were fed standard or erucic acid-enriched diets for 8 weeks. Lean and obese mice used to measure transcript levels of PAR bZip genes came from a cohort of mice from a previously reported study [149]. Mice were anesthetized by a ketamine/xylazine solution and euthanized by exsanguination at termination. Tissues were dissected, snap frozen in liquid nitrogen, and stored in -80°C.

Real Time-PCR

RNA was isolated from frozen tissues using RNA STAT-60 (Tel-Test, Inc.) and the RNeasy Mini Kit (Qiagen). cDNA was synthesized using the iScript cDNA Synthesis Kit (Bio-Rad). De-identified human cDNA samples were donated by the laboratory of Dr. Philip Kern of the Department of Internal Medicine (University of Kentucky). Quantitative real time-PCR was conducted using the 7900HT Fast Real Time-PCR System (Applied Biosystems) and SYBR Green or Taqman assays. CT values of measured transcripts were normalized to that of *Gapdh* or *Hprt*.

Statistical Analyses

Comparisons between two groups defined by one factor were performed using unpaired t-test. Comparisons defined by two factors were performed using two-way ANOVA. Statistical analyses were conducted using GraphPad Prism (version 6). For the microarray, analyses were conducted by the laboratory of Dr. Arnold Stromberg of the Department of Statistics (University of Kentucky). Data are summarized as mean \pm SEM, and statistical significance is defined by $p < 0.05$.

Results

Circadian genes are differentially deregulated in white adipose tissue of obese, ABCD2-deficient mice fed erucic acid.

A genome-wide microarray of adipose tissue was conducted in wild type and *Abcd2* KO mice fed either a standard diet or a diet enriched with erucic acid in order to identify genes involved in explaining the observed obesity phenotype. Of the 35,549 probes screened, 1,916 probes had a main effect of genotype, 4,032 probes had a main effect of diet, and 566 probes had an interaction effect between the two factors of genotype and diet (Figure 2.1).

Figure 2.1

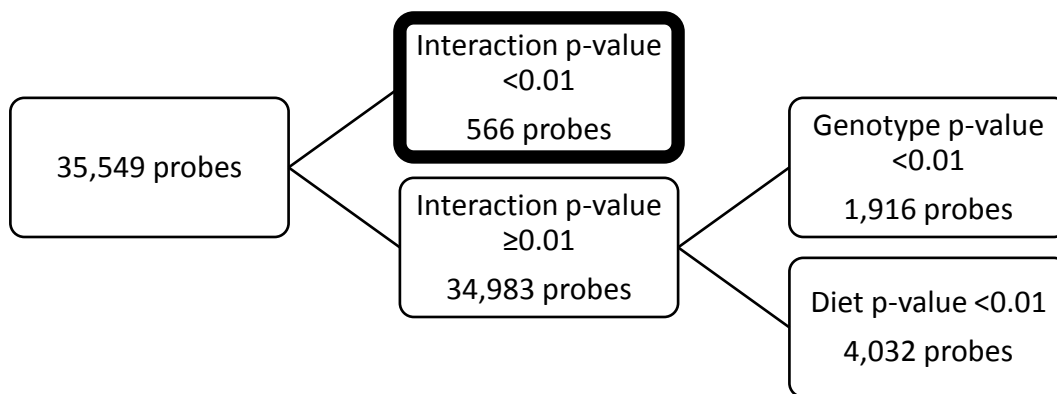


Figure 2.1. Diagram of statistically significant and non-significant probes from a 2x2 factorial microarray study of wild type and ABCD2 KO mice fed standard or erucic acid-enriched diets. 566 probes were significantly deregulated by an interaction between genotype and diet ($p < 0.01$). 1,916 probes had a main effect of genotype and 4,032 probes had a main effect of diet ($p < 0.01$).

The list of 566 probes that were differentially deregulated by interaction were processed through the Database for Annotation, Visualization, and Integrated Discovery (DAVID) version 6.7 for functional annotation clustering [190, 191]. The genes that were most overrepresented were clustered into annotation sources defined by the terms ‘rhythmic process’, ‘biological rhythms’, and ‘circadian rhythm’ (Table 2.1).

Table 2.1.

Annotation Source	Terms	p-value
GOTERM_BP_FAT	Rhythmic process	6.0E-5
SP_PIR_KEYWORDS	Biological rhythms	8.6E-4
KEGG_PATHWAY	Circadian rhythm	2.7E-3
GOTERM_BP_FAT	Circadian rhythm	8.7E-3

Table 2.1. Functional annotation clustering output from DAVID Bioinformatics Database.

The list of 566 probes that were differentially deregulated by an interaction between genotype and diet were most highly associated with ‘rhythmic process’, ‘biological rhythms’, and ‘circadian rhythm’ terms. The p-value represents the significance of the association measured by the DAVID Fisher Exact test.

Two sets of probes for both *Dbp* and *Tef* were identified within the list of 566 probes. After ranking the probes from lowest to highest p-value, both sets of *Dbp* probes were included in the list of the top 20 probes with the lowest p-value (Table 2.2).

Table 2.2

Gene Symbol	ProbF
Per3	1.52645E-06
Slc30a1	2.78176E-06
Hspa1b	1.01351E-05
Zcchc14	1.11562E-05
Cstb	1.91807E-05
Hist1h3b	2.12286E-05
Nedd8	2.42598E-05
S100a16	2.82557E-05
Snx33	3.36851E-05
Dbp	5.16747E-05
Per3	5.81648E-05
Dbp	6.26626E-05
Trim8	6.31615E-05
Mrps6	6.41546E-05
Nr1d2	6.83611E-05
Per3	7.42258E-05
4933424C09Rik	9.60619E-05
Fam110c	0.000119221
Kctd6	0.000124885
Ndrgl	0.000139583

Table 2.2. Gene symbols of the top 20 probes with the lowest p-value. The effect of a genotype by diet interaction is highly significant in two sets of *Dbp* probes.

Dbp, *Hlf*, and *Tef* are decreased in white adipose tissue of obese mice.

To confirm the findings from the microarray analysis in another mouse model of obesity, gene expression of *Dbp*, *Hlf*, and *Tef* were measured using real time-PCR in WAT of lean and obese ABCG5 ABCG8 (G5G8) knockout mice. All three members of the PAR bZip family, *Dbp*, *Hlf*, and *Tef* were significantly downregulated in obese G5G8 knockout mice compared to lean G5G8 knockout mice (Figure 2.2). *Ppara*, *Ppar γ* , and *Tnfa* were measured as positive controls and as expected, expression of *Ppara* and *Ppar γ* were decreased in obese mice while *Tnfa* expression was increased (Figure 2.2).

Figure 2.2

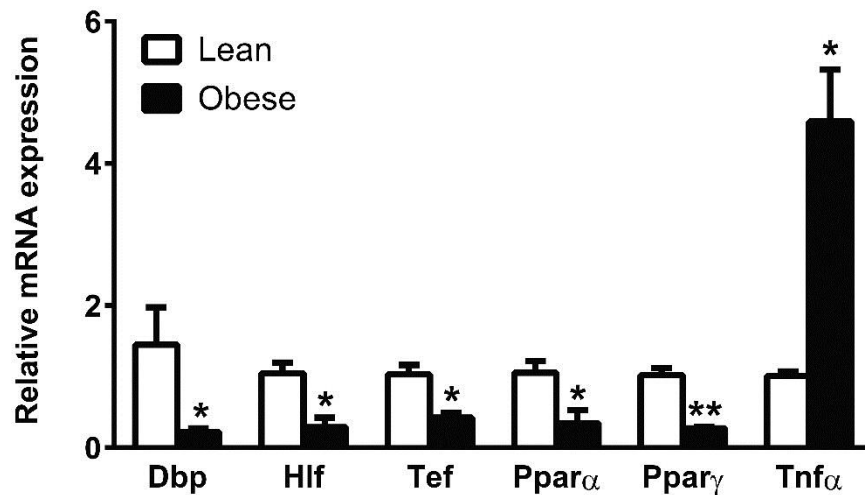


Figure 2.2. Gene expression of PAR bZip genes in WAT of 24-week-old male G5G8 knockout mice fed a low-fat diet (lean) or a high-fat diet (obese). *Dbp*, $t=2.472$, $df=9$, $p=0.0354$; *Hlf*, $t=2.866$, $df=9$, $p=0.0186$; *Tef*, $t=3.326$, $df=9$, $p=0.0088$; *Ppara*, $t=2.825$, $df=9$, $p=0.0199$; *Ppar γ* , $t=8.100$, $df=9$, $p<0.0001$; *Tnfa*, $t=4.450$, $df=9$, $p=0.0016$. $n=5$ for lean, $n=6$ for obese. * $p<0.05$, ** $p<0.01$.

Dbp and *Hlf* are decreased in white adipose tissue of obese, insulin-resistant humans.

Although the suppression of all three PAR bZip genes was observed in WAT of a mouse model of obesity, the clinical significance of this in humans is unclear. In order to better understand whether the clock-controlled PAR bZip genes are regulated by obesity in humans, gene expression was measured using RT-PCR in subcutaneous WAT in lean/insulin sensitive (IS) and obese/insulin resistant (IR) humans. The mean age between lean/IS and obese/IR subjects were similar while BMI and S_I , a measure of insulin sensitivity, were significantly increased in obese, insulin resistant subjects (Table 2.3).

Table 2.3

	Age (years)	BMI (kg/m ²)	S _I (min ⁻¹ /μU/mL)
Lean/IS	26	19	15.248
	51	23	6.276
	29	20	13.64
	48	22	5.068
	34	19	5.456
	35	26	8.31
	Mean ± SEM	37.2±15.2	21.5±8.8
Obese/IR	34	36	1.2
	35	35	1.979
	36	36	1.299
	38	37	2.15
	48	38	2.04
	49	37	1.008
	Mean ± SEM	40.0±16.3	36.5±14.9****

Table 2.3. Human subject characteristics. Age measured in years, body mass index (BMI) measured in kg/m², and insulin sensitivity index (S_I) of lean/insulin sensitive (IS) and obese/insulin resistant (IR) human subjects. S_I was calculated using the minimal model methodology. Age, *t*=0.5702, *df*=10, *p*=0.5812; BMI, *t*=12.53, *df*=10, *p*<0.0001; S_I, *t*=4.093, *df*=10, *p*=0.0022. *n*=6 per group. ***p*<0.01, *****p*<0.0001.

Gene expression of two of the PAR bZip genes, *Dbp* and *Hlf*, as well as the positive control, PPARG coactivator 1 alpha (*Pgc1α*), were significantly decreased in WAT of obese/IR subjects compared to lean/IS subjects (Figure 2.2). *Tef* expression tended to be decreased as well; however, the decrease was not statistically significant (Figure 2.3).

Figure 2.3

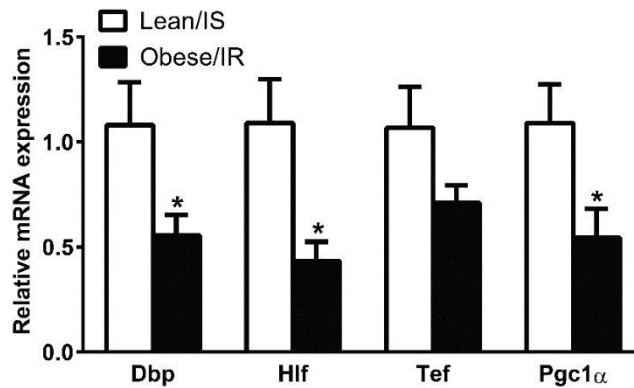


Figure 2.3. Gene expression of PAR bZip genes in WAT of lean/IS and obese/IR female human subjects. *Dbp*, *t*=2.338, *df*=10, *p*=0.0415; *Hlf*, *t*=2.892, *df*=10, *p*=0.0161; *Tef*, *t*=1.677, *df*=10, *p*=0.1244; *Pgc1α*, *t*=2.362, *df*=10, *p*=0.0398. *n*=6 per group. **p*<0.05.

Discussion

Our interest in the PAR bZip family of transcription factors was driven by the results from the microarray study comparing gene expression in WAT of wildtype and ABCD2 knockout mice fed control or erucic acid-supplemented diets. The MetS-like phenotypes observed with erucic acid feeding in ABCD2 knockout mice included obesity, hepatic steatosis, and insulin resistance [187]. The purpose of the microarray study was to identify genes that may be mechanistically involved in precipitating these phenotypes. Several core clock and clock-controlled genes were significantly deregulated when comparing wildtype mice fed a control diet versus ABCD2 knockout mice fed an erucic acid-supplemented diet including *Dbp* and *Tef* of the PAR bZip family. In our study, PAR bZip genes were decreased in a diet-induced model of obesity, confirming the findings of the microarray analysis. Furthermore, two members of the PAR bZip family, *Dbp* and *Hlf*, were decreased in humans with obesity and insulin resistance as well.

Our study provides evidence that PAR bZip genes in adipose tissue are inversely correlated with obesity and insulin resistance in both mice and humans. This suggests the notion that peripheral clocks are key factors involved in maintaining energy homeostasis. Indeed, the circadian clock has been found to regulate adipogenesis, lipogenesis, lipolysis, and fatty acid oxidation [106, 184, 185, 192, 193]. However, it cannot be concluded from our current study whether altered PAR bZip gene expression is simply an associated outcome of obesity or if it plays a pathogenic, causative role in adipose dysfunction. In order to better understand the impact of the PAR bZip family in adipose tissue function, further studies would need to be conducted in a tissue-specific PAR bZip knockout model.

In our study, we were able to translate our findings from mouse models of obesity to a human population of obese/IR subjects. While all three members of the PAR bZip family were significantly downregulated in mice, decreases in only *Dbp* and *Hlf* were significant in humans. This may be due to several limitations of the study including the use of a small sample size and the measurement of gene expression at only one time point. Another limitation of the study was the use of only males in the mouse experiment and only females in the human experiment. There are established sex differences in the characteristics of the circadian cycle, body temperature, melatonin release, feeding behavior, and sleep-wake cycles [194-198]. Additionally, differences in clock gene and protein expression have been observed in adipose tissue between morbidly obese males and females [199]. A more expansive study including measurements in both sexes during multiple time points is needed to get a better appreciation of the impact of suppressed PAR bZip gene expression on metabolic disease.

In summary, PAR bZip genes were downregulated in adipose tissue of multiple mouse models of obesity. These results were confirmed in human subjects, further suggesting the role of PAR bZip genes in adipose function. Taken together, our study extends findings from preclinical studies to humans and provides potential for identifying novel targets for the treatment of obesity.

CHAPTER 3: EFFECT OF PERIPHERAL CIRCADIAN DYSFUNCTION ON METABOLIC DISEASE IN RESPONSE TO A DIABETOGENIC DIET

Introduction

The liver and adipose tissue house peripheral clocks that regulate diurnal oscillations of factors involved in energy homeostasis such as glucose, insulin, and leptin [82, 115, 118]. Coordination between the liver and adipose tissue is essential for the regulation of glucose and lipid metabolism. This allows proper storage and release of fatty acids and glucose in response to the nutrient status. In the setting of disrupted peripheral clocks, it is thought that processes necessary for maintaining energy homeostasis is impaired [82, 105, 107, 192, 200]. Deletion of the core clock gene, *Bmal1*, specifically from the liver suppresses rhythmic expression of genes involved in glucose transport and gluconeogenesis while deletion specifically from adipose tissue alters feeding behavior and induces obesity [103, 104]. Given the interplay of adipose tissue and the liver, we hypothesized that the disruption of circadian clocks in both tissues would potentiate features of MetS.

Methods

Animals

Mice with loxP sites flanking exon 8 (*Bmal1^{fl/fl}*) were generously donated by Dr. Karyn Esser of the University of Kentucky and transgenic mice hemizygous for a *Cre recombinase* transgene driven by the adipocyte fatty acid binding protein promoter (*aP2-Cre^{+/-}*) were purchased from Jackson Laboratory (Bar Harbor, ME). Female *Bmal1^{fl/fl}* were bred to male *Bmal1^{fl/fl}-aP2-Cre^{+/-}* mice using trio breeding to obtain adipose-*Bmal1* deletion. Recombinant adenoviral vectors containing no insert (Ad-Empty) or cDNA for *Cre recombinase* (Ad-*Cre*) were amplified in HEK293Q cells, purified on cesium chloride gradients and dialyzed against PBS. Mice were injected with 4×10^{12} particles/kg via tail vein injection. *Bmal1^{fl/fl}* mice without the *aP2-Cre* allele were injected with Ad-Empty virus (control). *Bmal1^{fl/fl}* mice with the *aP2-Cre* allele were injected with either Ad-Empty virus or Ad-*Cre* virus to generate adipose-*Bmal1* knockout (ABKO) and liver- and adipose-*Bmal1* knockout (LABKO) mice, respectively.

Mice were maintained on a C57BL/6J background and housed 2-4 mice per cage in individually ventilated cages in a temperature-controlled room with access to standard rodent chow (Teklad 2918). For breeding, mice were maintained on a 14-hour light/10-hour dark cycle. Following

adenoviral injection at 7-weeks old, mice were transferred to a 12-hour light/12-hour dark cycle for the duration of the study.

All animal procedures were conducted conforming to Public Health Service policies for humane care and use of laboratory animals and were approved by the University of Kentucky Institutional Animal Care and Use Committee.

Indirect Calorimetry

Measurements for indirect calorimetry were performed on the TSE System (Chesterfield, MO). This system includes 24 chambers plus a reference chamber. O₂ (%), CO₂ (%), food intake and locomotor activity were directly measured from each chamber in sequence in 30 minute intervals. Reference measurements from room air were also taken in 30 minute intervals. The length of each measurement and reference measurement were determined by the measurement interval divided by the number of active chambers. Flow rate to the chambers was 0.45 L/min. Respiratory exchange ratio (RER) and energy expenditure (EE) were calculated by the system using measured values [CO₂%, O₂%, flow (L/min)]. Resting energy expenditure (REE) was defined as EE during the resting period (10:00 to 18:00) with a total activity count less than 150 beam breaks/30 min. Locomotor activity is defined as the number of times a mouse breaks two adjacent beams in succession or breaks the same beam twice. Mice were acclimated to chambers for 7 days then transferred to clean chambers immediately prior to the start of measurements. Data from the first and last days of measurements were not included in the analyses. Data across three days were averaged for each mouse.

Diet and Physiological Measurements

For 24-hour blood glucose measurements, mice 13-24-weeks old on standard rodent chow in 12-hour light/12-hour dark conditions were provided food only during the dark cycle for a 24-hour period. Blood glucose from tail vein pricks was measured every four hours for 24 hours beginning at circadian time 0, defined as the beginning of lights-on.

For the diet intervention study, male mice 8-weeks old were fed either a control diet (CD) comprised of 63% carbohydrate, 16% fat and 21% protein (Bio-Serv F4031) or a diabetogenic diet (DD) comprised of 26% carbohydrate, 59% fat and 15% protein (Bio-Serve F3282). Body weight was measured weekly and body composition was determined by EchoMRI-100 (Echo Medical Systems) during weeks 8, 12, 16, 20 and 24. Adiposity was calculated by dividing fat mass by total body mass.

During weeks 12, 16, 20 and 24, fasting glucose was measured following a 4-hour fast beginning at lights-on. Glucose tolerance and insulin sensitivity tests (GTT and IST) were conducted during weeks 16 and 24. For the GTT, 10 μ L/g body weight of a 20% glucose solution was injected intraperitoneally following a 4-hour fast beginning at lights-on. For the IST, 10 μ L/g body weight of insulin 0.2 IU/mL was injected intraperitoneally following a 1-hour fast beginning at lights-on. Blood glucose levels were measured before and 30, 60, 90 and 120 minutes after the injection from blood obtained from a tail-vein prick. All blood glucose measurements were conducted using a standard glucometer.

At the termination of the study, mice were administered ketamine/xylazine solution for sedation and euthanized by exsanguination. For the 24-hour gene expression, mice were sacrificed every four hours for 24 hours beginning at circadian time 0. For the diet intervention study, mice were sacrificed at circadian time 0. Blood was stored at 4°C for four hours, centrifuged at high speed for 10 minutes then serum collected and stored at -80°C. Tissues were dissected and immediately frozen in liquid nitrogen. For histological analysis, pieces of liver and adipose tissue were fixed in 10% formalin for 24 hours at room temperature then transferred to 70% ethyl-alcohol for long-term storage at 4°C.

Histology

Liver and epididymal fat sections were embedded in paraffin and cut into 5 μ m-thick sections. Sections stained with hematoxylin and eosin and Picrosirius Red were imaged at a 10x magnification. Adipocyte size and number were quantified using the NIS Elements software (Nikon Instruments, Inc., Tokyo, Japan). The image threshold and object count features were used to quantify three 700x700 μ m areas to represent each section (2 sections per mouse).

Hepatic Lipid Extraction and Lipid Measurements

Hepatic lipids were extracted from 100 μ g of tissue using the Folch method. Extracts were solubilized in 1% Triton in water as previously described [149]. Total cholesterol, triglycerides and non-esterified fatty acids (NEFAs) were measured using enzymatic, colorimetric assays (Wako Chemicals).

Real Time-PCR

RNA was isolated from frozen tissues using RNA STAT-60 (Tel-Test, Inc.) and the RNeasy Mini Kit (Qiagen). cDNA was synthesized using the iScript cDNA Synthesis Kit (Bio-Rad). Quantitative real time-PCR was conducted using SYBR Green and the 7900HT Fast Real Time-

PCR System (Applied Biosystems). For markers of lipolysis, TaqMan (Applied Biosystems) assays were used. Primer sequences for SYBR Green assay are listed in Table 3.1. CT values of measured transcripts were normalized to that of Gapdh and expressed relative to control mice on control diet using the $\Delta\Delta CT$ method.

Table 3.1

Gene	Primer sequence	
Bmal1	Forward	5'-ACACCAAGGAAGGATCAAGA-3'
	Reverse	5'-GGTACCAAAGAAGCCAATTCA-3'
Dbp	Forward	5'-ACCGGCCAGCTGTCTCCTGA-3'
	Reverse	5'-CCACAGCAGCGGCGCAAAAA-3'
Pparg	Forward	5'-CACAATGCCATCAGGTTTGG-3'
	Reverse	5'-GCTGGTCGATATCACTGGAGATC-3'
C/ebpa	Forward	5'-GACATCAGCGCCTACATCGA-3'
	Reverse	5'-TCGGCTGTGCTGGAAGAG-3'
C/ebpb	Forward	5'-ATTTCTATGAGAAAAGAGGCGTATGT-3'
	Reverse	5'-AAATGTCTTCACTTTAATGCTCGAA-3'
Zfp423	Forward	5'-TGGCCTGGGATTCCTCTGT-3'
	Reverse	5'-CTCTTGACTTGTCACGCTGTT-3'
Hsl	Forward	5'-GGAAAGAATTGATGGAGCCGGC-3'
	Reverse	5'-TCCATGCTGTGTGAGAACGCT-3'
F4/80	Forward	5'-CTTTGGCTATGGGCTTCCAGTC-3'
	Reverse	5'-GCAAGGAGGACAGAGTTTATCGTG-3'
Mcp-1	Forward	5'-TTAAAAACCTGGATCGGAACCAA-3'
	Reverse	5'-GCATTAGCTTCAGATTTACGGGT-3'
Hmgcr	Forward	5'-CTTGTGGAATGCCTTGTGATTG-3'
	Reverse	5'-AGCCGAAGCAGCACATGAT-3'
Hmgcs	Forward	5'-GCCGTGAACTGGGTCGAA-3'
	Reverse	5'-GCATATATAGCAATGTCTCCTGCAA-3'
Abcg5	Forward	5'-TGGATCCAACACCTCTATGCTAAA-3'
	Reverse	5'-GGCAGGTTTTCTCGATGAACTG-3'
Abcg8	Forward	5'-TGCCCACCTTCCACATGTC-3'
	Reverse	5'-ATGAAGCCGGCAGTAAGGTAGA-3'
Ldlr	Forward	5'-AGGCTGTGGGCTCCATAGG-3'
	Reverse	5'-TGCGGTCCAGGGTCATCT-3'
Srb1	Forward	5'-TCCCCATGAACTGTTCTGTGAA-3'
	Reverse	5'-TGCCCGATGCCCTTGA-3'
Cyp7a1	Forward	5'-TAGTGGCGGGCGTCCCTATT-3'
	Reverse	5'-GCCAGAGGATCACGAGGTG-3'
Cyp8b1	Forward	5'-GCCTTCAAGTATGATCGGTTCT-3'
	Reverse	5'-GATCTTCTTGCCCGACTTGTA-3'
Gapdh	Forward	5'-TGTGTCCGTCGTGGATCTGA-3'
	Reverse	5'-CCTGCTTACCACCTTCTTGAT-3'

Table 3.1. Sequences for primers. Forward and reverse primer sequences of SYBR Green assays.

Immunoblot Analysis

SDS-PAGE and immunodetection of proteins was conducted as previously reported [148]. To enrich for nuclear proteins, frozen tissues were homogenized in buffer containing Tris hydrochloride 20 mM, magnesium chloride 2 mM, sucrose 0.25 M and protease inhibitors. The homogenate was centrifuged at 2,000 g for 10 minutes and the remaining pellet was solubilized in protein sample buffer. An insulin syringe was used to shear DNA. For measuring total and phosphorylated AKT (p-AKT), the supernatant of the homogenate was collected. Protein concentrations were measured by BCA assay. The following primary antibodies were used: BMAL1 at 1:2000 dilution (Bethyl Laboratories A302-616A), total AKT at 1:5000 dilution (Cell Signaling Technology 4685), p-AKT at 1:5000 dilution (Cell Signaling Technology 9271), histone H3 at 1:2000 dilution (Cell Signaling Technology 4499), GAPDH at 1:200 dilution (Chemicon International MAB374). The secondary antibodies used were a goat anti-rabbit IgG horseradish peroxidase (HRP) conjugated antibody (Pierce Biotechnology 31460) and a horse anti-mouse IgG HRP conjugated antibody (Cell Signaling Technology 7076) at a 1:1000 dilution.

Statistical Analyses

Comparisons across groups defined by one factor (e.g., genotype) were performed using t-test or one-way ANOVA, and across groups defined by two factors (e.g., genotype and diet) using two-way ANOVA. For gene expression measured over a 24-hour period, variances across groups differed. Comparisons across groups defined by one factor (e.g., genotype) while accounting for lean mass were performed using one-way ANCOVA. Comparisons across groups defined by two factors (e.g., genotype and diet) while accounting for 8-week body weight were performed using two-way ANCOVA. Comparisons across groups in which time was a factor were performed using repeated measures ANOVA. Statistical analyses were conducted using GraphPad Prism (version 6) and SAS (version 9.3). Data are summarized as mean \pm SEM, and statistical significance is defined by $P < 0.05$.

Results

Liver and adipose peripheral clocks mediate centrally-regulated functions.

We generated adipose-*Bmal1* knockout (ABKO) and liver- and adipose-*Bmal1* knockout (LABKO) mice in order to study the role of adipose and liver peripheral clocks in metabolic disease. (Fig. 1). Peak mRNA and protein expression were blunted in adipose tissue of female ABKO and LABKO mice expressing the *aP2-Cre* transgene while mRNA and protein expression

were blunted in liver of LABKO mice injected with the Ad-*Cre* virus (Fig. 3.1A and B). Furthermore, the diurnal mRNA expression of *Dbp*, a BMAL1 target gene, was disrupted in adipose of ABKO and LABKO mice and in liver of LABKO mice (Fig. 3.1C).

Figure 3.1

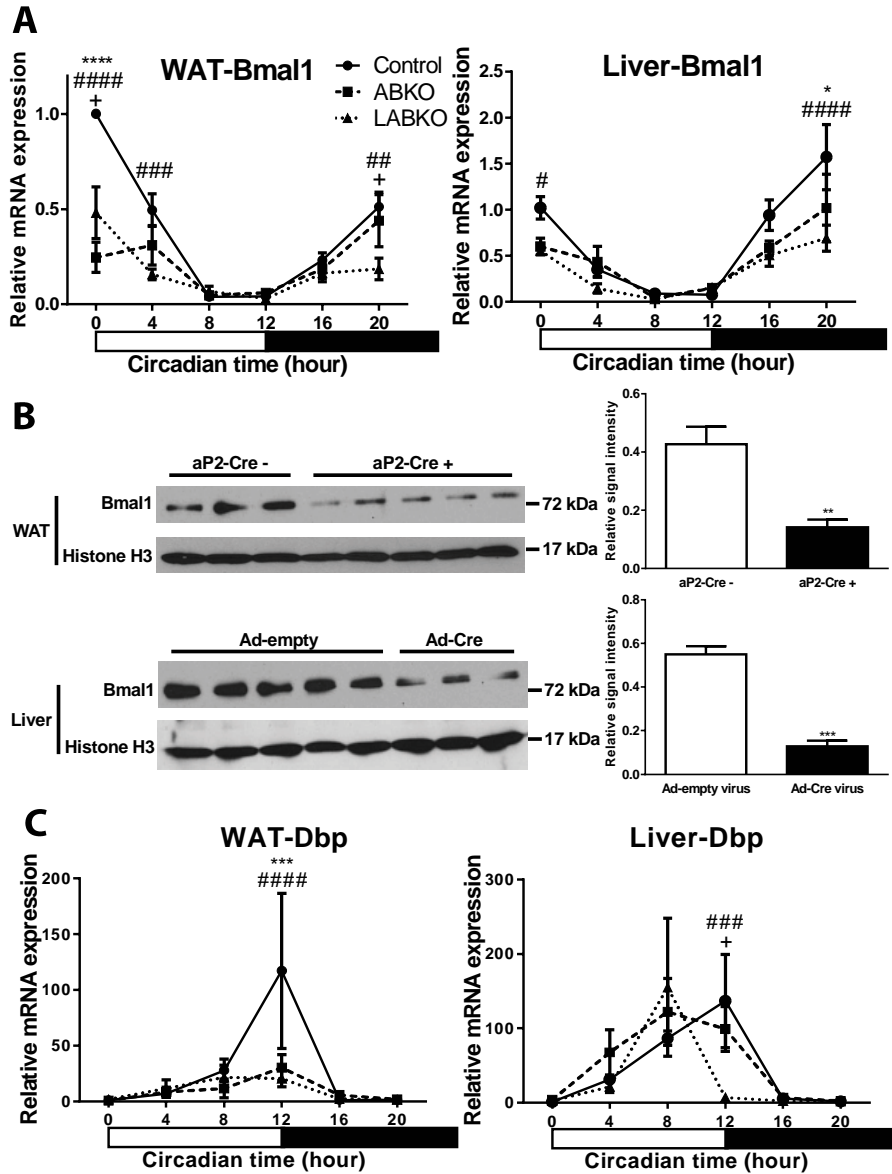


Figure 3.1. Deletion of *Bmal1* in WAT and liver of 13-24-week-old female mice on standard rodent chow. Hour 0 represents the beginning of lights-on. n=3-9 per group. A) *Bmal1* expression in white adipose tissue (WAT), genotype $F(2, 49)=18.23$, $p<0.0001$; time $F(2, 49)=29.76$, $p<0.0001$; interaction $F(10, 49)=6.604$, $p<0.0001$, and in liver, genotype $F(2, 55)=8.709$, $p=0.0005$; time $F(5, 55)=22.75$, $p<0.0001$; interaction $F(10, 55)=1.860$, $p=0.0714$. B) Western blot and densitometry analyses of BMAL1 in WAT of mice negative or positive for the

aP2-Cre transgene, $t=4.944$, $df=6$, $p=0.0026$, and in liver of mice injected with Ad-empty or Ad-*Cre* virus, $t=7.732$, $df=6$, $p=0.0002$, at hour 0. C) *Dbp* expression in WAT, genotype $F(2, 49)=2.481$, $p=0.0941$; time $F(5, 49)=6.358$, $p=0.0001$; interaction $F(10, 49)=2.223$, $p=0.0317$, and in liver, genotype $F(2, 55)=0.9127$, $p=0.4075$; time $F(5, 55)=11.35$, $p<0.0001$; interaction $F(10, 55)=1.874$, $p=0.0695$. *=Comparison between control and ABKO, #=Comparison between control and LABKO, +=Comparison between ABKO and LABKO for Figures 1A and C. *#.+ $p<0.05$, **.# $p<0.01$, ***.## $p<0.001$, ****.### $p<0.0001$.

To determine whether peripheral *Bmall* regulates behavioral changes related to metabolism, measures of food intake, locomotor activity and energy expenditure were taken in female mice maintained on a standard rodent chow diet (Fig. 3.2). Both ABKO and LABKO mice had increased total food intake. The increase was observed in both the light and dark phase, although the increase did not reach statistical significance in the dark phase in ABKO mice. (Fig. 3.2A and B). Total locomotor activity was increased in ABKO mice compared to control mice. This was due to increased activity predominantly in the light phase and tended to be increased in the dark phase (Fig. 3.2C and D). Further deletion of *Bmall* in the liver reversed this effect (Fig. 3.2D). Other differences in activity patterns were also observed. Compared to control and LABKO mice, ABKO mice had a greater and more prolonged peak in activity following the onset of the dark phase. ABKO mice also exhibited bursts of activity midway through the light and dark phases (Fig. 3.2C).

Figure 3.2

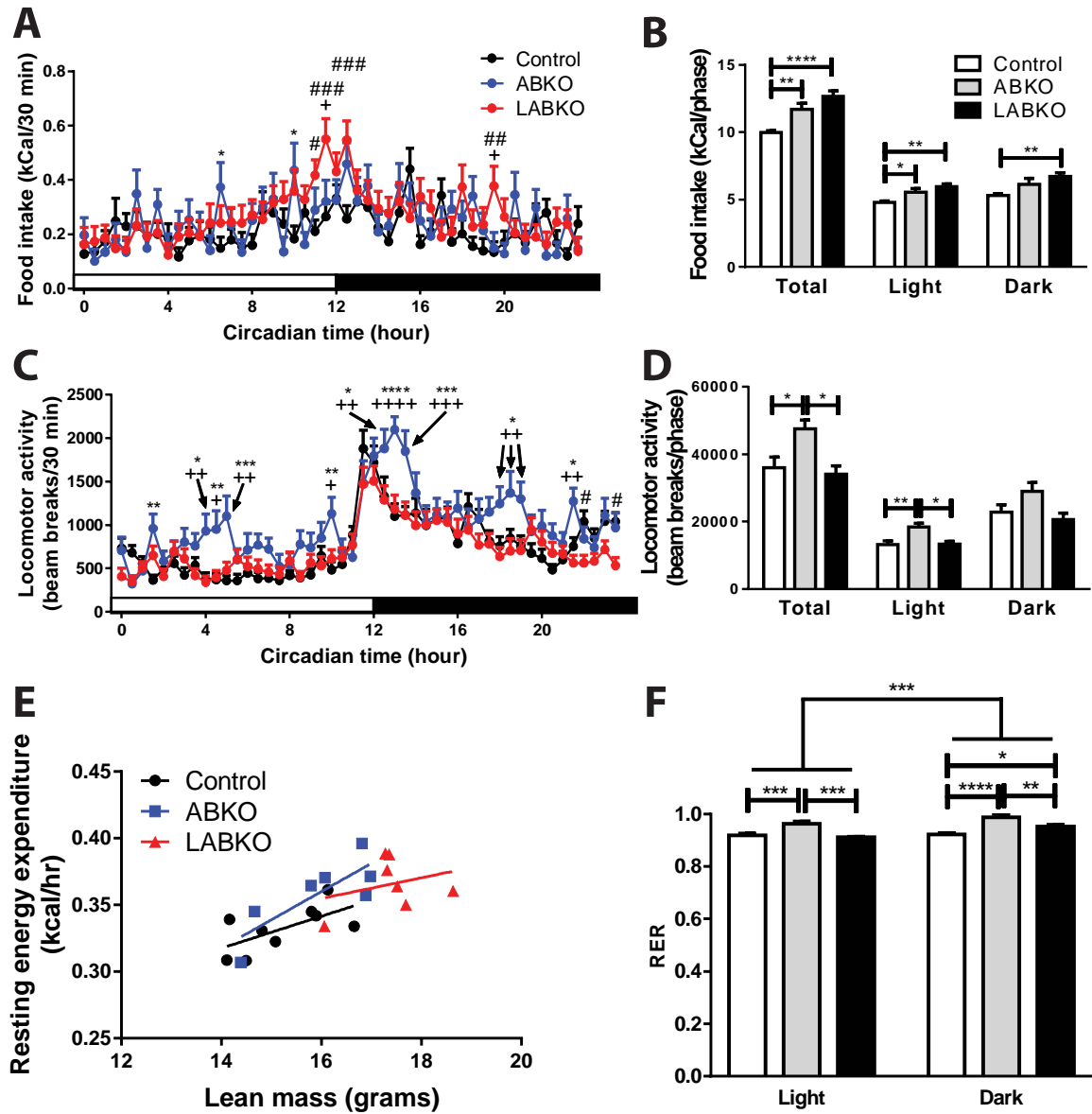


Figure 3.2. Food intake, physical activity and energy expenditure changes in 12-week-old female mice on standard rodent chow. Hour 0 represents the beginning of lights-on. $n=7-9$ per group. A) Food intake over 24 hours, genotype $F(2, 3842)=10.28, p<0.0001$; time $F(47, 3842)=3.594, p<0.0001$; interaction $F(94, 3842)=1.361, p=0.0124$. B) Food intake during the light phase, $F(2, 20)=9.791, p=0.001$; dark phase, $F(2, 20)=5.956, p=0.0093$; both phases, $F(2, 20)=16.65, p<0.0001$. C) Locomotor activity defined as the sum of ambulatory (break of two adjacent beams in succession) and fine (break of the same beam twice) activity over 24 hours, genotype $F(2, 3888)=54.14, p<0.0001$; time $F(47, 3888)=16.03, p<0.0001$; interaction $F(94, 3888)=1.741, p<0.0001$. D) Locomotor activity during the light, $F(2, 20)=7.541, p=0.0036$; dark phase, $F(2, 20)=3.555, p=0.0477$; both phases, $F(2, 20)=5.853, p=0.01$. E) Resting energy expenditure (REE) relative to lean mass, slope $p=0.458$; intercept $p=0.171$. F) Respiratory exchange ratio (RER) during the light and dark phase, genotype $F(2, 42)=29.12, p<0.0001$; phase $F(1, 42)=13.01, p=0.0008$; interaction $F(2, 42), p=0.0546$. Effects of genotype are indicated by

horizontal lines terminating in vertical lines. *=Comparison between control and ABKO, #=Comparison between control and LABKO, +=Comparison between ABKO and LABKO for Figures 2A and C. *.,#+p<0.05, **,##,++p<0.01, ***,###,+++p<0.001, ****,####,++++p<0.0001.

Resting energy expenditure (REE) was analyzed using lean mass as a covariate. After controlling for lean mass, there were no significant differences among genotypes on REE (Fig. 3.2E). The respiratory exchange ratio (RER) was higher overall in the dark phase and highest in ABKO mice within both light and dark phases indicating a greater utilization of glucose for energy (Fig. 3.2F). Body weight, lean mass, fat mass and adiposity were all increased in LABKO mice compared to control and ABKO mice (Fig. 3.3A-D).

Plasma glucose oscillates following a diurnal pattern [82, 104, 115]. ABKO mice had higher blood glucose concentrations throughout the light phase which was maintained upon feeding during the dark phase. The increase in glucose was reversed in LABKO mice, resulting in a similar blood glucose pattern between control and LABKO mice (Fig. 3.3E).

Figure 3.3

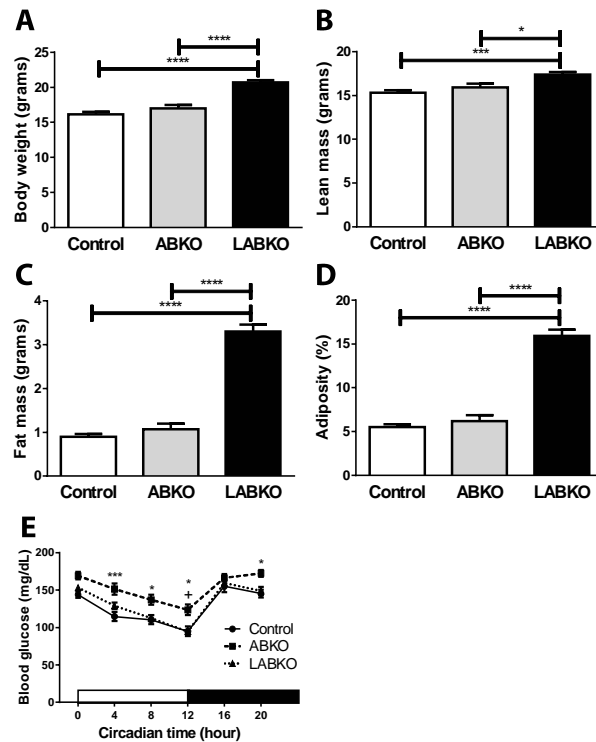


Figure 3.3. Body weight, body composition and blood glucose of 13-24-week-old female mice fed a standard rodent chow. n=7-9 per group. A) Body weight, $F(2, 20)=37.99$, $p<0.0001$. B) Lean mass, $F(2, 20)=10.63$, $p=0.0007$. C) Fat mass, $F(2, 20)=124.9$, $p<0.0001$. D) Percent adiposity, $F(2, 20)=106.3$, $p<0.0001$. E) Blood glucose measured beginning at circadian time 0, genotype $F(2, 74)=10.72$, $p<0.0001$; time $F(5, 370)=65.51$, $p<0.0001$; interaction $F(10, 370)=1.058$, $p=0.3938$. n=17-31 per group. Effects of genotype are indicated by horizontal lines

terminating in vertical lines. *=Comparison between control and ABKO, +=Comparison between ABKO and LABKO for Figure 3E. *+,p<0.05, ***p<0.001, ****p<0.0001.

Disruptions in liver and adipose peripheral clocks lead to increased body weight and adiposity.

To assess the development of obesity and obesity-related phenotypes, a second cohort of male mice was fed a low-fat, control diet (CD) or high-fat, diabetogenic diet (DD) for 16 weeks. The diabetogenic diet itself decreased *Bmal1* mRNA expression in epididymal adipose tissue but not in the liver (Fig. 3.4A and C). However, this decrease was not reflected in BMAL1 protein levels observed at hour 0 (Fig. 3.4B).

Figure 3.4

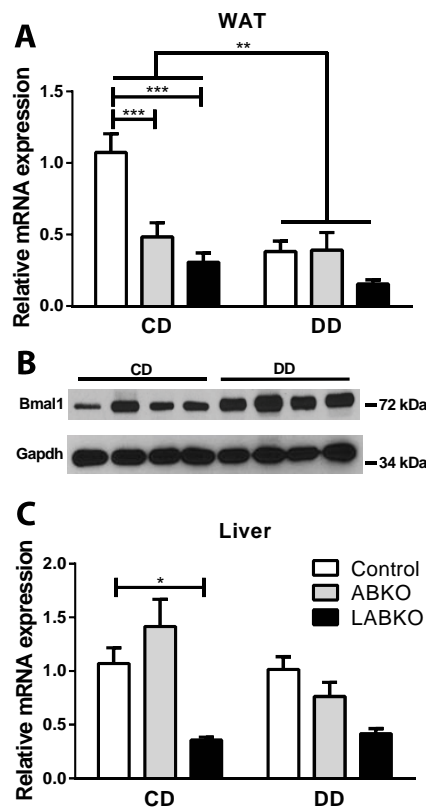


Figure 3.4. Deletion of *Bmal1* in WAT and liver of 24-week-old male mice on control diet (CD) or diabetogenic diet (DD) for 16 weeks. A) *Bmal1* expression at circadian time 0 in WAT, genotype, $F(2, 39)=8.433, p=0.0009$; diet $F(1, 39)=9.94, p=0.0031$; interaction $F(2, 39)=4.676, p=0.0151$. $n=4-11$ per group. B) Western blot analysis of BMAL1 in WAT of control mice on CD or DD. C) *Bmal1* expression at circadian time 0 in liver, genotype $F(2, 37)=8.64, p=0.0008$; diet $F(1, 37)=2.305, p=0.1374$; interaction $F(2, 37)=2.611, p=0.0869$. $n=5-9$ per group. Effects of genotype are indicated by horizontal lines terminating in vertical lines. Effects of diet are indicated by brackets terminating in horizontal lines. * $p<0.05$, ** $p<0.01$, *** $p<0.001$.

As in the cohort of female mice, male LABKO mice were slightly heavier prior to the initiation of diet at 8-weeks old (Fig. 3.5A and B). At 24 weeks, the overall analysis of variance indicated a

main effect of diet and a main effect of genotype on body weight, weight gain and adiposity (Fig. 3.5C-E). Body weight at 24 weeks was significantly increased in LABKO mice fed either diet (Fig. 3.5A and C) The increase in weight gain over a 16-week period appeared to be greater in control diet-fed LABKO mice but the difference did not reach statistical significance while diabetogenic diet-fed LABKO mice had significantly increased weight gain (Fig. 3.5D). A two-way ANCOVA was performed for 24-week body weight using 8-week body weight as the covariate and genotype and diet as the two factors in order to determine whether the increased body weight at 24 weeks in LABKO mice was predicted by elevated body weight at 8 weeks. The 8-week body weight covariate was significantly associated with 24-week body weight ($p=0.002$) as was genotype ($p=0.003$) and diet ($p<0.001$), but there was no genotype by diet interaction ($p=0.149$). Adiposity followed a similar pattern as 24-week body weight for both diet groups (Fig. 3.5E) Within diet, as there were no differences in lean mass between genotypes (data not shown), the increase in body weight and weight gain was due to increased adiposity.

Figure 3.5

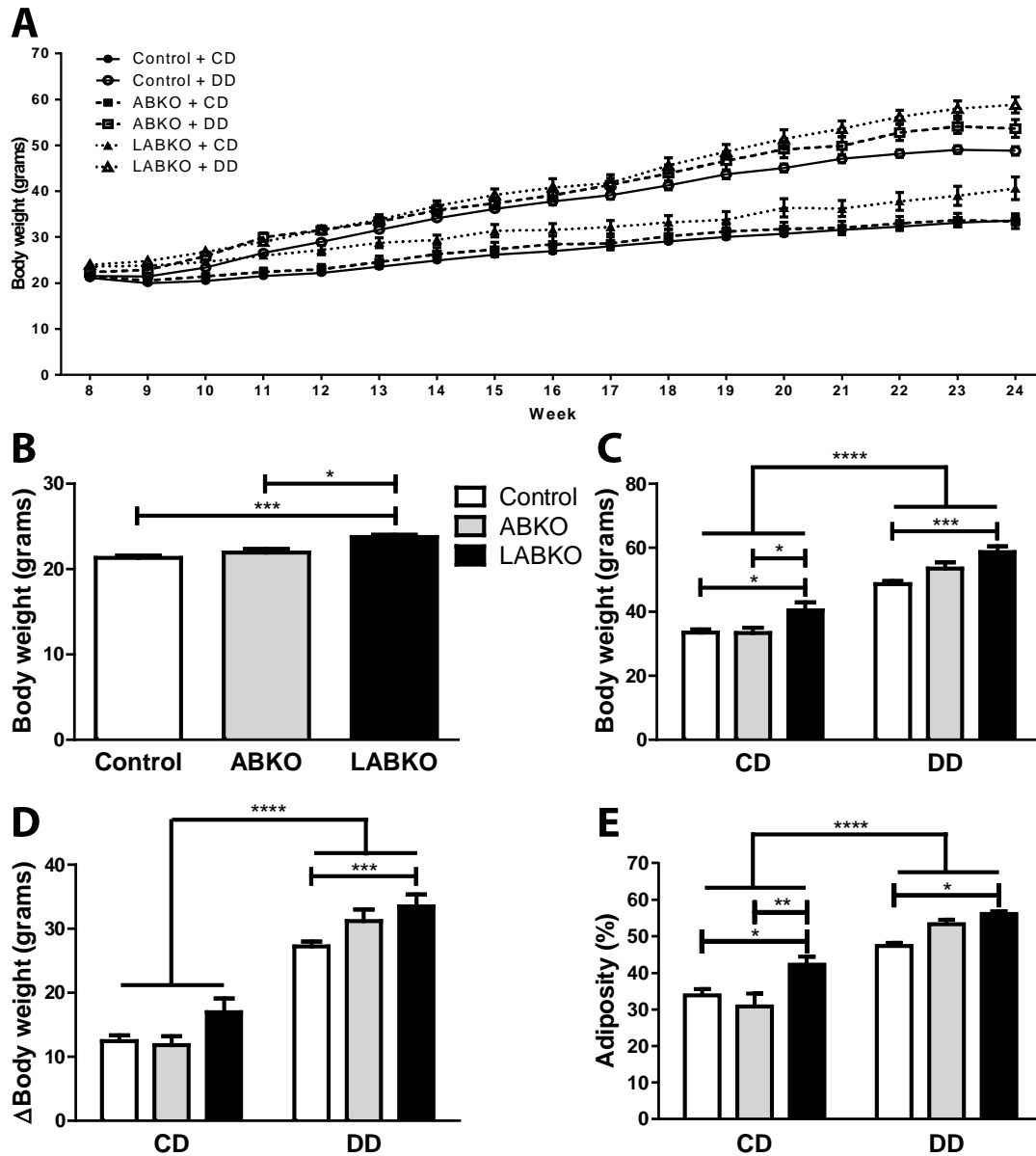


Figure 3.5. Body weight and composition of male mice fed a control diet (CD) or a diabetogenic diet (DD) for 16 weeks. n=5-18 per group. A) Body weight from week 8 to 24. B) Body weight prior to initiation of diets at week 8, $F(2, 59)=8.981$, $p=0.0004$. C) Body weight at the end of study at week 24, genotype $F(2, 56)=15.12$, $p<0.0001$; diet $F(1, 56)=204.1$, $p<0.0001$; interaction $F(2, 56)=2.003$, $p=0.1444$. D) Change in body weight from week 8 to week 24, genotype $F(2, 56)=9.023$, $p=0.0004$; diet $F(1, 56)=228.7$, $p<0.0001$; interaction $F(2, 56)=2.032$, $p=0.1407$. E) Percent adiposity at week 24, genotype $F(2, 56)=8.202$, $p=0.0008$; diet $F(1, 56)=95.17$, $p<0.0001$; interaction $F(2, 56)=3.521$, $p=0.0363$. Effects of genotype are indicated by horizontal lines terminating in vertical lines. Effects of diet are indicated by brackets terminating in horizontal lines. * $p<0.05$, ** $p<0.01$, *** $p<0.001$, **** $p<0.0001$.

The diabetogenic diet resulted in overall increased adipocyte size and the appearance of crown-like structures (Fig. 3.6). Among groups fed the control diet, adipocyte area was similar between genotypes with a tendency for increased size in LABKO mice (Fig. 3.6A and B). This resulted in a greater number of larger adipocytes reflected by the rightward shift in the histogram (Fig. 3.6C). However, this genetic difference was lost in mice fed the diabetogenic diet despite both ABKO and LABKO mice having increased fat mass compared to controls (Fig. 3.5D, Fig. 3.6).

Adipose inflammation appeared to increase the presence of crown-like structures in the diabetogenic diet-fed mice, but was not affected by genotype (Fig. 3.6A). Similarly, the diabetogenic diet increased the expression of both *F4/80* (genotype F(2, 39)=0.4142, p=0.6637; diet F(1, 39)=63.71, p<0.0001; interaction F(2, 39)=0.4215, p=0.6590) and *Mcp-1* (genotype F(2, 39)=3.123, p=0.0552; diet F(1, 39)=19.12, p<0.0001; interaction F(2, 39)=1.555, p=0.2241) (data not shown). *Mcp-1* expression appeared to be higher in both ABKO and LABKO mice, but was only significant in the LABKO group (Control: 3.266±0.291, LABKO: 8.767±3.976) (data not shown).

To determine whether the increase in adiposity could be explained by increased adipogenesis or decreased lipolysis, markers of these processes were measured in control diet-fed mice. There was a significant increase in *C/ebpβ* expression in LABKO mice, but other measured genes of adipogenesis (*Pparγ*, *C/ebpa*, *Zfp423*) and lipolysis (*Hsl*, *Pnpla2*, *Abhd5*) were unchanged by genotype (Fig. 3.6D).

Figure 3.6

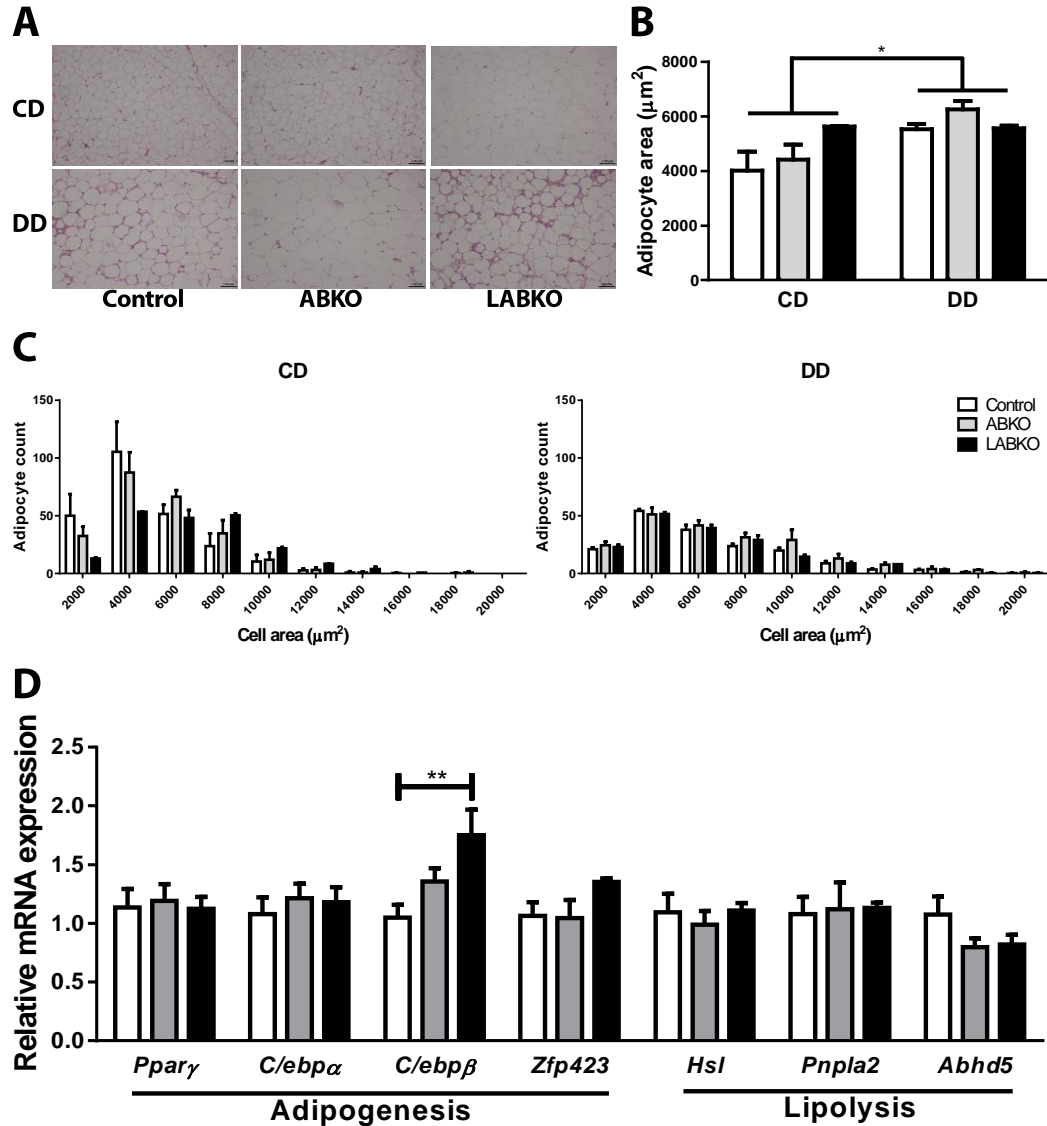


Figure 3.6. Adipose histology, quantification and measure of adipogenesis and lipolysis in WAT at circadian time 0 in 24-week-old male mice fed a control diet (CD) or a diabetogenic diet (DD) for 16 weeks. A) Representative images of H&E stain from epididymal adipose. B) Adipocyte area, genotype $F(2, 14)=1.392$, $p=0.281$; diet $F(1, 14)=6.985$, $p=0.0193$; interaction $F(2, 14)=1.599$, $p=0.2369$. $n=2-4$ per group. C) Histogram of adipocyte count distribution of specified adipocyte area. D) Gene expression of adipogenic and lipolytic genes. For *C/ebp β* , $F(2, 20)=5.893$, $p=0.0097$. $n=5-9$ per group. Effects of genotype are indicated by horizontal lines terminating in vertical lines. Effects of diet are indicated by brackets terminating in horizontal lines. * $p<0.05$, ** $p<0.01$.

Loss of glycemic control does not correspond with increased body weight and adiposity.

To determine whether peripheral clocks play a role in the loss of glycemic control associated with obesity, fasting glucose, glucose tolerance and insulin sensitivity were measured in male mice challenged with a diabetogenic diet. There was a main effect of diet on fasting glucose but no effect of genotype in either diet (Fig. 3.7A and B). Similarly, there was a main effect of diet on blood glucose concentrations following an intraperitoneal injection of glucose but no differences between genotypes (Fig. 3.7C and D). Both ABKO and LABKO mice fed a diabetogenic diet had greater reductions in blood glucose following an intraperitoneal injection of insulin than control mice (Fig. 3.7E and F). To determine whether adipose tissue of ABKO and LABKO mice respond better to insulin, total and p-AKT were measured. Though p-AKT was increased in WAT of ABKO and LABKO mice, total AKT expression was increased as well. Therefore, there were no significant differences in p-AKT (Fig. 3.7G).

Figure 3.7

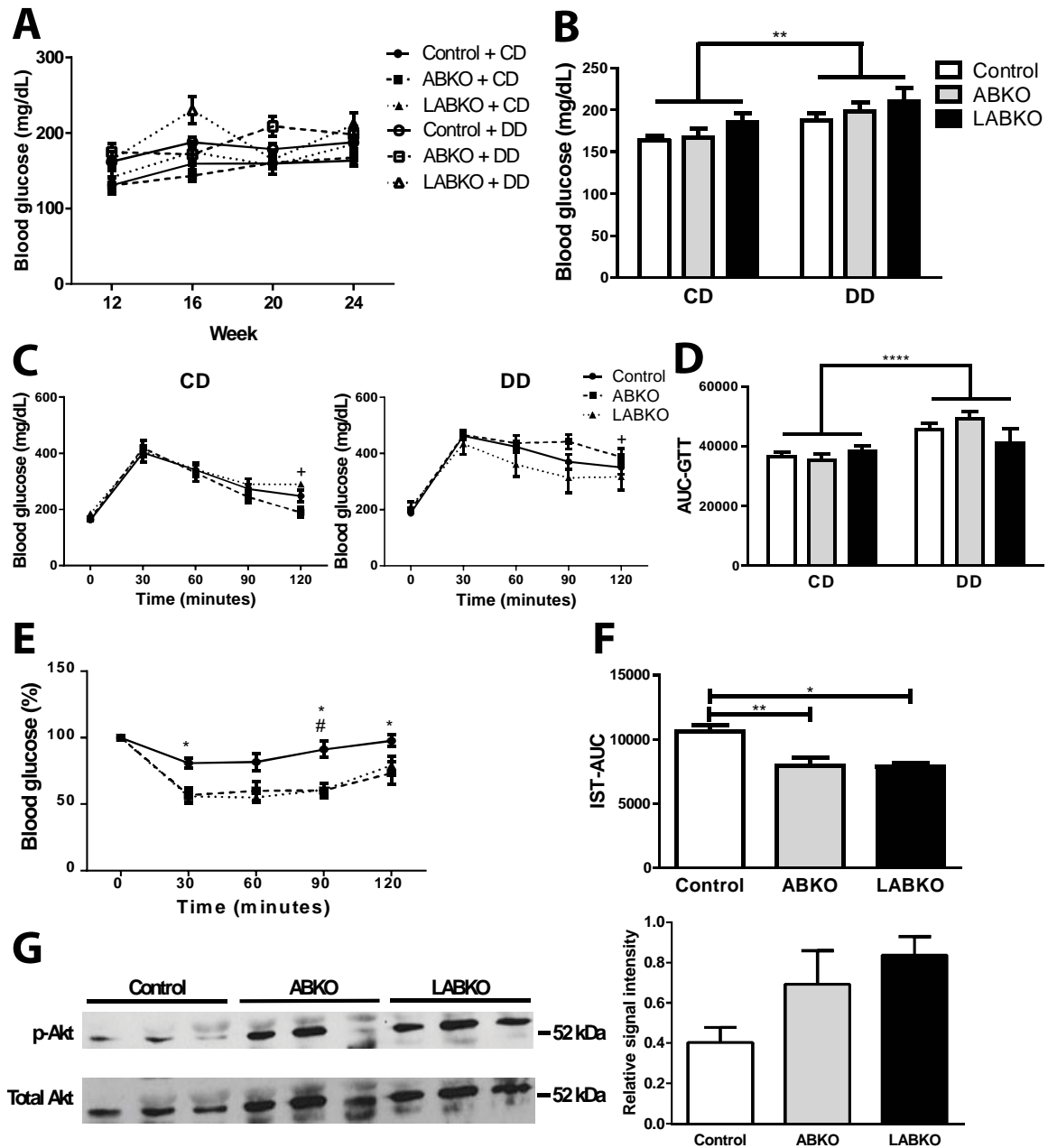


Figure 3.7. Glycemic control in 24-week-old male mice fed a control diet (CD) or a diabetogenic diet (DD) for 16 weeks. $n=5-18$ per group. A) Fasting blood glucose concentrations from week 12 to 24. B) Fasting blood glucose concentrations following a 4-hour fast, genotype $F(2, 56)=1.956$, $p=0.1509$; diet $F(1, 56)=8.497$, $p=0.0051$; interaction $F(2, 56)=0.05681$, $p=0.9448$. C) Glucose tolerance following a 4-hour fast in mice fed CD, genotype $F(2, 28)=0.8944$, $p=0.4202$; time $F(4, 112)=75.99$, $p<0.0001$; interaction $F(8, 112)=1.436$, $p=0.1894$, and in mice fed DD, genotype $F(2, 28)=1.29$, $p=0.291$; time $F(4, 112)=80.27$, $p<0.0001$; interaction $F(8, 112)=1.909$, $p=0.0654$. D) Area under the curve (AUC) calculated from glucose tolerance test, genotype $F(2, 56)=0.3693$, $p=0.6929$; diet $F(1, 56)=18.25$, $p<0.0001$; interaction $F(2, 56)=1.989$, $p=0.1464$. E) Insulin sensitivity following a 1-hour fast in mice fed

DD, genotype $F(2, 28)=7.759$, $p=0.0021$; time $F(4, 112)=33.28$, $p<0.0001$; interaction $F(8, 112)=3.42$, $p=0.0015$. F) AUC calculated from insulin sensitivity test, $F(2, 28)=7.768$, $p=0.0021$. G) Western blot and densitometry analyses of total and p-AKT in WAT of mice on diabetogenic diet injected with insulin, $F(2, 6)=3.495$, $p=0.0985$. Effects of genotype are indicated by horizontal lines terminating in vertical lines. Effects of diet are indicated by brackets terminating in horizontal lines. *=Comparison between control and ABKO, #=Comparison between control and LABKO, +=Comparison between ABKO and LABKO for Figures 7B and D. * $^{\#,+}$ $p<0.05$, ** $p<0.01$, **** $p<0.0001$.

Disruptions in liver and adipose peripheral clocks increase hepatic cholesterol in LABKO mice.

There was a main effect of diet on serum total cholesterol but no significant differences between genotypes in either diet groups. Serum triglycerides and non-esterified fatty acids (NEFAs) were not affected by diet or genotype (data not shown). However, it should be noted that mice were not fasted for these measures. As expected, there was a main effect of diet on liver weights. However, there were no differences in liver weights or percent liver weight between genotypes in either diet group (data not shown). Despite any lack of differences, ABKO mice appeared to have decreased lipid deposition in the liver compared to control and LABKO mice within the diabetogenic diet groups (Fig. 3.8A). There was a main effect of diet on hepatic total cholesterol and triglycerides (Fig. 3.8B and C). Within mice given a diabetogenic diet, LABKO mice had the highest level of hepatic total cholesterol (Fig. 3.8B). A similar pattern was observed for triglycerides, but these differences did not reach statistical significance (Fig. 3.8C). In an effort to explain the increase in hepatic cholesterol in LABKO mice fed a diabetogenic diet, genes involved in cholesterol synthesis and regulation were measured in liver. *Hmgcr* and *Hmgcs*, involved in cholesterol synthesis, exhibited similar patterns of expression with LABKO mice on control diet and both ABKO and LABKO mice on diabetogenic diet having increased expression (Fig. 3.8D). Sterol transporters, *Abcg5* and *Abcg8*, were both suppressed by diet but no significant differences between genotypes were observed (Fig. 3.8D). Although genes involved in cholesterol uptake, *Ldlr* and *Srb1*, had the highest expression in LABKO mice on a control diet there were no differences in *Ldlr* and *Srb1* expression between genotypes in mice on a diabetogenic diet (data not shown). Bile acid synthesis genes, *Cyp7a1* and *Cyp8b1*, were unchanged by diet or genotype (data not shown).

Figure 3.8

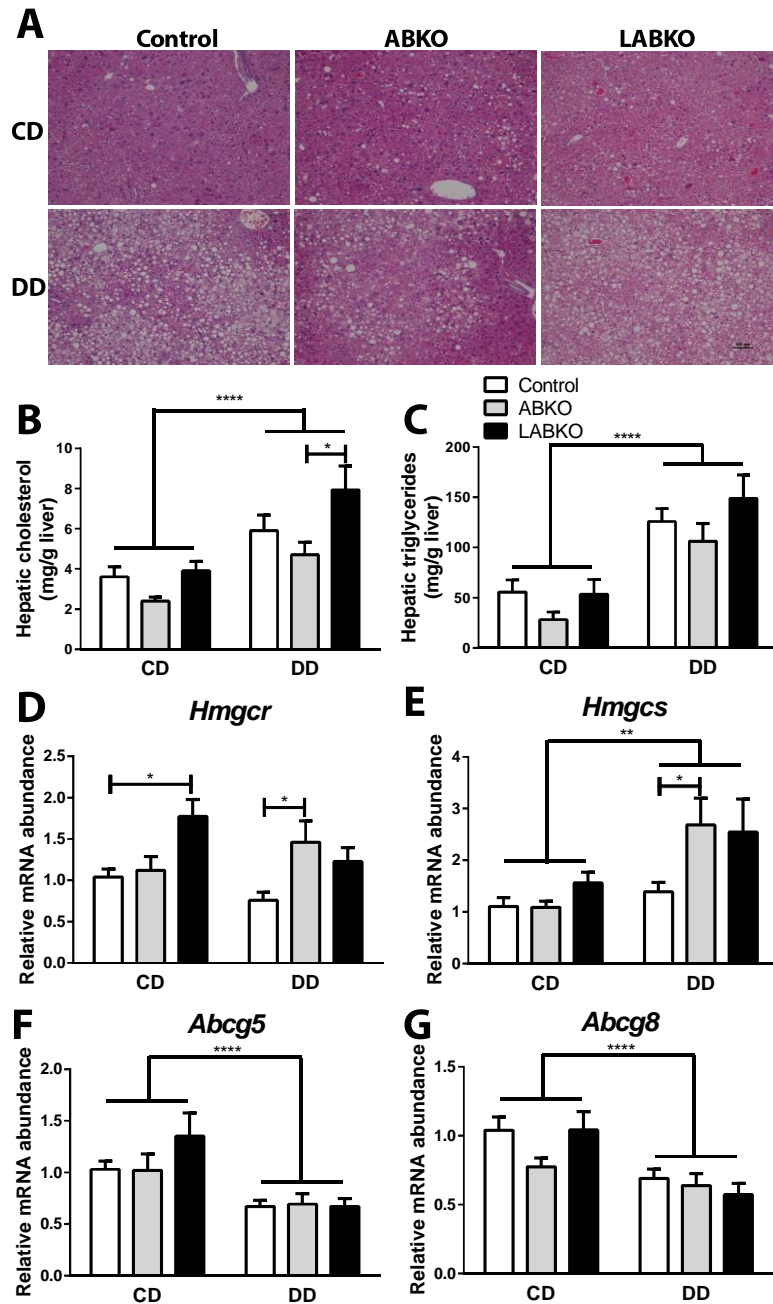


Figure 4.8. Liver histology, hepatic lipids and gene expression from liver isolated at circadian time 0 in 24-week-old male mice fed a control diet (CD) or a diabetogenic diet (DD) for 16 weeks. A) Representative images of H&E stain. B) Total cholesterol, genotype F(2, 26)=5.095, p=0.0136; diet F(1, 26)=25.42, p<0.0001; interaction F(2, 26)=0.9054, p=0.4167. C) Triglycerides genotype F(2, 26)=2.519, p=0.1000; diet F(1, 26)=44.3, p<0.0001; interaction F(2, 26)=0.3547, p=0.7047. n=4-7 per group. D) Gene expression of *Hmgcr*, genotype F(2, 39)=6.118, p=0.0049; diet F(1, 39)=1.268, p=0.267; interaction F(2, 39)=3.374, p=0.0445. E) Gene expression of *Hmgcs*, genotype F(2, 39)=3.582, p=0.0373; diet F(1, 39)=12.54, p=0.001; interaction F(2, 39)=2.471, p=0.0976. F) Gene expression of *Abcg5*, genotype F(2, 39)=0.8746,

p=0.4251; diet F(1, 39)=19.89, p<0.0001; interaction F(2, 39)=1.024, p=0.3685. G) Gene expression of *Abcg8*, genotype F(2, 39)=2.004, p=0.1484; diet F(1, 39)=18.92, p<0.0001; interaction F(2, 39)=1.747, p=0.1876. n=5-9 per group. Effects of genotype are indicated by horizontal lines terminating in vertical lines. Effects of diet are indicated by brackets terminating in horizontal lines. *p<0.05, **p<0.01, ****p<0.0001.

Discussion

Our study confirms and extends previous findings indicating that peripheral oscillators, particularly in adipose, modulate feeding and locomotor activity. The loss of *Bmal1* in adipose tissue and the liver exacerbates obesity but no other metabolic co-morbidities. The central clock synchronizes the oscillations of peripheral clocks. However, an essential feature of peripheral clocks is the ability to be uncoupled from the central clock via entrainment by the feeding/fasting cycle [92, 201, 202]. Time-restricting food consumption to the rest phase results in obesity while food consumption solely during the active phase is protective against obesity [126-130]. In our study, we sought to determine the impact of disrupted adipose tissue and liver clocks on centrally-regulated functions related to metabolism such as feeding behavior and locomotor activity. It has previously been shown that deletion of *Bmal1* from adipose alters plasma polyunsaturated fatty acid concentrations, leading to alterations in the hypothalamic regulation of feeding behavior [104]. We corroborated these findings and observed that ABKO mice exhibit impaired feeding patterns and have increased food intake during the light phase. In both studies, the *aP2-Cre* transgene was used for adipose deletion. AP2 is commonly used to drive the expression of *Cre recombinase* for adipose-specific deletion as it is abundantly expressed in adipose. However, AP2 is also expressed in other tissues such as macrophages, embryonic tissues and brain [203, 204]. In our study, we observed residual *Bmal1* mRNA and protein expression in both adipose and liver. This is likely due to incomplete penetrance of *Cre recombinase* as well as the presence of other cell types expressing *Bmal1*. Deletion of *Bmal1* from the liver and adipose tissue in LABKO mice also resulted in increases in food intake during the light phase as well as during the dark phase. ABKO mice tended to be more active, particularly during the light phase in our studies. However, a previous study did not observe any differences in locomotor activity with *Bmal1* deletion from adipose tissue [104]. This discrepancy between studies is likely due to differences in environmental conditions or the diet used. Nonetheless, alterations in activity during both the light and dark phase in ABKO mice indicate that adipose *Bmal1* plays a role in modulating physical activity and movement. Interestingly, increased activity was reversed in LABKO mice. Previous studies have demonstrated that liver-specific deletion of *Bmal1* is insufficient to alter locomotor activity and feeding behavior [103]. Together, these findings

demonstrate that disrupting the liver clock in the setting of adipose clock disruption impacts physical activity. Thus, coordination of functional adipose and liver clocks is necessary to properly mediate centrally-regulated functions. Furthermore, the differences in food intake and activity between genotypes suggest tissue-specific roles of *Bmal1*.

ABKO mice had increased overall food intake similar to that of LABKO mice but body weight and adiposity were not significantly increased like that of LABKO mice. This is likely due to the increased activity observed in ABKO but not in LABKO mice. Although we cannot rule out a direct role of peripheral *Bmal1* in regulating energy metabolism, our findings suggest that changes in feeding behavior and activity in ABKO and LABKO mice are the primary regulators of body weight and composition.

Blood glucose concentrations exhibit diurnal variations and several models of dysfunctional circadian rhythm exhibit impaired glycemic control [82, 105, 115]. Over a 24-hour period, ABKO mice with food access during the dark phase tended to have slightly elevated blood glucose concentrations compared to control and LABKO mice while the diurnal pattern remained similar between groups. Therefore, in the setting of restricted food availability to the dark phase, disrupting adipose and liver *Bmal1* was insufficient to impair the diurnal pattern of blood glucose.

Due to the high association between obesity and other features of MetS, we expected that in the presence of a diabetogenic diet, the disruption of *Bmal1* in two metabolic tissues would exacerbate insulin resistance and fatty liver disease. Although LABKO mice were more obese than control mice, there was no further loss of glycemic control or evidence of increased hepatic inflammation and fibrosis in either ABKO or LABKO mice. Overall, the disruption of peripheral clocks from the liver and adipose tissue was insufficient to exacerbate metabolic disease beyond the development of obesity. One possibility for this observation may be explained by the effects a diet high in fat can have on circadian rhythms. A high-fat diet can lengthen the circadian period in mice prior to any body weight effect and attenuate diurnal feeding behavior and clock gene expression [205]. Consistent with these findings, we found that 16 weeks of a diabetogenic diet suppresses peak *Bmal1* expression in white adipose tissue though protein expression was slightly increased. As this reflects expression at a single time point, the discrepancy may reflect a phase shift in BMAL1 expression or post-transcriptional regulation. Peak *Bmal1* expression was not affected in the liver however. Others have demonstrated slight to significant attenuations in liver *Bmal1* oscillations depending on the duration of high-fat feeding [205, 206]. It is likely that although disrupting multiple peripheral clocks indeed alters central behavior, these effects seem

to be overcome by the effects of a high-fat diet thereby muting any exacerbations in metabolic disease.

Similar to the role of circadian rhythms in the development of obesity and insulin resistance, evidence suggest lipid homeostasis is dependent on circadian function. *Clock*-mutant mice have increased plasma triglycerides, cholesterol, and atherosclerotic lesions [207]. Additionally, a number of rhythmic transcripts involved in cholesterol synthesis and metabolism have been identified in the open access bioinformatics database, CircaDB. Hepatic cholesterol and triglycerides were divergently altered in ABKO and LABKO mice fed a diabetogenic diet, suggesting the involvement of liver *Bmal1* in the regulation of cholesterol. Cholesterol synthesis, measured by transcript levels of *Hmgcr* and *Hmgcs*, tended to be increased in both ABKO and LABKO mice fed a diabetogenic diet. However, no additional changes in genes involved in cholesterol transport and bile acid synthesis that would explain the varying abundance of hepatic lipids were observed. It should be noted that transcript levels of *Hmgcs* and *Cyp8b1* reach peak amplitude approximately at the beginning of the light cycle, *Hmgcr*, *Ldlr*, *Cyp7a1*, *Abcg5* and *Abcg8* at the beginning of the dark cycle and *Srb1* at mid-light cycle [208]. Consequently, measuring gene expression throughout a 24-hour period would enhance the capability of identifying essential differences.

A limitation of our study is the use of both male and female mice. Estradiol during development plays a role in diurnal rhythms and estrogen receptor beta is regulated by the clock machinery [209, 210]. Additionally, sexually dimorphic differences in clock gene expression in the SCN and locomotor activity in response to light-induced phase shifts by leptin is observed in mice [211]. To minimize the limiting effects of sex, only females were used for indirect calorimetry experiments while only males were used for the diet intervention portion of the study.

Our study and others have demonstrated the selectivity of the clock's influence on metabolism and the potential that exists in targeting circadian factors as a potential therapeutic for metabolic disease. Here we add knowledge to how disruptions in multiple peripheral clocks may differentially regulate behavior and influence the development of obesity.

CHAPTER 4: ROLE OF BILE ACID-FGF15/19 AXIS IN THE REGULATION OF ABCG5 AND ABCG8

Introduction

Elevated cholesterol increases the risk of CVD by contributing to the development of atherosclerosis and is highly associated with NAFLD [212, 213]. The relationship between cholesterol and atherosclerotic CVD has been widely studied, leading to the development of lipid-lowering agents that target a number of cholesterol-modulating pathways including cholesterol synthesis (HMG-CoA reductase inhibitors), cholesterol absorption (ezetimibe), and LDL receptor regulation (PCSK9 inhibitors). More recently, emerging evidence implicates hepatic cholesterol in the pathogenesis of NAFLD and NASH, the more severe form of disease. Increased dietary cholesterol and fat act synergistically in wildtype mice to increase hepatic fat, inflammation, and fibrosis indicative of NASH [214]. In LDL receptor-deficient mice fed a high fat, high-carbohydrate diet, the addition of cholesterol worsens dyslipidemia and hepatic steatosis as well as induces NASH-associated inflammation and fibrosis [74]. In humans, increased hepatic free cholesterol is detected in NAFLD [71]. We have previously observed that mice deficient of the cholesterol transporter, ABCG5 and ABCG8 (G5G8), have decreased biliary cholesterol secretion, increased hepatic cholesterol, and worsened obesity, insulin resistance, and NAFLD when fed a high-fat diet [149]. Conversely, overexpression of adenoviral G5G8 in obese *db/db* mice increases biliary cholesterol secretion and reduces triglycerides, insulin resistance, and ER stress [147]. These data suggest that G5G8 may be a promising target for accelerating cholesterol elimination and improving features of NAFLD.

The majority of cholesterol elimination occurs through the conversion of cholesterol to bile acids (bile acid synthesis) and by direct clearance through the biliary pathway [157]. Of the cholesterol entering the bile, up to 90% is transported via the ABCG5 and ABCG8 (G5G8) heterodimer [143, 215, 216]. Ursodiol (Urso) is a pharmacologic bile acid that has been found to increase G5G8 protein abundance, biliary cholesterol secretion, and fecal neutral sterol elimination in mice [150]. Although the molecular mechanism(s) by which Urso regulates G5G8 is not clear, possibilities include the alleviation of ER stress and bile acid signaling.

Fecal neutral sterol elimination is increased in mice receiving Urso and ezetimibe. However, the combination does not increase cholesterol synthesis, suggesting there is no increase in total sterol loss [150]. Rather, increases in ileal fibroblast growth factor 15 (*Fgf15*) and suppression of bile acid synthesis indicate a diversion of the cholesterol pool away from the bile acid synthesis

pathway to the biliary secretion pathway [150]. FGF15 in mice and FGF19 in humans (FGF15/19) are expressed in the enterocytes of the ileum, stimulated by farnesoid X receptor (FXR) in response to bile acids, and transported to the liver where it binds to its receptor, fibroblast growth factor receptor 4 (FGFR4), to suppress bile acid synthesis among other effects [163, 217, 218]. FXR agonists in clinical trials have shown promise for the treatment of NAFLD and NASH, presumably through effects mediated in part by FGF19 [170, 171]. FGF19 administration improves parameters of obesity and insulin sensitivity in obese mice and is involved in regulating hepatic glycogen and fatty acid synthesis [173-175, 219]. However, it is unknown whether FGF15/19 plays a role in regulating G5G8 and biliary cholesterol secretion. Our study suggests that FGF15/19 increases G5G8 protein and promotes localization to the canalicular surface of hepatocytes. Furthermore, Urso causes a similar localization of G5G8 that appears to be dependent on FGF15/19 signaling via FGFR4 receptor.

Methods

Animal Husbandry and Procedures

C57BL/6J mice were purchased from Jackson Laboratory (Bar Harbor, ME). Mice heterozygous for the *Abcg5* and *Abcg8* (G5G8) mutant alleles were bred using trio matings to generate homozygous G5G8 knockout (KO) and wildtype (WT) littermates as previously described [149]. Mice were housed in individually ventilated cages in a temperature-controlled room maintained on a 14:10 light:dark cycle and had free access to water and standard rodent diet (Teklad 2918).

Male mice 10-12 weeks of age were injected intraperitoneally with recombinant human FGF19 protein (ProSpec CYT-700) at 1 µg/g body weight (BW) or PBS at 0 hours and 4 hours after lights-on. Mice were anesthetized under urethane 1g/kg BW at 8 hours after lights-on and basal bile was collected for 30 minutes by ligating the bile duct and cannulating the gallbladder. Bile flow was calculated gravimetrically assuming a density of 1 g/mL. Following exsanguination, tissues were dissected, frozen in liquid nitrogen, and stored at -80°C until analysis. Blood was stored at 4°C for four hours. After centrifugation at high speed for 10 minutes, serum was collected and stored at -80°C until analyzed. A portion of liver was embedded in OCT compound for histology.

Male and female mice 7 weeks of age were injected subcutaneously with FGFR4 antisense oligonucleotide (ASO) (Ionis Pharmaceuticals) 25 mg/kg BW twice weekly for a total of 5 weeks. At the beginning of week 5, mice were fed either a control diet (Research Diets, Inc. AIN-

76A) or a diet supplemented with 0.3% (w/w) ursodiol (Epic Pharma, LLC, NDC: 42806-503-01) for a total of 7 days. Basal bile and tissues were collected as described above.

Real Time-PCR

RNA was isolated from liver samples using RNA STAT-60 (Tel-Test, Inc.) and the RNeasy Mini Kit (Qiagen). The iScript cDNA Synthesis Kit (Bio-Rad) was used to synthesize 20 μ L of cDNA from RNA 100 ng/ μ L. Relative changes in gene expression were measured by quantitative real time-PCR using SYBR Green and the 7900HT Fast Real Time-PCR System (Applied Biosystems). *Gapdh* was used as the normalization control for measured transcripts.

Immunoblot Analysis

Membrane protein preparations from frozen tissues, SDS-PAGE, and immunoblotting were conducted as previously reported [147, 149]. ABCG5 was detected in 40 μ g of protein using a 1:20,000 dilution of chicken anti-ABCG5 polyclonal antibody [147, 149]. ABCG8 was detected using a 1:100 dilution of monoclonal antibody [153]. Beta-actin was detected using a 1:50,000 dilution of monoclonal antibody (Sigma-Aldrich A5441).

Lipid Analysis

Hepatic lipids were extracted from frozen liver (~100 mg) using the Folch method, dried in CHCl_3 + 2% Triton and suspended in 1% Triton in water as previously reported [147]. Enzymatic, colorimetric assays (Wako Diagnostics) were used to measure free and total cholesterol from serum, hepatic lipid extracts, and bile as well as phospholipids from bile. Bile acids in bile were measured using an enzymatic assay that measures 3 α -hydroxy bile acids as previously reported [220].

Immunofluorescence Microscopy

Cryosections (8 μ m) were cut, post-fixed in 4% PFA at room temperature for 30 min, then rehydrated in three changes of PBS. Sections were treated with 0.1% Triton X-100 for 15 min and then incubated in Buffer A (PBS + 1% bovine serum albumin (BSA)) for 1 h at 22°C. Primary antibodies (ABCG5, 1:8000; ZO-1, 1:125) were diluted in Buffer A. Spotted sections were circumscribed with a wax pencil, overlaid with 100 μ L of diluted antibody, and incubated overnight (4°C). Sections were then washed with three changes of PBS. Conjugated secondary antibodies directed against avian IgG (G5, Alexafluor 488) and rabbit IgG (ZO-1, Alexafluor 568) were diluted in Buffer A (1 μ g/mL) and incubated for 60 min (22°C). Slides were washed

with 3 changes of PBS. Sections were spotted with aqueous mounting media containing DAPI and overlaid with glass coverslips.

Sections were imaged with a Zeiss Axiovert 200IM microscope equipped with ApoTome and a 63X oil immersion objective. Five optical sections (0.25 μm /section) in each channel (RGB) were captured in the Z plane and converted to a two dimensional image by Extended Focus calculation in the AxioVision imaging software suite. Channels were pseudocolored (ABCG5, green; ZO-1, red; DAPI, blue) and displayed individually and as merged RGB images.

Statistical Analysis

Statistical analyses were conducted using GraphPad Prism (version 7.00). Data are presented as mean \pm SEM with statistical significance defined as $p < 0.05$. Unpaired t-tests were performed for comparisons between two groups. Two-way ANOVAs were performed for comparisons of groups defined by two factors and Bonferroni's multiple comparisons tests were performed for post hoc analyses.

Results

FGF19 suppresses bile acid synthesis and increases hepatic G5G8

In order to determine whether FGF19 regulates G5G8 protein expression, recombinant FGF19 (1 $\mu\text{g/g}$ BW) or carrier (PBS) was administered to mice at 0 and 4 hours after lights-on and tissues collected at 8 hours after lights-on. Mice injected with FGF19 had decreased expression of *Fxr* and increased expression of small heterodimer partner (*Shp*) in the liver (Figure 4.1A). SHP mediates suppression of *Cyp7a1* through interactions with FGF15/19 [163]. Genes involved in bile acid synthesis, *Cyp7a1*, *Cyp8b1*, and *Cyp27a1*, were decreased with FGF19 administration (Figure 4.1A). The changes we observed were as expected based on previous reports and confirmed the efficacy of the recombinant FGF19 in the present study [163, 218, 221]. *Abcb4* and *Abcb11* transport phospholipids and bile salts, respectively, into bile and were unaffected following FGF19 administration (Figure 4.1A). *Abcg8* mRNA increased by ~30% while ABCG5 protein increased by ~50% and ABCG8 by ~200% (Figures 4.1A and B).

Figure 4.1

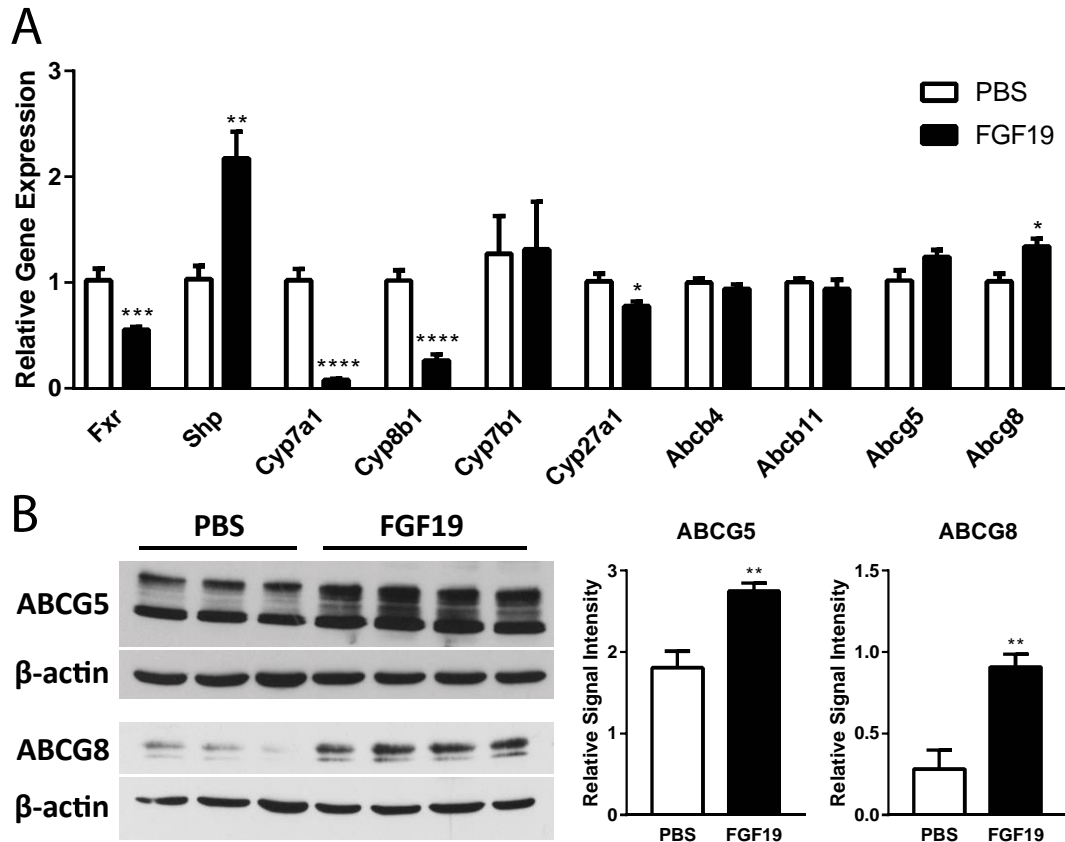


Figure 4.1. FGF19 suppresses bile acid synthesis and increases hepatic G5G8. Mice were injected with PBS or FGF19 1 $\mu\text{g/g}$ body weight at 0 and 4 hours after lights-on then euthanized at 8 hours. A: RT-PCR analysis of genes involved in bile acid synthesis and biliary cholesterol secretion in liver of mice injected with PBS (n=5) or FGF19 (n=7). B: Western blot analysis and densitometry of ABCG5 and ABCG8 protein expression in liver of mice injected with PBS (n=3) or FGF19 (n=4). Data are presented as mean \pm SEM. * $p < 0.05$, ** $p < 0.01$, *** $p < 0.001$, **** $p < 0.0001$.

FGF19 increases biliary total lipid concentrations

Consistent with our findings of increased G5G8 protein expression, biliary total cholesterol increased by nearly 50% following FGF19 administration (Figure 4.2A). There were also significant increases in biliary phospholipid and bile acid concentrations with FGF19 (Figures 4.2B and C). Therefore, mice injected with FGF19 had increased total lipid concentrations in bile (Figure 4.2D). However, FGF19 administration did not alter basal bile flow measured 4 hours following the last injection (Figure 4.2E). The cholesterol saturation index (CSI) was calculated to determine the extent of cholesterol solubility in bile. While total lipid concentrations were

increased in bile of mice given FGF19, the CSI remained equal to that of mice receiving PBS (Figure 4.2F).

Figure 4.2

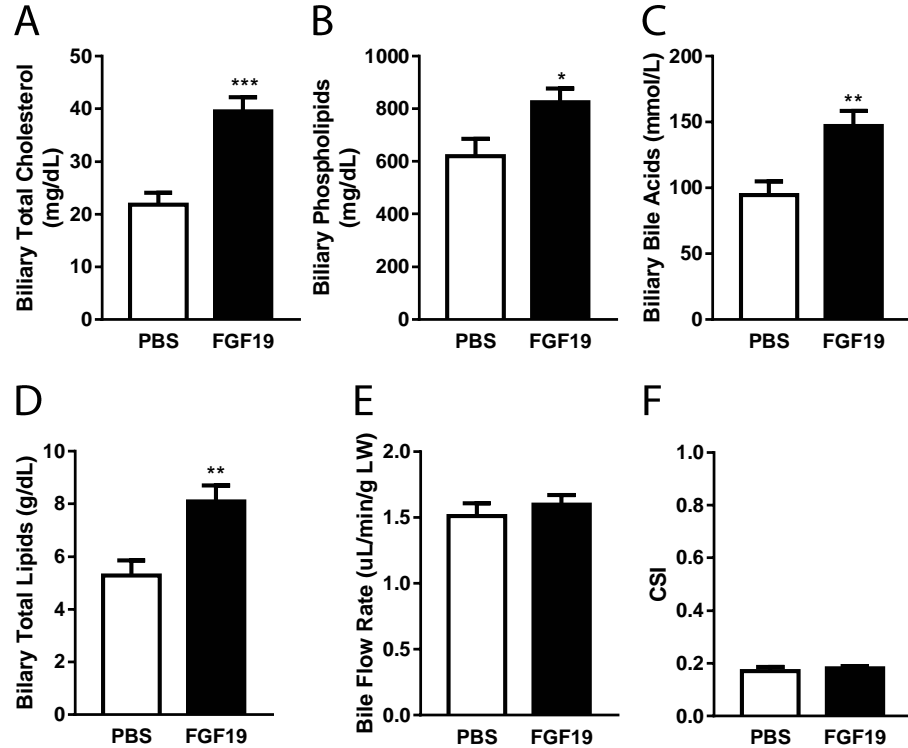


Figure 4.2. FGF19 increases biliary total lipid concentrations. Mice were injected with PBS or FGF19 1 $\mu\text{g/g}$ body weight at 0 and 4 hours after lights-on then euthanized at 8 hours. A: Total lipids measured in bile of mice injected with PBS (n=6) or FGF19 (n=6). B: Phospholipids measured in bile of mice injected with PBS (n=6) or FGF19 (n=7). C: Bile acids measured in bile of mice injected with PBS (n=6) or FGF19 (n=6). D: Total cholesterol measured in bile of mice injected with PBS (n=6) or FGF19 (n=7). E: Bile flow rate normalized to liver weight (LW) of mice injected with PBS (n=6) or FGF19 (n=7). F: The cholesterol saturation index (CSI) of bile in mice injected with PBS (n=6) or FGF19 (n=6). Data are presented as mean \pm SEM. * $p < 0.05$, ** $p < 0.01$, *** $p < 0.001$.

FGF19 localizes G5G8 to the canalicular surface of hepatocytes

Previously, we reported the development of a new antibody against ABCG5 which afforded us the opportunity to evaluate the effect of FGF19 on the localization of endogenous G5G8 [149]. Liver sections were imaged by immunofluorescence microscopy. Canalicular structures were delineated by an antibody against the tight junction protein, zonula occludens-1 (ZO-1) (Figures 4.3A, D, G, and J). ABCG5 was observed in liver of control mice but not in G5G8 KO mice, verifying the specificity of the ABCG5 antibody (Figures 4.3B and E). In control mice injected

with PBS, G5G8 appeared to be discrete puncta that were dispersed in the cytosol of hepatocytes (Figure 4.3E). Administration of FGF19 or Urso co-localized ABCG5 with ZO-1 (Figures 4.3G-L). These data suggest that FGF19 facilitates the mobilization of G5G8 to the apical surface of hepatocytes lining the bile canaliculi.

Figure 4.3

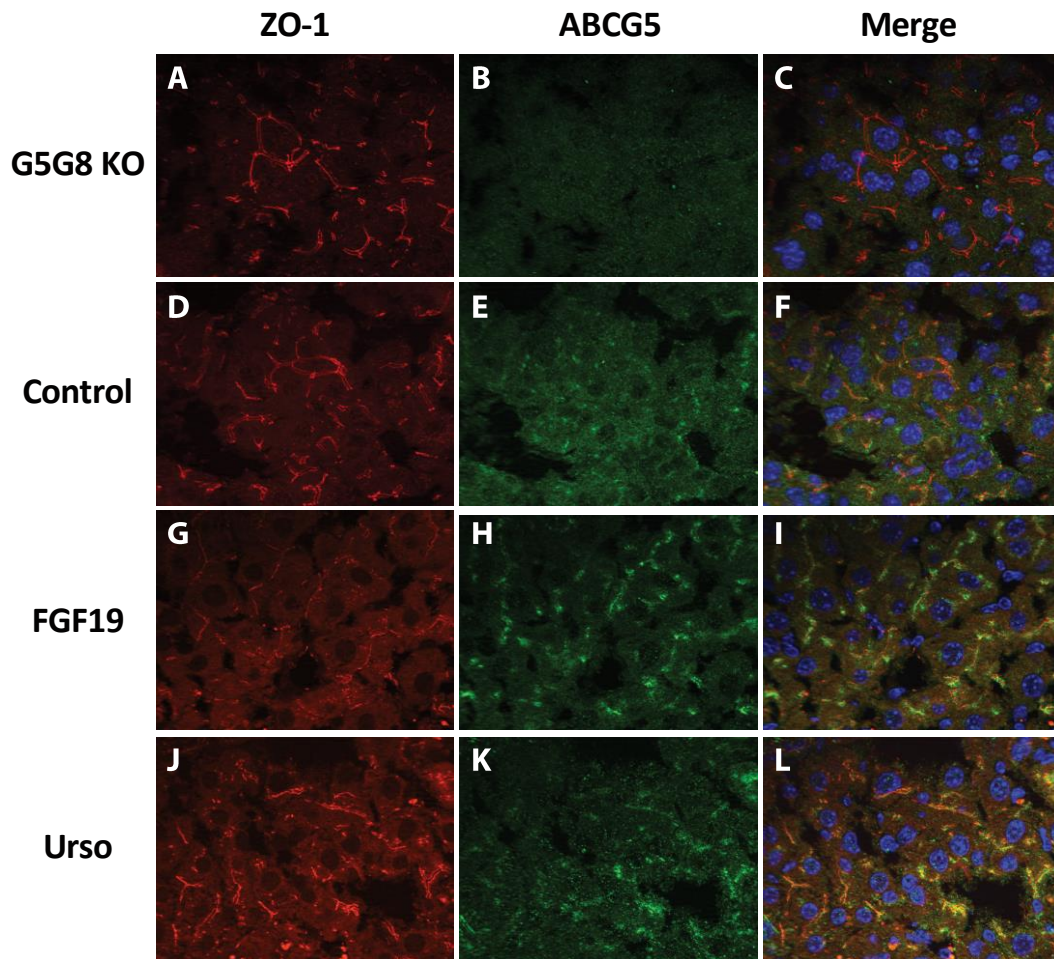


Figure 4.3. FGF19 localizes G5G8 to the canalicular surface of hepatocytes.

Immunofluorescence microscopy of mouse ZO-1 (A, D, G, J) and ABCG5 (B, E, H, K) in liver of G5G8 KO (A, B, C), control (D, E, F), FGF19-injected (G, H, I), and Urso-supplemented (J, K, L) mice.

FGF19 does not disrupt cholesterol homeostasis in the absence of G5G8

We observed that FGF15/19 increases G5G8 while simultaneously decreasing bile acid synthesis, suggesting that cholesterol is diverted from the catabolic to the secretory pathway. In the absence of G5G8, free cholesterol was expected to accumulate in hepatocytes. Therefore, it was hypothesized that in the absence of G5G8, overexpression of FGF15/19 would disrupt cholesterol

homeostasis in the liver. WT and G5G8 KO mice were injected with FGF19. G5G8 KO mice had decreased biliary total cholesterol but there were no differences in biliary phospholipid or bile acid concentrations (Figures 4.4A-C). Serum and hepatic cholesterol were measured to determine whether cholesterol would accumulate in G5G8 KO mice receiving FGF19. While there were no differences in serum total and hepatic total and free cholesterol, there was a slight but significant increase in serum free cholesterol in G5G8 KO mice (Figures 4.4D and E). Free cholesterol was measured in fast protein liquid chromatography (FPLC)-fractionated serum to determine its distribution in lipoprotein fractions. The FPLC profile did not reveal any major differences or the presence of LpX-like particles that would account for the increase in free cholesterol (not shown). *Abcg5* and *Abcg8* were confirmed to be significantly downregulated in G5G8 KO mice (Figure 4.4F). Absence of G5G8 had no effect on gene expression in mice treated with FGF19 (Figure 4.4F).

Figure 4.4

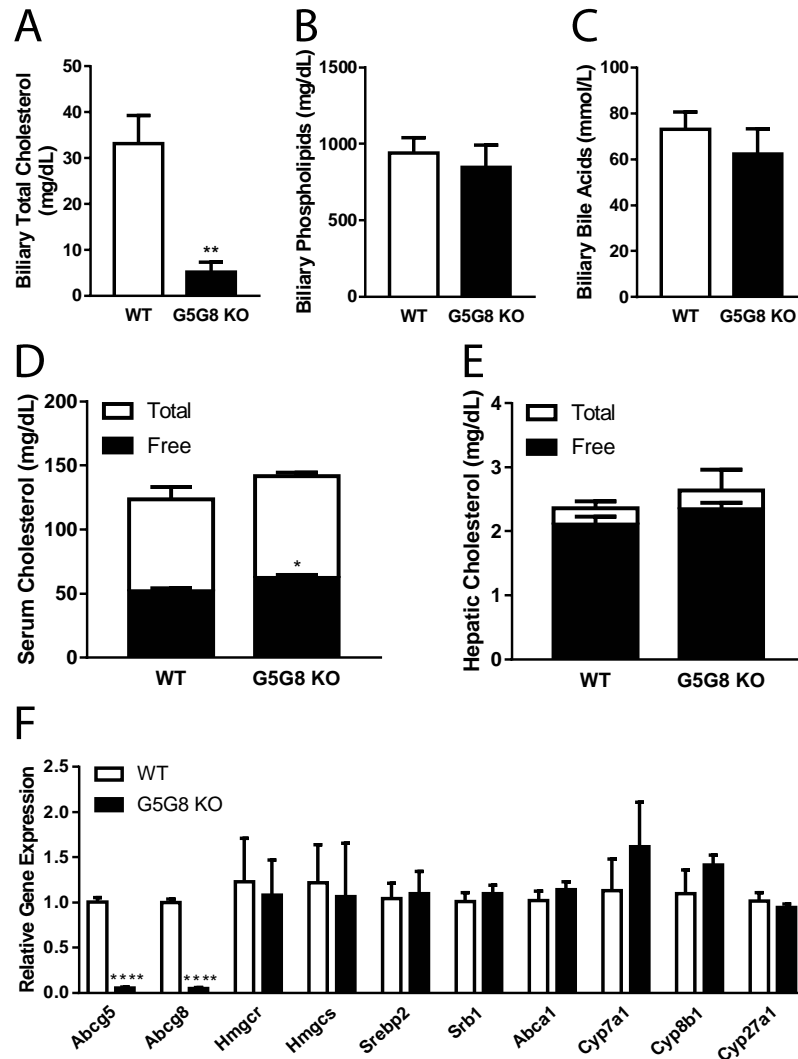


Figure 4.4. FGF19 does not disrupt cholesterol homeostasis in the absence of G5G8.

Wildtype (WT) and G5G8 knockout (KO) mice were injected with FGF19 1 μ g/g body weight at 0 and 4 hours after lights-on then euthanized at 8 hours. A: Total cholesterol measured in bile of WT and KO mice (n=4). B: Phospholipids measured in bile of WT and KO mice (n=4). C: Bile acids measured in bile of WT and KO mice (n=4). D: Total and free cholesterol measured in serum of WT and KO mice (n=4). E: Total and free cholesterol measured in liver of WT and KO mice (n=4). F: RT-PCR analysis of genes involved in cholesterol metabolism and bile acid synthesis in liver in WT and KO mice (n=4). Data are presented as mean \pm SEM. *p<0.05, **p<0.01, ****p<0.0001.

FGF15/19-FGFR4 signaling is required for Urso to localize G5G8 to the canalicular surface of hepatocytes

Previous studies revealed that Urso can increase G5G8 resulting in increased biliary cholesterol secretion. Urso has similar effects on G5G8 abundance and localization as FGF19, but it is

unknown whether these effects are dependent on FGF19 signaling through its receptor, FGFR4. To address this question, mice injected with control or FGFR4 ASO were fed a control or Urso-containing diet. In either the male or female group, there was no difference in body weight between control and Urso-fed mice receiving control or FGFR4 ASO (Figure 4.5A). Expression of *Fgfr4* was similar between males and females within the control ASO treatment group; therefore, comparisons were conducted irrespective of sex (Figure 4.5B). Mice receiving FGFR4 ASO had significantly decreased expression of *Fgfr4*, confirming the knockdown of *Fgfr4* in the liver (Figure 4.5C). Interestingly, there was also a slight reduction of *Fgfr4* with Urso within the control ASO treatment group (Figure 4.5C).

Figure 4.5

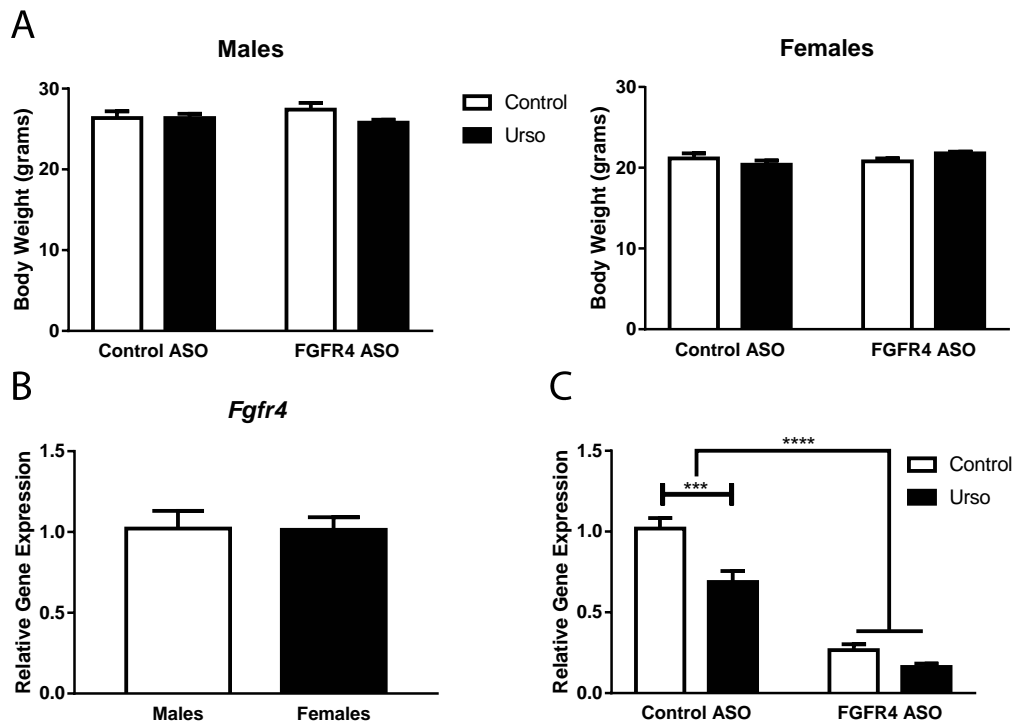


Figure 4.5. FGF19-FGFR4 signaling is required for Urso to localize G5G8 to the canalicular surface of hepatocytes. Male and female mice were injected with control or FGFR4 ASO 25 mg/kg body weight twice weekly for 5 weeks and fed standard or Urso 0.3%-supplemented diet for 7 days. A: Body weight measured post-treatment at 12 weeks of age (n=5). B: RT-PCR of *Fgfr4* in liver of mice injected with control ASO (n=5). C: RT-PCR of *Fgfr4* in liver of male and female mice injected with control of FGFR4 ASO (n=10). Data are presented as mean \pm SEM. ***p<0.001, ****p<0.0001.

Immunofluorescence microscopy revealed that in mice receiving control ASO, Urso promoted co-localization of ABCG5 and ZO-1 on the canalicular surface of hepatocytes (Figure 4.6). In the

presence of FGFR4 ASO, the effect of Urso on the localization of ABCG5 was impaired (Figure 4.6).

Figure 4.6

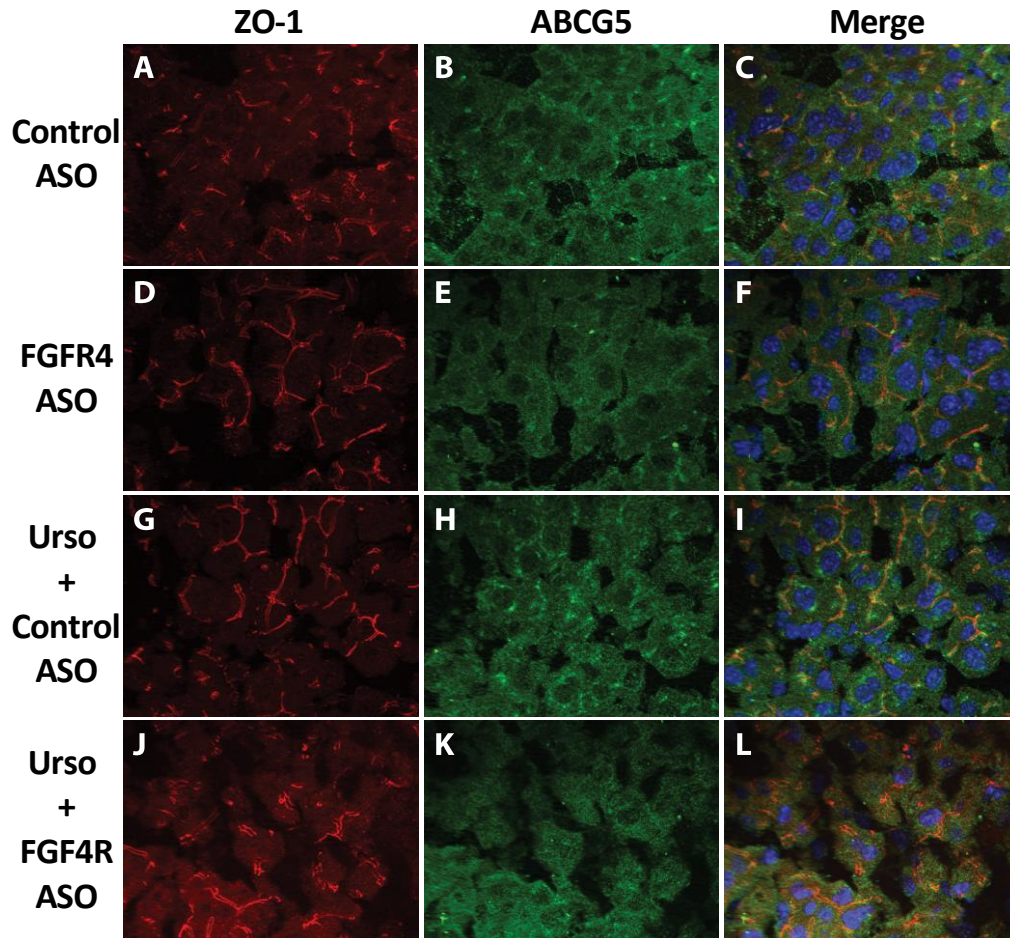


Figure 4.6. FGF15/19-FGFR4 signaling is required for Urso to localize G5G8 to the canalicular surface of hepatocytes. Immunofluorescence microscopy of mouse ZO-1 (A, D, G, J) and ABCG5 (B, E, H, K) in liver of mice receiving control ASO (A, B, C), FGFR4 ASO (D, E, F), Urso and control ASO (G, H, I), or Urso and FGFR4 ASO (J, K, L).

Discussion

The present study demonstrates that FGF19 upregulates and promotes canalicular localization of G5G8 in hepatocytes. However, treatment with FGF19 in the absence of G5G8 did not acutely disrupt cholesterol regulation in the liver, suggesting the involvement of G5G8-independent mechanisms for maintaining cholesterol homeostasis. Additionally, Urso regulates localization of G5G8 through an FGF15/19-FGFR4-dependent mechanism. Our findings suggest that biliary sterol elimination and bile acid synthesis share a common pathway mediated by FGF15/19-

FGFR4 signaling. However, the mechanism(s) by which FGF15/19 regulates G5G8 awaits further investigation.

The formation of bile involves the transport of bile acids, phospholipids, and cholesterol from hepatocytes into bile canaliculi. This process is tightly regulated in order to facilitate cholesterol solubilization in the form of mixed micelles. Increased biliary cholesterol concentrations relative to phospholipid and bile acid concentrations create supersaturated conditions that are favorable for gallstone formation [222]. Increased cholesterol gallstones are associated with polymorphisms in G5G8 that are thought to contribute to increased G5G8 activity [223, 224]. Therefore, it is plausible that biliary cholesterol secretion, mediated by G5G8, is regulated by bile acids in the enterohepatic circulation. During the fed state, bile acids are released from the gallbladder and bind to the nuclear receptor, FXR, to stimulate FGF15/19 in the small intestine [163]. FGF15/19 enters the liver via the enterohepatic circulation and binds to the FGFR4- β Klotho receptor complex to inhibit *Cyp7a1*, suppressing bile acid synthesis [163]. Emptying of the gallbladder and subsequent repletion requires various signals that integrate the status of the intestine, liver, and gallbladder. We observed in the present study that FGF15/19 plays a role in regulating G5G8. This may be a mechanism by which enterohepatic bile acids mediate biliary cholesterol secretion. FGF15/19 has been found to promote gallbladder filling by increasing cyclic adenosine monophosphate (cAMP) [172]. Mice deficient of FGF15 have empty gallbladders while FGF19 administration promotes gallbladder filling [172]. Interestingly, it has been demonstrated that localization of G5G8 to the canalicular surface involves cAMP signaling [225]. Both FGF19 and Urso induced expression of G5G8 at the site of bile canaliculi in the present study. Taken together, these data support the notion that in response to circulating bile acids, FGF15/19 regulates biliary cholesterol secretion in a feed forward mechanism.

Acute FGF19 administration suppressed bile acid synthesis and increased biliary total cholesterol. Therefore, we hypothesized that impairing biliary cholesterol secretion via G5G8 in the setting of increased FGF19 would disrupt hepatic cholesterol metabolism. Although serum free cholesterol was mildly increased in G5G8 KO mice, there were no changes in hepatic cholesterol or genes involved in cholesterol synthesis, transport, and bile acid synthesis. There were slight increases in *Cyp7a1* and *Cyp8b1* gene expression in G5G8 KO mice suggesting a possible compensatory response to promote non-G5G8-mediated cholesterol elimination, though these changes were not significant. Alternatively, there may be G5G8-independent, non-biliary pathways that are involved in maintaining cholesterol homeostasis. Supporting this notion, we have previously reported that Urso can increase fecal neutral sterols in G5G8 KO mice to a similar extent as in

wildtype mice [150]. Although we did not observe significant effects of acute FGF19 administration in G5G8 KO mice in this study, further studies using a more chronic dosing regimen of FGF19 are warranted to assess the effect of persistently elevated FGF19.

Urso is a hydrophilic bile acid that is used for the treatment of primary biliary cirrhosis and cholesterol gallstones. Urso facilitates the elimination of toxic bile acids that accumulate in hepatocytes and cholangiocytes as well as possess anti-apoptotic and anti-inflammatory properties [151]. Additionally, we have previously reported that Urso may be beneficial in liver diseases such as NAFLD and NASH by increasing G5G8 and biliary cholesterol secretion [150]. However, clinical data regarding the efficacy of Urso in NAFLD and NASH are inconsistent. While one study of standard dose Urso observed improvements in serum liver enzymes and steatosis, others found either no or slight improvements in serum liver enzymes with no improvements in liver histology with standard or high dose Urso [226-231]. The lack of efficacy observed in human studies may be explained, in part, by our findings in mice that Urso causes a simultaneous suppression of bile acid synthesis that minimizes the overall cholesterol elimination achieved via G5G8 [150]. The present study suggests that Urso regulates G5G8 by promoting canalicular localization and that this effect shares a common pathway with FGF15/19-mediated suppression of bile acid synthesis.

Among the multiple effects of Urso, the alleviation of ER stress may be one mechanism by which Urso regulates G5G8. The formation of functional G5G8 heterodimers requires N-linked glycosylation of both ABCG5 and ABCG8 within the ER prior to transport onto the canalicular surface of cells [152, 153]. Molecular chaperones, calnexin and calreticulin, facilitate folding of immature ABCG5 and ABCG8 in the ER and calreticulin stimulates the expression of G5G8 at the cell surface [154]. Proper G5G8 formation and trafficking may be impaired under conditions of ER stress such as obesity. Accordingly, decreased G5G8 in obese, insulin resistant *ob/ob* mice can be rescued by overexpression of adenoviral GRP78, an ER chaperone [147]. Previous reports demonstrate that tauroursodeoxycholic acid (TUDCA) is a chemical chaperone that alleviates ER stress-induced cell apoptosis as well as insulin resistance and fatty liver in obese, diabetic mice [232, 233]. Furthermore, TUDCA increases G5G8 protein in livers of wildtype and *db/db* mice [148]. TUDCA is the hydrophilic, tauro-conjugated form of Urso and in mice, most bile acids are conjugated to taurine [234, 235].

Urso may also play a regulatory role in sterol homeostasis. In the setting of an expanded bile acid pool, bile acid synthesis decreases through negative feedback signaling by FGF15/19. The bile acid synthesis pathway is the major route by which cholesterol catabolism occurs. Therefore,

increases in bile acid synthesis require upregulation of biliary cholesterol secretion through G5G8 in order to maintain hepatic sterol balance.

Our current study extends knowledge on the dynamic role of FGF15/19 signaling in the simultaneous regulation of bile acid synthesis and biliary cholesterol secretion. Additionally, we observed that Urso mediates the localization of G5G8 to the canalicular surface through a FGF15/19-FGFR4-dependent mechanism. Although the mechanisms by which this effect occurs are unclear, it likely involves the regulation of multiple processes including ER stress and bile acid signaling.

CHAPTER 5: A FUTURE DIRECTION IN CLINICAL APPLICATION: EFFECT OF EZETIMIBE-URSODIOL COMBINATION THERAPY ON BIOMARKERS OF LIVER FUNCTION AND STEROL BALANCE IN SUBJECTS WITH NAFLD

As the prevalence of NAFLD and NASH rises, the need for safe and effective therapies for treatment is becoming increasingly more urgent. A number of available pharmacologic agents including ezetimibe (EZ) and ursodiol (Urso) have been tested in clinical trials but have either failed or demonstrated minimal efficacy. EZ reduces intestinal absorption of dietary and biliary cholesterol by inhibiting NPC1L1 while Urso increases G5G8 and biliary cholesterol secretion. It has been demonstrated in multiple mouse models that increasing cholesterol elimination by promoting hepatic G5G8-mediated biliary secretion is dependent on intestinal absorption of cholesterol. In *Ldlr* KO mice, overexpression of G5G8 in both the intestine and liver increased biliary cholesterol and fecal neutral sterols while fractional absorption, hepatic cholesterol, LDL-cholesterol, and VLDL-cholesterol were decreased [145]. However, overexpression of G5G8 only in the liver in *Ldlr* KO mice increased biliary cholesterol secretion but decreased fractional absorption, LDL-cholesterol and VLDL-cholesterol only when intestinal absorption was inhibited by EZ [146]. Furthermore, adenoviral overexpression of G5G8 in the liver of *db/db* mice led to a paradoxical increase in plasma cholesterol that could only be suppressed in the presence of EZ [147]. These data suggest that concomitant regulation of biliary secretion and intestinal absorption of cholesterol is necessary for maintaining cholesterol homeostasis.

In humans, several studies suggest that EZ may be effective for the treatment of NAFLD. In a 6-month-long study in NASH patients with dyslipidemia, EZ improved liver enzymes, histology, and LDL-cholesterol [236]. EZ in combination with weight loss decreased intrahepatic lipids in obese patients [237]. EZ decreased alanine aminotransferase (ALT) after 12 months and steatosis after 24 months in newly-diagnosed NAFLD patients [237]. Urso has long been used in liver disease including NAFLD though results from clinical studies have been conflicting. Urso (13-15 mg/kg) has been shown to improve liver enzymes but have no effect on histology [226-228]. In a 6-month long study assessing a high dose of Urso (28-35 mg/kg), there were no changes in liver enzymes or histology [230]. However, a 12-month long study of high dose Urso yielded a decrease in ALT along with improvements in glycemic control [231]. As suggested by results from preclinical studies, the minimal effects of EZ and Urso monotherapy may be due to the interdependence of biliary secretion and intestinal absorption. Therefore, it is hypothesized that a combination therapy of EZ to inhibit intestinal absorption of cholesterol with Urso to

simultaneously promote biliary cholesterol secretion will increase cholesterol elimination, resulting in improvements in biomarkers of liver function and sterol balance in NAFLD.

To test this hypothesis, a prospective, open-label, pre-/post-treatment, pilot study in subjects with NAFLD is proposed (Appendix 1). Enrolled subjects will undergo 6 months of intervention with EZ 10 mg daily and Urso 13-15 mg/kg daily with measurements conducted before and after treatment. The primary endpoints will be the decrease in ALT and ALT/aspartate aminotransferase (AST) ratio and the secondary endpoints will be the decrease in hepatic fat fraction and changes in total cholesterol, LDL-cholesterol, HDL-cholesterol, triglycerides, fasting glucose and insulin, HbA1c, IL-8, IL-6, CK18, and plasma campesterol/lathosterol ratio. It is anticipated that after 6 months of EZ-Urso, ALT and ALT/AST ratio will be decreased. However, a limitation of the study is the possibility that these changes will not be observed in a small, pilot study. Nonetheless, useful information can be gathered from measures of hepatic fat fraction, glycemic control, inflammation, and plasma lipids. In preclinical studies, overexpression of G5G8 in obese, *db/db* mice decreased fasting glucose, triglycerides, and ER stress indicating that EZ-Urso may have significant effects on glycemic control [147]. Expanding the target patient population to include those with MetS and measuring hepatic fat fraction as the primary endpoint may optimize the potential to identify statistically significant differences pre- and post-treatment.

Urso increases biliary cholesterol secretion, fecal neutral sterols, and G5G8 in a dose-dependent manner, and these effects are maintained with the addition of EZ in mice [150]. However, a negative sterol balance is not achieved, evidenced by a lack of a compensatory increase in cholesterol synthesis [150]. This is explained at least in part by a suppression in bile acid synthesis that is caused by the presence of Urso. Therefore, it is possible that EZ-Urso may not be effective in the treatment of NAFLD. However, several differences between mice and humans exist that suggest that the effects of EZ-Urso in mice may not translate into humans. In humans, EZ decreases fractional cholesterol absorption by approximately 50%, and the maximal reduction in LDL-cholesterol is 20% [238-240]. Mice have a significantly greater response to EZ with up to a 96% inhibition in intestinal cholesterol absorption [241]. The increased efficacy of EZ in mice may limit the effect of Urso on promoting biliary cholesterol secretion compared to humans. Additionally, there is conflicting data regarding the role of Urso as an FXR agonist. Urso has been considered to be a weak agonist [162, 242, 243]. In mice, Urso has been shown to increase ileal *Fgf15* and decrease *Cyp7a1* to suppress bile acid synthesis [150]. However, a recent study in humans demonstrated that short term Urso decreased FGF19 and FXR activation and stimulated bile acid synthesis, acting as an FXR antagonist [244]. Although Urso increases G5G8 in mice,

the effect in humans is unknown. Hepatic G5G8 abundance will not be directly measured in the proposed study, but the campesterol/lathosterol ratio will provide an indication of the effectiveness of EZ and Urso on cholesterol elimination. Presumably, lathosterol as a measure of cholesterol synthesis will increase to maintain sterol balance in response to increased cholesterol elimination. Chronic treatment with EZ alone can increase hepatic cholesterol synthesis [245]. Therefore, further studies comparing EZ and Urso monotherapies to the combination therapy are needed to determine relative efficacies.

CHAPTER 6: SUMMARY

Imbalances in the regulation of glucose and lipid metabolism lead to the development of MetS. There are a multitude of molecular and biochemical pathways that are not specific to individual features of MetS but rather are interconnected. This dissertation focuses on the role of two distinct yet related aspects of metabolic regulation, circadian rhythms and the cholesterol-bile acid axis, in order to identify novel therapeutic targets for features of MetS.

The existence of a relationship between disrupted circadian rhythms and metabolic disease is unequivocal as evidenced by a number of observational studies as well as animal and prospective human studies. In analyzing the role of the central clock in conditions of altered sleep/wake cycles, evidence indicates that asynchrony between the internal clock and centrally-mediated behaviors such as feeding and physical activity precipitates MetS and its associated phenotypes. Less is known about the significance of peripheral clocks, though increasing evidence supports the role of peripheral clock components as direct transcriptional regulators of glucose and lipid metabolism.

In a mouse model of obesity, we conducted microarray analysis in order to identify potential genes of interest in adipose tissue that may be involved in the development of obesity. Of the genes that were significantly deregulated, genes associated with circadian rhythms including the clock-controlled PAR bZip family were the most overrepresented. During initial studies, we confirmed the expression of the PAR bZip genes in adipose tissue of mice and humans. Furthermore, we consistently observed a suppression of PAR bZip genes with obesity and insulin resistance. Measurements made during a single time point indicate a relationship between clock-controlled genes and mediators of obesity in adipose tissue. However, whether the decreases in PAR bZip genes were a cause of obesity and insulin resistance or an associated outcome could not be determined from these studies.

The PAR bZip transcription factors exhibit functional redundancy, and therefore mice require deletion of all three genes to have a significant impact on target genes. This adds a level of complexity in generating tissue-specific KO mice for studying the role of the PAR bZip family. In an effort to simplify procedures while maintaining our focus on the impact of disrupted peripheral clocks in the liver and adipose tissue, we generated and conducted a study in mice deficient of *Bmal1* in adipose tissue alone (ABKO) and in both adipose tissue and liver (LABKO). The objective of this study was to determine the role of peripheral *Bmal1* in the development of obesity and insulin resistance. Female ABKO and LABKO mice exhibited

alterations in feeding and activity patterns indicating that peripheral clocks mediate centrally-regulated, diurnal functions. Male LABKO mice became more obese but no other significant obesity-related phenotypes were observed, even when challenged on a diabetogenic diet. A high-fat diet has been shown to modulate locomotor activity periodicity as well as the expression of core clock and clock-controlled genes in the hypothalamus, liver, and adipose tissue. In our study, the effects of disrupted liver and adipose clocks were likely masked and confounded by the effects of a high-fat diet, which brings into question the impact of altering peripheral circadian rhythms in the setting of a high fat diet. Since a high-fat diet itself impairs circadian rhythmicity, it is difficult to delineate between the circadian- and non-circadian-related effects of the diet. It is likely that the macronutrient composition of a diet not only has a direct effect on clock genes and diurnal behaviors regulating metabolism but also has an impact on the degree of metabolic disease observed when peripheral circadian dysfunction precedes a high-fat diet. ABKO and LABKO mice also exhibited differences in hepatic cholesterol levels and expression of genes involved in cholesterol metabolism. Cholesterol and bile acid synthesis display diurnal patterns of activity and are transcriptionally-regulated by core clock genes [177-181]. Altered expression of cholesterol metabolic genes including *Hmgcr* and *Srebp2* is associated with NAFLD [73]. The link between circadian rhythms and metabolism has revealed a novel approach of timing rather than simply restricting food intake for the treatment and/or prevention of metabolic diseases. In mice, a high-fat diet consumed at the beginning of the wake phase was less detrimental to body weight and glycemic control compared to a high-fat diet consumed at the end of the wake phase [127]. Similarly, a clinical study of overweight or obese individuals consuming more calories earlier in the day achieved greater weight loss and improved blood glucose levels compared to those consuming more during the latter part of the day [131]. Although these studies demonstrate compelling evidence supporting the timing of food intake as a therapeutic for metabolic diseases, it is unclear how impactful this strategy may be in humans in the setting of a standard American diet high in carbohydrates, fat, and cholesterol. Further clinical studies assessing the timing of diets with varying macronutrient compositions will provide additional knowledge on the magnitude of the effects of circadian rhythms on metabolism.

Elevated hepatic free cholesterol has been implicated in NAFLD and NASH. Recent findings in mice have identified a potential combination drug therapy for the treatment of NAFLD. In these experiments, Urso-EZ promoted biliary cholesterol secretion by increasing G5G8 while simultaneously inhibiting intestinal cholesterol absorption. Although a compensatory increase in cholesterol synthesis was expected, signifying an increase in overall cholesterol elimination, no major changes were observed. Rather, there was a significant upregulation of *Fgf15*

corresponding with a suppression of bile acid synthesizing genes. It was hypothesized that the increase in G5G8 and decrease in bile acid synthesis by Urso were dependent mechanisms mediated by FGF15/19 signaling. In subsequent experiments, FGF19 and Urso were found to promote canalicular localization of G5G8. In the presence of FGFR4 ASO, this effect by Urso was abolished, indicating that the effects of Urso on G5G8 are dependent on FGF15/19 signaling. Urso regulates G5G8 in mice likely through multiple mechanisms involved in alleviating ER stress, inducing FXR, and signaling through the FGF15/19 pathway. Further studies in *in vitro* models expressing FGF15/19 and G5G8 are needed in order to differentiate between the regulation of G5G8 and bile acid synthesis. By understanding the mechanism(s) of Urso, therapeutic strategies to increase G5G8 without affecting bile acid synthesis can be explored for the treatment of NAFLD.

The availability of Urso and EZ as FDA-approved drugs facilitates the translatability of the previously conducted preclinical study to humans. Although evidence in mice suggest that the effects of Urso-EZ may be mitigated by the suppression of bile acid synthesis, the impact on humans warrants further investigation. Species differences in drug response as well as conflicting results from trials assessing Urso and EZ monotherapy are all potential reasons why positive responses may still be observed in humans. The pilot study proposed in Chapter 5 may not yield statistically significant differences in the primary endpoint pre- and post-treatment, but it will still provide critical information regarding the underlying mechanisms by which Urso may be effective in the treatment of NAFLD.

Although there are no FDA-approved drugs indicated for NAFLD and NASH currently, the potent FXR agonist, obeticholic acid (OCA), has been shown to be efficacious in NASH patients in clinical trials. An initial proof-of-concept study demonstrated an improvement in ALT, hepatic fibrosis, and insulin sensitivity as well as a reduction in body weight in NAFLD patients with T2DM after 6 weeks of treatment with the semi-synthetic bile acid [170]. The Farnesoid X Receptor Ligand Obeticholic Acid in NASH Treatment (FLINT) trial was a larger, multi-center study assessing the efficacy of OCA in NASH patients [171]. After 72 weeks of treatment, there was a significantly greater percentage of patients receiving OCA that had a decrease in NAFLD activity score by at least 2 points compared to those receiving placebo [171]. Although the effects of OCA on hepatic G5G8 in humans have not been formally tested, OCA and Urso are similar in that both induce choleresis and possess anti-apoptotic properties [246, 247]. However, FXR activation by OCA decreases bile acid pool size while Urso replaces endogenous bile acids and is incorporated into the bile acid pool [235, 248]. A decrease in the bile acid pool favors the

formation of cholesterol gallstones. Furthermore, increasing biliary cholesterol secretion by G5G8 causes a supersaturation of bile, leading to the precipitation of cholesterol crystals [249, 250]. Conversely, previous studies in mice have suggested FXR activation may prevent cholesterol gallstone formation by inducing *Abcb11* and *Abcb4*, transporters for bile acids and phospholipids, respectively [251]. On one hand, FXR activation by OCA may induce gallstones by 1) decreasing the bile acid pool size and 2) increasing biliary cholesterol secretion. On the other hand, FXR-mediated increases in ABCB11 and ABCB4 may prevent gallstones by lowering the cholesterol saturation index. Whether Urso is less likely to induce gallstone formation compared to OCA will depend on a combination of factors affecting bile acid pool size, G5G8 activity, and FXR activation. Therefore, studies comparing Urso to OCA need to be conducted in order to assess the effects of OCA on G5G8 and gallstone formation.

In the FLINT study, OCA increased serum total cholesterol and LDL-cholesterol while decreasing HDL-cholesterol [171]. The increase in serum cholesterol was effectively managed by lipid-lowering therapy and resolved upon discontinuation of OCA [171]. The observed changes on cholesterol was likely due in part to the effects of FXR on suppressing bile acid synthesis. Additionally, FXR activation in mice has been shown to reduce HDL-cholesterol by inducing SR-B1 and promoting RCT [252, 253]. Although it cannot be determined from these studies whether an increase in G5G8-mediated biliary cholesterol secretion and subsequent reabsorption of biliary-derived cholesterol could contribute to the increase in serum cholesterol, the addition of EZ may mitigate the increase in cholesterol if OCA has a similar effect on G5G8 as Urso. However, it is to be noted that FXR activation reduces intestinal cholesterol absorption, indicating that the overall effect of adding EZ may be minimized [253]. In addition to lowering serum cholesterol, EZ is effective in the prevention of cholesterol gallstones [254]. Therefore, studies comparing Urso to OCA both alone and in combination with EZ will determine whether 1) OCA is more effective in improving biomarkers of NAFLD and NASH and 2) the addition of EZ is sufficient to offset the potential negative effects of OCA. Information gathered from these future studies will address critical questions regarding the safety and efficacy of Urso and OCA as treatments for NAFLD.

APPENDICES

Appendix 1

The effect of Ezetimibe-Ursodiol combination therapy on biomarkers of liver function and sterol balance in subjects with NAFLD

Drug Identification: Zetia (Ezetimibe)/Ursodiol Combination

Date: 5 May 2015

Protocol Version 4

Sponsor Principal Investigator: Gregory Graf, PhD

University of Kentucky Pharmaceutical Sciences

345 Biological Pharmaceutical Complex

489 S. Limestone

Lexington, KY 40536-0595

Gregory.Graf@uky.edu

Phone: (859) 257-4749

Fax: (859) 257-7564

CONFIDENTIAL STATEMENT

This document contains confidential information, which should not be copied, referred to, released or published without written approval from Gregory Graf, PhD or the University of Kentucky. Investigators are cautioned that the information in this protocol might be subject to change and revision. Any conclusion regarding efficacy and safety must be considered provisional.

INVESTIGATOR'S STATEMENT AND SIGNATURE

The effect of Ezetimibe-Ursodiol combination therapy on biomarkers of liver function and sterol balance in subjects with NAFLD

I have read and understand this protocol, attachments, and Investigator Brochures for both Zetia and Ursodiol. I agree to conduct the study as outlined in the protocol and to comply with all the terms and conditions set out therein. I confirm that I will conduct the study in accordance with ICH GCP guidelines and the ethical principles of the Helsinki Declaration.

Sponsor/Principal Investigator:

Signature: _____

Date: _____

Printed Name: _____

CONTACT DETAILS OF KEY PERSONNEL

Role	Name	Contact Information
Sponsor/Principal Investigator	Gregory Graf, PhD	Email: gagraf2@uky.edu Phone: (859) 257-4749 Fax: (859) 257-7564
Sponsor Medical Monitor	Alla Grigorian, MD	Email: alla.grigorian@uky.edu Phone: (859) 338-7825 Fax: (859) 323-6445
Serious Adverse Event Reporting	Merck's Global Safety	Fax: (215) 993-1220

BACKGROUND AND RATIONALE

Name and Description of Investigational Products

This study will determine if two FDA approved drugs administered in combination will reduce biomarkers of nonalcoholic fatty liver disease (NAFLD). Ezetimibe (EZ), marketed as “Zetia” is an inhibitor of cholesterol absorption that is indicated for cholesterol lowering. Its mechanism of action is to block the Niemen Pick C 1 Like 1 protein (NPC1L1). It is available in a single formulation (10 mg tablet) prescribed o.p.d. Ursodiol (Urso) is marketed under multiple names by multiple suppliers including UrsoForte, a 500 mg tablet prescribed at 13-15 mg/kg/day, cf. It is indicated for primary biliary cirrhosis. The mechanism(s) of action of Urso are not fully understood, but are thought to be multifaceted and include opposing the effects of toxic bile acids, anti-apoptotic properties, and acting as a chemical chaperone among others.

Background & Hypothesis

Overweight and obesity is an epidemic that affects almost half of the US population at an estimated cost of \$147 billion annually [255]. Obesity is strongly associated with the Metabolic Syndrome, a cluster of clinical phenotypes associated with increased risk of diabetes and heart disease. It is now recognized that nonalcoholic fatty liver disease (NAFLD) is the hepatic manifestation of Metabolic Syndrome [256]. Although more difficult to diagnose than diabetes or cardiovascular disease, current estimates for the incidence of NAFLD range from 17-33% and 5-17% for nonalcoholic steatohepatitis (NASH), the more severe expression of NAFLD.[256] Current treatment of NAFLD is limited to lifestyle modification. Other therapeutic approaches are often employed such as insulin sensitizing agents, anti-oxidants and anti-inflammatories, but none are particularly effective at reversing the disease [257, 258]. This pilot study will determine if there is sufficient evidence to pursue a combination therapy of EZ + Urso to effectively accelerate cholesterol elimination, reduce hepatic lipids and improve liver function tests.

A growing body of literature supports an active role for cholesterol in the development of nonalcoholic fatty liver disease (NAFLD) and the progression to nonalcoholic steatohepatitis (NASH). Our previously published studies in preclinical models of diet-induced obesity indicate that reduced biliary cholesterol secretion accelerates the development of obesity and exacerbates hepatic steatosis and inflammation [149]. Conversely, our new preliminary data show that accelerating biliary cholesterol secretion through the ABCG5 ABCG8 sterol transporter (G5G8) reduces plasma glucose and triglycerides (TG) and restores insulin signaling in obese, db/db mice. In both cases, changes in G5G8 activity and liver phenotypes correlated with alterations in markers of endoplasmic reticulum (ER) stress. ER stress has been linked to hepatic insulin resistance and the upregulation of lipogenic, inflammatory, and apoptotic pathways in multiple cell types and in preclinical models of NAFLD [259].

Perhaps paradoxically, increasing G5G8-mediated biliary cholesterol secretion increases plasma and hepatic cholesterol, an effect blocked by co-administration of EZ. Ezetimibe (EZ) is an inhibitor of cholesterol absorption and reduces delivery of cholesterol to both liver and bile [260]. Similar to accelerated biliary secretion, the inhibition of cholesterol absorption with EZ improves liver function in preclinical models [261-263]. Our new preliminary data demonstrate that this effect of EZ is G5G8-dependent. Thus, the effect of accelerated biliary cholesterol secretion is mitigated by intestinal absorption, and similarly, the effect of EZ is limited by G5G8. These observations suggest that simultaneous acceleration of biliary secretion and inhibition of intestinal absorption will act cooperatively to promote cholesterol elimination from the body. Ursodiol (Urso) is a hydrophilic bile acid indicated for cholestasis and the dissolution of cholesterol gallstones, but it also acts as a molecular chaperone that alleviates ER stress, increases G5G8 and improves NAFLD in preclinical models [148, 264]. We hypothesize that EZ-Urso combination therapy will act cooperatively to achieve a “cholesterol drain” that promotes fecal elimination of cholesterol and alleviates clinical features of NAFLD (Fig 1).

Published & Preliminary Data in Preclinical Models

The inclusion of cholesterol in a high fat, high sucrose diet increases the severity of NAFLD resulting in steatohepatitis in LDL receptor deficient mice [74]. In a mouse model of Alström Syndrome, the development of NAFLD was associated with the accumulation of hepatic free cholesterol due to an increase in hepatic uptake and a decrease in biliary elimination.⁷ In a mouse model of Alström Syndrome, the development of NAFLD was associated with the accumulation of hepatic free cholesterol due to an increase in hepatic uptake and a decrease in biliary elimination [265]. In this model, hepatic G5G8 was strongly repressed despite the accumulation of hepatic sterols. We subsequently tested the hypothesis that the loss of G5G8 would contribute to NALFD [149]. Indeed, the loss of G5G8 resulted in accelerated loss of glycemic control and hepatic insulin resistance. Liver weight was increased and hepatic lipid accumulation was substantially greater in G5G8 KO mice compared to wild-type controls (Fig 2). The expression of inflammatory genes was increased as was the number of TUNEL and F4/80 positive cells. These changes were associated with an increase in markers of ER-stress (phospho-eIF2 α) and suppression of insulin signaling (decreased phospho-Akt & serine phosphorylation of IRS1). These data suggest that active biliary secretion opposes hepatic accumulation of cholesterol and TG and is important in the maintenance of insulin sensitivity.

Ezetimibe (EZ) inhibits cholesterol absorption by blocking Niemann-Pick C1-Like 1 (NPC1L1), the primary transporter responsible for cholesterol absorption at the apical surface of enterocytes [266]. In addition, EZ has been shown to reduce insulin resistance and steatosis in both rats and mice [262, 263, 267]. However, the ability of EZ to promote cholesterol elimination from the body is dependent on G5G8 [268]. Therefore,

we repeated this study in WT and G5G8 KO mice maintained on high fat diets containing EZ (0.005%). Despite the presence of EZ, liver weight and lipids were increased in G5G8 deficient mice compared to wild-type controls (Fig 3). The key implication of this observation is that the efficacy of EZ as a therapeutic in the treatment of NAFLD is dependent on G5G8 and biliary

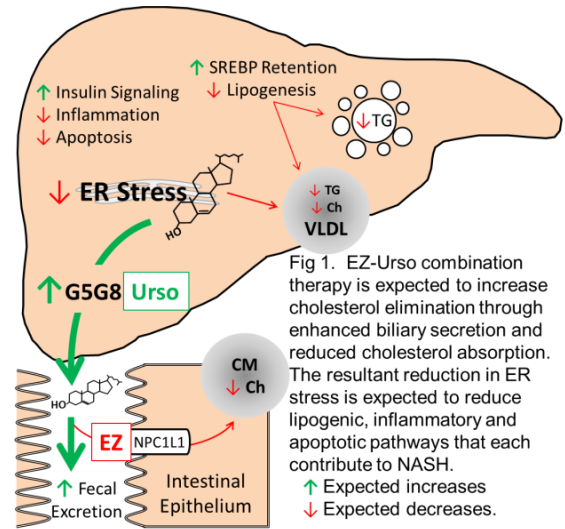


Fig 1. EZ-Urso combination therapy is expected to increase cholesterol elimination through enhanced biliary secretion and reduced cholesterol absorption. The resultant reduction in ER stress is expected to reduce lipogenic, inflammatory and apoptotic pathways that each contribute to NASH.
 ↑ Expected increases
 ↓ Expected decreases.

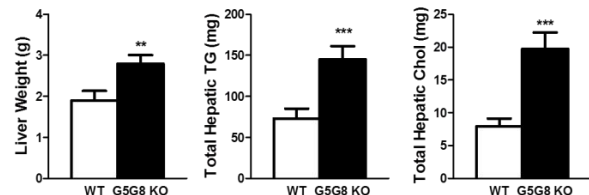
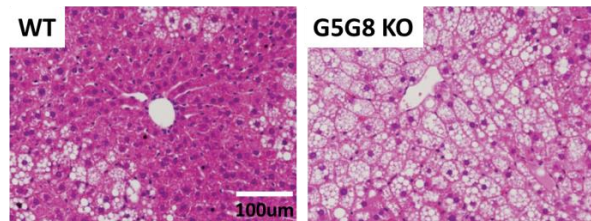


Fig 2. The absence of G5G8 (G5G8 KO) exacerbates NALFD in mice fed a high fat, plant sterol free diet compared to wild-type (WT) controls. Images are H&E stained liver sections. Bars are mean \pm SEM (n=6). **p<0.01, *p<0.001. Adapted from Su et al., 2012

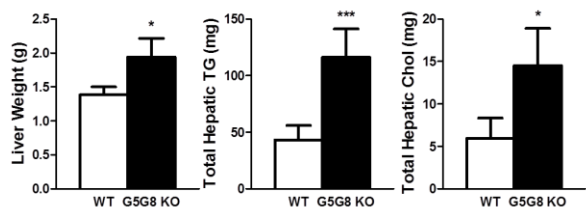


Fig 3. Ezetimibe does not correct NAFLD phenotypes in G5G8 KO mice. Bars are mean \pm SEM (n=6). *p<0.05, **p<0.001

cholesterol secretion.

While these studies establish that biliary cholesterol secretion is essential for liver function in the setting of obesity, the therapeutically relevant question is whether this pathway can be targeted in the treatment of NAFLD. Therefore, we conducted an experiment to determine if accelerating biliary cholesterol secretion could correct liver dysfunction in a model of NAFLD. Obese, db/db mice were infected with either a control virus or an adenovirus encoding G5G8 (AdG5G8). Expression of the mature, functional forms of

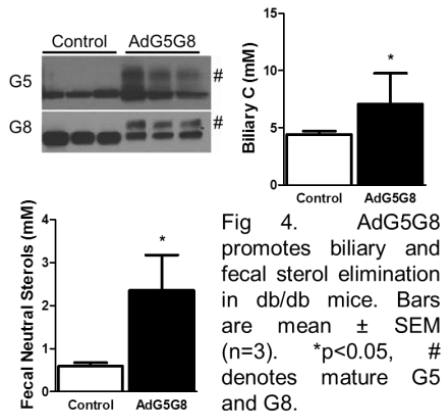


Fig 4. AdG5G8 promotes biliary and fecal sterol elimination in db/db mice. Bars are mean \pm SEM (n=3). *p<0.05, # denotes mature G5 and G8.

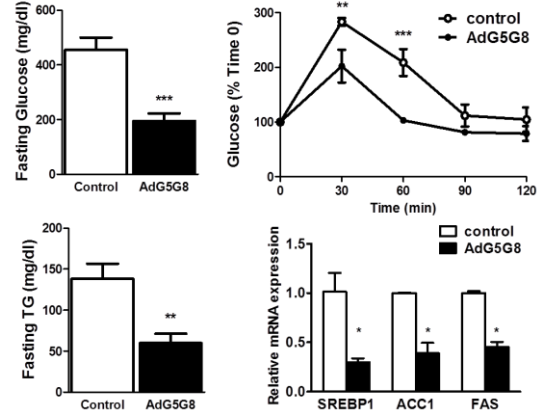


Fig 5. AdG5G8 reduces fasting glucose, improves glucose tolerance, reduces plasma TGs and suppresses lipogenic gene expression in liver of db/db mice. Sterol element binding protein 1 (SREBP1), ACC1 (acetyl CoA carboxylase), FAS (fatty acid synthase). Bars are mean \pm SEM (n=4-6) *p<0.05, **p<0.01, ***p<0.001

G5 and G8 was confirmed by western blotting (Fig 4). As expected, AdG5G8 increased biliary cholesterol and fecal neutral sterols. Differences in body weight and adiposity were not observed over the 72 hr treatment period. AdG5G8 reduced fasting glucose and improved glucose tolerance in db/db mice (Fig 5). There was also a decrease in fasting triglycerides and a suppression of SREBP and its lipogenic target genes.

ER stress and activation of the integrated stress response (ISR) is thought to play a causative role in liver dysfunction in obese mice [232, 269]. Phosphorylation of eIF2 α by a series of stress-activated kinases results in a cascade of signaling events that leads to reduced phosphorylation of protein kinase B (Akt), a key mediator of insulin signaling [270, 271]. Markers of ER stress were further increased obese G5G8 deficient mice compared to wild-type controls [149]. Therefore, we determined if AdG5G8 could reverse these effects. AdG5G8 reduced phospho-eIF2 α and increased phospho-Akt (Fig 6). Collectively, these published and preliminary data support a role for G5G8 mediated biliary cholesterol secretion in the maintenance of hepatic insulin signaling, glycemic control and TG metabolism. Further, they suggest therapeutics which accelerate biliary cholesterol secretion may be effective in the treatment of NAFLD and its more severe form, NASH.

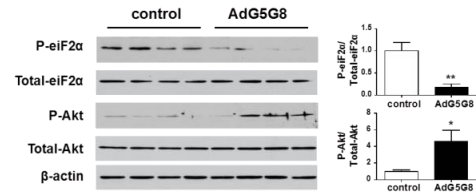


Fig 6. AdG5G8 reduces phospho (P)-eIF2 α and increases P-Akt in liver of db/db mice. Densitometric analysis of total to phosphorylated proteins is shown on the right. Bars are mean \pm SEM (n=4) *p<0.05, **p<0.01

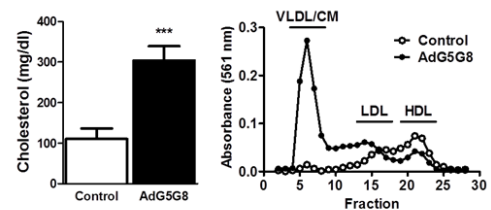


Fig 7. Cholesterol in total and FPLC-fractionated plasma from db/db mice administered a control adenovirus or AdG5G8. Fractions containing VLDL and chylomicrons (CM), LDL and HDL are indicated by horizontal lines. Bars are mean \pm SEM (n=4), **p<0.001

Increased biliary cholesterol secretion and fecal sterol elimination would presumably lower plasma cholesterol levels in db/db mice. However, we observed a paradoxical increase in plasma cholesterol following AdG5G8 administration (Fig 7). FPLC fractionation of serum indicates that the majority of cholesterol is associated with large

lipoprotein particles (fractions 5-8) such as VLDL or chylomicrons (CM). These fractions are very low triglycerides and enriched in ApoB48 compared to mice treated with control virus (not shown). This suggested that the accumulation of these particles was due to reabsorption of secreted biliary cholesterol.

Therefore, we administered AdG5G8 to mice in the absence and presence of EZ (Fig 8). When cholesterol absorption is inhibited, AdG5G8 does not generate large, cholesterol rich particles in plasma and total plasma cholesterol is reduced. These data indicate that in the presence of EZ, AdG5G8 promotes biliary secretion of cholesterol that is trapped within the proximal small intestine, fails to be re-absorbed and is ultimately lost in the feces. Similar observations were made in atherosclerosis studies in which a G5G8 transgene expressed in both liver and intestine lowered LDL cholesterol and reduced lesion

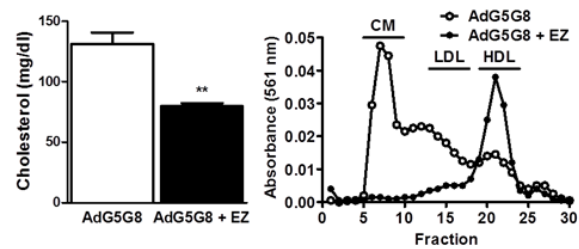


Fig 8. Cholesterol in total and FPLC-fractionated plasma from C57Bl/6J mice administered a control adenovirus or AdG5G8. Fractions containing CM, LDL and HDL are indicated by horizontal lines. Bars are mean \pm SEM (n=4), **p<0.001

area whereas a liver specific transgene was ineffective in the absence of EZ [146, 272]. The key implication of our new and previously published observations is that the intestine mitigates the efficacy of increased biliary cholesterol secretion in the elimination of cholesterol in the feces.

Clinical Studies with EZ or Urso Monotherapy

A number of clinical trials have evaluated either EZ or Urso in the treatment of NAFLD or specifically NASH. Yoneda et al. reported reductions in serum ALT, GGT, plasma triglycerides and hepatic fat (biopsy) in a 6-month pre-/post treatment open-label trial in 10 patients [273]. High sensitivity CRP was also reduced, suggesting improvements in inflammation, but measures of insulin resistance were unchanged. EZ in addition to weight loss was compared to weight loss alone in an obese, Australian cohort (BMI=33, n=15) [237]. EZ was effective at reducing intrahepatic lipids after adjusting for the effects of weight loss, but did not result in added benefit for other measures of NAFLD. In a non-obese population (n=8), EZ reduced plasma ALT by 40% at 6 and 12 months, but failed to reduce hepatic fat as determined by ultrasound [274]. In the largest study to date (n=45) in a Japanese population, EZ reduced ALT at 12 months and resulted in modest, but significant, reductions in steatosis, ballooning, and other indices of NAFLD by 24 months [274, 275]. Although limited in numbers of both studies and patients, EZ has shown promise in the treatment of NAFLD. Results with Urso have been mixed. Low-dose Urso (13-15 mg/kg/day) reduced some markers of inflammation including serum ALT, but failed to significantly improve NASH in two separate studies [226, 227]. High-dose Urso (28-32 mg/kg/day) failed to reduce ALT at either 3 or 6 months in one trial (n=12) [230], but in a separate study lowered ALT levels by an average of 40% at 3, 6, 9 and 12 months and normalized ALT values in 25% of patients (ALT<35 IU/ml) compared to no reductions or normalizations in the placebo group [276]. In the latter study, Urso also reduced HbA1c and HOMA-IR values suggesting improved insulin sensitivity. If our hypothesis is correct, the limited benefit of each of these agents is likely due to the interdependent nature of biliary cholesterol secretion and intestinal absorptive with respect to cholesterol elimination.

Conclusions

Our studies and others support an interdependence of biliary secretion and intestinal absorption for effective fecal cholesterol elimination. As a consequence, monotherapies that reduce cholesterol absorption will be limited by biliary secretion rates. Similarly, compounds that increase biliary secretion will be limited by intestinal reabsorption. A key element of our hypothesis is that a combination therapy that simultaneously increases biliary secretion and

reduces cholesterol absorption will result in a “*cholesterol drain*” that actively promotes cholesterol elimination from the body. No currently available therapeutic is indicated for the treatment of NAFLD. The completion of this pilot study will determine if there is sufficient evidence to warrant larger and better-controlled trials to determine if EZ-Urso combination will promote a negative sterol balance, reduce hepatic lipids and improve biomarkers of liver function in subjects with NAFLD. In addition, the fact that these agents are already FDA approved, have been used in large numbers of patients, and are well-tolerated greatly reduces the time required for this therapeutic approach to be tested in the NAFLD population should the clinical pharmacology goals be achieved. Thus, the present study has to the potential to have an immediate impact in the development of therapeutic approaches in the treatment of NAFLD, including NASH.

REGULATORY GUIDELINES

This study will be performed in accordance with US 21 Code of Federal Regulations Parts:

50, Protection of Human Subjects;

54, Financial Disclosure by Clinical Investigators and

56, Institutional Review Boards

RESEARCH OBJECTIVES

Aims

Determine if ezetimibe-ursodiol combination therapy (EZ-Urso) reduces hepatic fat, improves liver function tests and reduces markers of inflammation in subjects with NAFLD. Subjects diagnosed with NAFLD will be recruited to participate in an open label, pre-post treatment 6-month clinical trial to determine if EZ-Urso combination therapy provides benefit in subjects with NAFLD. Pre- and post-treatment measures of liver enzymes, steatosis by MRI quantification, inflammatory cytokines, apoptotic markers and plasma lipids will be determined.

Determine the extent to which a “cholesterol drain” is achieved and associates with markers of NAFLD and obesity-related liver phenotypes. The extent of cholesterol loss is directly reflected by the rate of cholesterol synthesis. Pre- and post-treatment plasma lathosterol, a late intermediate in the cholesterol synthesis pathway, will be determined by GC-MS. A reduction in plasma campesterol, a marker of sterol absorption, and a lowering of the campesterol/lathosterol ratio are also reflective of a greater dependence on *de novo* synthesis to maintain cellular sterol levels in tissues. The extent to which each of these associates with key measures of the severity of NAFLD will be determined. Similarly, associations with plasma glucose, insulin, and HOMA-IR will be determined to assess insulin resistance, which is strongly associated with the development of NAFLD.

INVESTIGATIONAL PLAN

Description of Overall Study Design

The study will be conducted as a prospective open label trial with pre- and post-treatment measures for all dependent variables. This trial will enroll subjects with a clinical diagnosis of nonalcoholic fatty liver disease (NAFLD) by magnetic resonance imaging (MRI), computed tomography (CT) or ultrasound, including those diagnosed with nonalcoholic steatohepatitis (NASH). Subjects will be consented, blood collected and a MRI conducted on the first visit. Subjects will be advised on the proper use of the pharmacotherapy and given the first three month's supply of EZ and Urso. For the remaining three months, study drug will be delivered by US mail along with return packaging for the prior three month's study medication in order to monitor compliance. Subjects will be called routinely to encourage compliance, retention, and monitor side effects or adverse events. After six months of pharmacotherapy, subjects will return for a follow-up assessment of plasma parameters, MRI and a post-study questionnaire.

Duration of Subject Enrollment: 6 months

Duration of Study: 18 months

Dosing Rationale

No study to date has assessed EZ-Urso combination therapy in the treatment of NAFLD or NASH. Our data in preclinical models suggest that combination therapy will be more effective than either single agent. Although high-dose Urso is required to reduce ALT as a monotherapy, noncompliance is a significant concern. Side effects at this dose included diarrhea and abdominal discomfort in a significant number of subjects [276]. In addition, currently available formulations require 6-9 tablets daily for subjects between 64-72 inches tall and BMIs ranging from 25 to 50. Based on these factors, EZ-Urso combination therapy will include EZ in its standard formulation (10 mg/day) and Urso (13-15 mg/kg/day).

Safety Analysis

Subjects will be monitored for adverse events through scheduled phone calls once a month. Subjects experiencing severe adverse events will be told to discontinue the study medications immediately and contact their physician. Mild to moderate adverse events will be reviewed by Dr. Grigorian to determine appropriate actions to ensure subject safety. Adverse events will be documented and reported in accordance with IRB, and Merck. Subjects will be informed that they may withdraw from the study at any time.

SUBJECT POPULATION:

Recruitment Method

Subjects will be recruited either through pre-screening by UK HealthCare Hepatology or through referring physicians. Fliers containing information about the study and contact information will be distributed to UK HealthCare Hepatology and to outside physicians' offices. The flier will also contain a checklist for Dr. Grigorian and other referring physicians to use for pre-screening. Subjects seen by Dr. Grigorian at UK HealthCare Hepatology will be pre-screened during their normally scheduled routine appointment to determine if they meet the study eligibility

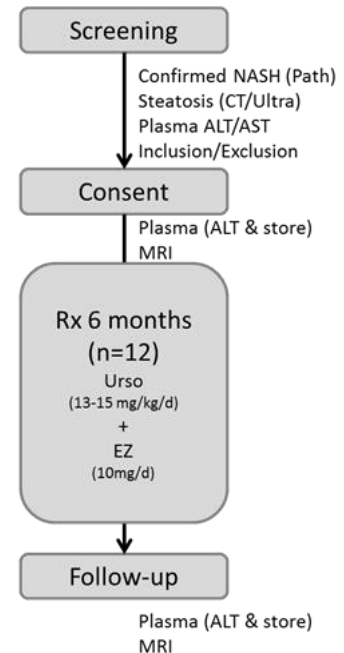


Fig 9. Study Design

requirements. Referring physicians will be asked to inform subjects deemed potentially eligible using the pre-screen checklist about the study and to provide the subject with the completed checklist to keep if they decide to enroll in the study. All potential subjects, both from UK HealthCare Hepatology and outside physicians' offices, will contact the study coordinator listed on the flier to set up the first appointment which will take place at the Clinical Services Core (CSC) facility.

Selection of Subjects

Twelve individuals will be enrolled of any gender, race or ethnicities who meet the inclusion/exclusion criteria outlined in Table 1. Subjects will be between the age of 18 and 75 years with normal renal function, alanine aminotransferase (ALT) in excess of 50% of the normal range and an ALT/aspartate aminotransferase (AST) ratio greater than 1.0 who are typically referred to the hepatologist by their primary care physician. Hepatic steatosis is generally confirmed by either MRI, CT or ultrasound, but a clinical diagnosis of NASH requires liver biopsy and analysis by a pathologist. Subjects with advanced liver disease with cirrhosis will not be recruited as the mechanism of action of the proposed therapeutics is unlikely to provide benefit in these subjects. Having a diagnosis of secondary steatosis or other liver diseases and women who are pregnant or breastfeeding will be excluded. Subjects reporting alcohol intake at levels reported to promote liver disease will be excluded. A critical element of the trial is the precise determination of hepatic fat fractions prior to and after pharmacotherapy. Thus, individuals too large for the available research MRI instrument, with known claustrophobia or medical devices or conditions incompatible with MRI will be excluded. Individuals from vulnerable populations will not be recruited.

Inclusion/Exclusion Criteria

Table 1

Inclusion	Exclusion
18-75 yrs	Normal ALT within last 6 mo
ALT >1.5 normal (>55 F, 60 M)	
ALT/AST ratio >1.0	Advanced fibrosis based on 1) biopsy, if available (Stage 3 or 4 NAFLD), 2) imaging, or 3) lab (platelet count <150,000)
	Alcohol (>20g/day F, >30g/day M)
Steatosis (MRI, CT or Ultrasound)	2 ^o steatosis, other liver disease
Normal kidney function (CrCl >30mL/min)	Rx (Urso, EZ, Vit E, fish oils, TZD, insulin, sulfonylureas, HMG-CoA reductase inhibitors)
	Pregnancy/Breastfeeding
	BMI > 50, largest body circ >160cm, claustrophobia, other incompatibilities listed in MRI screening form
	Hypersensitivity to Ezetimibe or ursodiol

Concomitants Medications/Treatments to Avoid

Individuals already taking either EZ or Urso will not be included. In addition, individuals taking therapeutics with reported benefits or complications in the treatment of NAFLD/NASH (vitamin E, fish oils), thiazoladinediones (TZDs), insulin, sulfonylureas, HMG-CoA reductase inhibitors) will also be excluded as these may confound the interpretation of the results.

Subject Withdrawal Criteria

Voluntary withdrawal: Subjects will be asked to contact the study coordinator in the event that voluntary withdrawal from the study is desired. The study coordinator will document the reason for withdrawal and schedule a follow-up if withdrawal is due to an adverse event.

PI-determined withdrawal: If the subject no longer meets inclusion/exclusion criteria or experiences a serious adverse event or suspected unexpected serious adverse reaction, the subject will be withdrawn from the study. For serious adverse events or suspected unexpected serious adverse reactions, any necessary follow-up will be conducted.

If a subject withdraws or is withdrawn from the study, no additional data will be collected and no replacement will be enrolled. The study design accounts for a 25% dropout rate with a minimum of 9 subjects needed to reach statistical significance.

STUDY PROCEDURES/EXAMINATIONS

Initial Contact

Interested potential subjects will contact the study coordinator and pre-screening will be conducted to determine if the potential subject meets criteria for age, alcohol consumption, concomitant medications, weight loss, pregnancy/breastfeeding, MRI, and hypersensitivity to the study drugs. If the participant is determined eligible, the study coordinator will set up an initial appointment (Visit 1) with the CSC in order to obtain consent. If applicable, subjects will be reminded at this time to bring the pre-screen checklist completed by their physician to the appointment. Additionally, subjects will be asked to present to this visit after a 12 hour fast.

Visit 1

Eligibility will be confirmed and informed consent will be obtained. Demographics and contact information including name, age, gender, race, phone number, email address, mailing address, availability, and referring physician will be obtained or confirmed if information was already provided during the initial contact. Subjects will be assigned a unique identification number at this point. Weight will be obtained to determine ursodiol dosing. Data to be collected from the chart review include ALT, AST, GGT, lipid panel (total cholesterol, LDL, HDL, TG), and HbA1c. Subjects will be given a 3-month supply of their study medication and counseled on each medication. Subjects will be expected to keep a daily log of when medication was taken to ensure compliance. This log will be provided to the subject at this time. Subjects will be told that about 7-10 days prior to their completion of the 3-month supply, another 3-month supply of their study medication will be mailed to them along with a daily log and a pre-paid package. Subjects are to mail back their medication bottles any remaining medication they did not take and their study diary in this pre-paid package. The procedure for reporting adverse effects will be explained. During this time, the study coordinator will schedule the next appointment for the subject (Visit 7).

Visits 1 and 7

Subjects will present to each visit after a 12 hour fast. Medical history and medication history will be obtained. Vital signs (BP, HR), height, weight, waist and hip circumference, and the largest body circumference will be measured. This information will be used for determining waist to hip ratio and to confirm subject is compatible with the MRI machine. Blood will be drawn via

peripheral venipuncture by a trained phlebotomist. A total of 25 mL of blood will be collected into green PST, gold SST, and purple tubes for both standard and non-standard labs listed below in Table 2. After the clinic visit, subjects will be asked to return to undergo an MRI at the UK Magnetic Resonance Imaging and Spectroscopy Center (MRISC). Subjects will be given directions to the MRISC and \$25 cash compensation. Subjects will be asked to finish consuming any food at least 3.5 hours prior to the MRI appointment. The study coordinator will confirm subjects' contact information in case a phone call is warranted between the time the subject leaves the clinic and returns to the MRISC. At this time, subjects will be allowed to leave the premises until the MRI appointment. Upon completion of the MRI visit, subjects will be given an additional \$25 cash compensation for a total of \$50 cash compensation per visit.

Study Flow Chart

Procedure	Screening	Treatment at Home					Follow-up
	Visit 1	Visit 2	Visit 3	Visit 4	Visit 5	Visit 6	Visit 7
		Telephone Call					
Informed Consent	X						
Demographics	X						
Medical History	X						X
Medication History	X						X
Inclusion/Exclusion	X						
Height/Weight	X						X
Waist and Hip Measurement	X						X
Blood Pressure and Heart Rate	X						X
Clinical Labs	X						X
Study Labs	X						X
MRI	X						X
Questionnaire							X
Adverse Events	X	X	X	X	X	X	X
Study Drug issued ¹	X			X			
Daily Log issued ¹	X			X			
Study Drug compliance ²				X			X

1 = First 3-month's supply of study drug will be given to the participant at the on-site study visit 1. The last 3-month's supply will be sent via US mail directly to the participant. The package will include an envelope with paid postage for return shipment of the previous 3-month's medications.

2 = Compliance will be monitored at mid-point and end of study via pill counts and daily log.

Dose Titration

Ursodiol dosing will be titrated up the final dose of 13-15mg/kg/day over a one week period. Subjects will take ursodiol 500mg/day for three days then 1000mg/day for four days then 13-15mg/kg/day from thereafter. This will be done to increase the tolerability of adverse effects.

Magnetic Resonance Imaging (MRI)

MRIs for all subjects will be obtained through the UK Magnetic Resonance Imaging and Spectroscopy Center (MRISC) in order to more accurately determine the extent of hepatic steatosis. Beyond being a noninvasive procedure, a key advantage of MRI for hepatic fat determination over biopsy is that multiple areas of the liver can be analyzed. Thus, we employ a noninvasive approach that better estimates the extent of steatosis throughout the liver. In addition, we can monitor changes in hepatic fat fractions pre- and post-treatment. MRI exams will be conducted by Dr. Peter Hardy, PhD, a Research Assistant Professor in the Division of Radiological and Medical Physics and Dr. James Lee, MD, an Assistant Professor in Radiology. Briefly, a 20mm voxel will be placed at four independent locations (upper and lower right & left lobe) of the liver avoiding major vascular structures, liver edge or bile ducts. STEAM single voxel proton spectroscopy will be performed. TR will be prolonged to minimize T1 effect and multiple and short TEs will be performed to limit the effects of J-coupling and estimate T2. Spectra will be analyzed and area under the curve will be calculated and recorded by our Peter Hardy and James Lee. Hepatic fat in each subject will be calculated as the mean fat fraction from the four scans.

Shipment of Drug

Subjects will be given a 3-month supply of medication during their initial visit. Approximately 7-10 days prior to the end of month 3, study personnel will mail the remaining 3 month's supply of medication to the subject along with a daily log. This shipment will also include a pre-paid package in which subjects will use to mail back empty bottles and any unused medication. These packages will be mailed to the IDS pharmacy.

IDS Mailing Address

Stephen Sitzlar
University of Kentucky
1000 S. Limestone Street, Rm A03.101 Pavilion A
Lexington, KY 40536

Telephone Calls and Follow-up

Medical and medication history will be updated as needed. Phone interviews will be conducted monthly to monitor compliance as well as known side effects of each medication and any unexpected side effects or adverse events. Subjects will be contacted 5-7 days before each clinic visit as a reminder of their upcoming appointment. Following 6 months of pharmacotherapy, subjects will return to the CSC facility for a blood draw, scheduled MRI and completion of a post-study questionnaire.

Laboratory Blood Sampling

Blood obtained from subjects at each visit will be taken to both the UK HealthCare clinical laboratory and to the study laboratory of Dr. Graf located in the Biological Pharmaceutical Building for measurements of labs listed in Table 2. Two green PST tubes, one gold SST tube, and one purple tube will be delivered to the UK HealthCare clinical laboratory while remaining plasma will be divided into aliquots and transported to the study laboratory of Dr. Graf where the samples will be stored at -80°C until use. The non-standard of care labs that will be performed in the laboratory of Dr. Graf include measurement of inflammatory markers (interleukin-8, -6, tumor necrosis factor α) and a marker of apoptosis (CK18). Plasma lipids will be extracted and analyzed by gas chromatography-mass spectrometry for the determination of intermediate

metabolites of cholesterol synthesis (lathosterol) as well as phytosterols (campesterol, sitosterol, stigmasterol) to estimate rates of cholesterol synthesis and absorption before and after pharmacotherapy.

Any remaining aliquots of plasma will remain in the study laboratory of Dr. Graf for long-term storage. This will be done so that if new biomarkers of NAFLD/NASH emerge, these samples may be analyzed in the future; this will be included with informed consent.

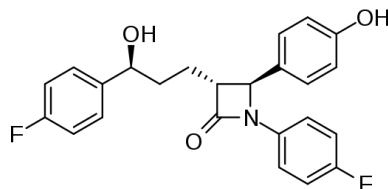
Table 2

Lab	Standard of care	Visit 1	Visit 7
ALT	X	X	X
AST	X	X	X
GGT		X	X
Lipid profile		X	X
Insulin		X	X
Glucose		X	X
HbA1c		X	X
TNF α		X	X
IL-8		X	X
IL-6		X	X
CK18		X	X
Sterols		X	X

DRUG SUBSTANCE

Ezetimibe

ZETIA (ezetimibe, IND: 52,791) is in a class of lipid-lowering compounds that selectively inhibits the intestinal absorption of cholesterol and related phytosterols. The chemical name of ezetimibe is 1-(4-fluorophenyl)-3(R)-[3-(4-fluorophenyl)-3(S)-hydroxypropyl]-4(S)-(4-hydroxyphenyl)-2-azetidinone. The empirical formula is C₂₄H₂₁F₂NO₃. Its molecular weight is 409.4 and its structural formula is:



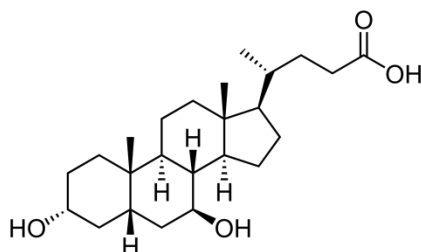
Ezetimibe is a white, crystalline powder that is freely to very soluble in ethanol, methanol, and acetone and practically insoluble in water. Ezetimibe has a melting point of about 163°C and is stable at ambient temperature. ZETIA is available as a tablet for oral administration containing 10 mg of ezetimibe and the following inactive ingredients: croscarmellose sodium NF, lactose monohydrate NF, magnesium stearate NF, microcrystalline cellulose NF, povidone USP, and sodium lauryl sulfate NF.

Name and address of Manufacturer:

Merck Sharp & Dohme Corp.
126 E. Lincoln Avenue
MS: RY34-A238
Rahway, NJ 07065-0900

Ursodiol

URSO 250 (ursodiol, 250 mg) is available as a film-coated tablet for oral administration. URSO Forte (ursodiol, 500 mg) is available as a scored film-coated tablet for oral administration. Ursodiol (ursodeoxycholic acid, UDCA) is a naturally occurring bile acid found in small quantities in normal human bile and in larger quantities in the biles of certain species of bears. It is a bitter-tasting white powder consisting of crystalline particles freely soluble in ethanol and glacial acetic acid, slightly soluble in chloroform, sparingly soluble in ether, and practically insoluble in water. The chemical name of ursodiol is 3 α ,7 β -dihydroxy-5 β -cholan-24-oic (C₂₄H₄₀O₄). Ursodiol has a molecular weight of 392.56. Its structure is shown below:



Inactive ingredients: microcrystalline cellulose, povidone, sodium starch glycolate, magnesium stearate, ethylcellulose, dibutyl sebacate, carnauba wax, hydroxypropyl methylcellulose, PEG 3350, PEG 8000, cetyl alcohol, sodium lauryl sulfate and hydrogen peroxide.

Name and address of Manufacturer:

Forest Research Institute
Harborside Financial Center
Plaza V, Suite 1900
Jersey City, NJ 07311

INVESTIGATIONAL DRUG ACCOUNTABILITY

Both drugs in this study (EZ and Urso) will be stored in the Investigational Drug Service (IDS) pharmacy during the duration of the study. Merck will directly ship the required amount of EZ to the IDS pharmacy where IDS staff will maintain proper storage and security of drug. Urso will be purchased from Forest, properly stored, and secured by IDS pharmacy. Both drugs will be packaged and labeled by IDS pharmacy staff. The subject's initial supply of medication will be dispensed from the IDS pharmacy to either the study coordinator or other study personnel who will then deliver the supply to the subject. Subjects will be instructed to return any unused drug via mail (see section **Shipment of Drug**). Any unused drug that is returned to IDS will be properly disposed of on-site by study personnel. This will be documented in the case report form (CRF).

ADVERSE EVENTS

Reporting Procedures for Exchange of Adverse Event Information

Adverse Event or **AE** shall mean any untoward medical occurrence in a Study subject who is administered the Study Drug regardless of whether or not a causal relationship with the Study Drug exists. By way of example and without limitation, an AE can be any unfavorable and unintended sign (for example, an abnormal laboratory finding), symptom, or disease temporally associated with the use of the Study Drug.

“Serious Adverse Event” or **“SAE”** shall mean any untoward medical occurrence in a Study subject who is administered the Study Drug that results in death, a life-threatening drug experience, requires inpatient hospitalization or prolongation of existing hospitalization, results in persistent or significant disability/incapacity, or is a congenital anomaly/birth defect that occurs in the offspring of a patient taking the drug, cancer, or is a new cancer if the cancer is the condition of the study, or overdose. Other important medical events that may jeopardize the subject or may require intervention to prevent one of the outcomes listed previously should also be considered “serious.”

“Suspected Unexpected Serious Adverse Reaction” or **“SUSAR”** shall mean any Serious Adverse Event, the nature, severity or frequency of which is not consistent with information in the most current investigator’s brochure, or with respect to a marketed product the most current Summary of Product Characteristics (SPC) or Package Insert.

Serious Adverse Event and Suspected Unexpected Serious Adverse Reaction, Potential Incident, or Incident Reporting: Principal Investigator shall forward to Merck’s Global Safety (“Merck GS”) group any SAE, SUSAR or Incident information, including, but not limited to, all initial and follow-up information involving any Study subject in the Study. Notification shall be in the form of a completed CIOMS I/MedWatch (or other mutually agreed upon format) within 24 hours of learning of the information. This information shall be transmitted to Merck GS using the contact information provided below or such other modified contact information as provided by Merck in writing. All information shall be transmitted in the English language and contain the reporter’s name and the Study subject identifier code. SUSAR information will be reported unblinded if the Study Drug has been blinded in the Study.

- Merck may define certain Non-Serious Events of Interest. If any Non-Serious Events of Interest are defined, Merck will provide such information in writing to Principal Investigator at the time of Protocol approval, execution of the study contract or anytime thereafter. Reporting of any defined Non-Serious Events of Interest will be handled in the same manner as SAEs unless mutually agreed otherwise in writing by the parties.
- All reports of Study Drug exposure during pregnancy or lactation whether associated with an AE or not, must be reported to Merck GS in accordance with the timelines and contact information for an SAE. Principal Investigator shall follow pregnancies to term to obtain the outcome of the pregnancy. The outcome of the pregnancy shall be forwarded to Merck GS.
- Institution and Principal Investigator shall fully comply with all of their respective reporting obligations to the applicable regulatory authorities with respect to any AE, SAE or SUSAR that arises from the Study.
- SAE reports and any other relevant safety information are to be forwarded to Merck GS FAX number: (215) 993-1220.

In the event Principal Investigator or Institution becomes aware of a defect or possible defect in the Study Drug provided under this Agreement, Institution and Principal Investigator agree to notify Merck within one business day of first becoming aware of the defect or possible defect.

Principal Investigator agrees to notify Merck within twenty-four (24) hours in the event that the FDA or any other regulatory authority notifies the Study site of a pending inspection that concerns the Study or Institution’s ability to perform clinical research. In addition, Principal Investigator will

forward to Merck any written communication received as a result of the inspection within twenty-four (24) hours of receipt of such communication and agrees to allow Merck to assist in responding to any citations involving the Study Drug. Such responses shall be made as soon as possible under the circumstances or within any earlier deadline set by the issuing regulatory authority. Principal Investigator shall also provide to Merck a complete description of documents and any correspondence provided to any inspector. In the event the FDA or other regulatory authority requests or requires any action to be taken to address any citations, Principal Investigator and Institution agree, after consultation with Merck, to take such action as necessary to address such citations.

A copy of all 15 Day Reports and Annual Progress Reports are to be submitted as required by the applicable regulatory authority by the Principal Investigator. Principal Investigator agrees to cross reference this submission according to local regulations, to the Study Drug number (IND, CSA, etc) at the time of submission. Additionally Principal Investigator agrees to submit a copy of these reports to Merck (Attn: Global Safety; FAX 215-993-1220) at the time of submission to the appropriate regulatory agency.

Merck may provide the Principal Investigator and Institution, at Study initiation and on an ongoing basis, with information regarding the Study Drug, including but not limited to safety information. The Principal Investigator and Institution agree to hold this information in confidence.

Adverse Event Follow-up

All AEs, including clinically significant changes in physical examinations findings, or isolated clinically significant laboratory findings must be followed until the event resolves, the condition stabilizes, the event is otherwise explained, or the subject is lost to follow-up. If resolved or stabilized, a resolution date should be documented on the case report form (CRF).

Adverse events ongoing at the final visit or early termination visit will be followed until that adverse event is resolved.

Pregnancy

Pregnancy is an exclusion criterion for this study. Female subjects must be instructed that if up to 9 months after study drug administration she suspects she may be pregnant, she is to immediately contact the Research Coordinator who will schedule a serum pregnancy test within 48 hr to confirm pregnancy. Pregnancy will be followed until resolution (i.e., termination [voluntary or spontaneous] or birth) to assess for pregnancy-associated AEs or SAEs such as congenital anomaly.

- **Reproductive Risks:** It is not known whether receiving the study drug used in this study are harmful to an unborn child. Pregnancy after administration of either Ezetimibe or Ursodiol may involve risks to the mother, and her embryo or fetus. Therefore, females who are capable of reproducing, must use effective contraceptive methods. These methods must be used from the time of screening until the end of the study. Examples of effective birth control are: hormonal contraceptives (the pill, implant, transdermal patch, or injection), barrier methods (condom with spermicide, diaphragm with spermicide), IUD, or a male partner who has had a vasectomy.
- **Lactating women:** It is not known whether either of the study drugs or its metabolites are excreted in human milk. Because many drugs are excreted in human milk, women who are breastfeeding will be excluded from the study.

POTENTIAL RISK:

Blood Draws

The risks associated with blood draws include pain, bruising, soreness and possible infection at the site of blood withdrawal, as well as possible fainting.

MRI

The risks associated with MRI include anxiety and possible discomforts from lying on one's back, but are otherwise minimal as no contrast reagents will be used.

Study Drug

Both EZ and Urso have been used in large numbers of patients for a number of years and are well-tolerated.

- Side effects listed for Ezetimibe when administered alone include upper respiratory tract infection, diarrhea, arthralgia, sinusitis, and pain in extremity and occurred in excess of 2% of placebo treated subjects.
- Side effects of Ursodiol include diarrhea, elevated creatinine, elevated blood glucose, leukopenia, peptic ulcer, skin rash, and thrombocytopenia. These adverse reactions occurred at similar rates in placebo treated subjects.

All participants will be monitored for side effects through routine calls from the research coordinator. Subject safety will be monitored according to GCP guidelines. Any changes to the risk/benefit ratio will be reported accordingly to IRB and FDA regulations.

Privacy/Social

The only other risk is possible loss of privacy or social distress from the examination (height, weight, waist and hip circumference and blood pressure) and medical record review. All subjects will be assigned a study identification number. These risks are deemed minimal.

Only the Principal Investigator, Chief Physician, the CCTS CSC research nurses, and the study coordinator will have access to the subjects' identities and private information. The study coordinator will create a unique identification number for each enrolled subject during the first CSC visit. The tubes of blood collected will only be identified by the individual's assigned unique identification number. All information collected on the subject (age, height, weight, waist and hip circumference, blood pressure, heart rate, fasting lipid panel, glucose, liver tests, and medication list) will only be identified by the unique identification number assigned. Plasma will be collected and stored temporarily in the Biochemical Analysis Laboratory and permanently in the Graf Laboratory. Plasma samples and subject data will be associated through the unique identification number. All electronic information is encrypted and stored on secure server with password protection (see data management plan).

BENEFIT VS. RISK

The study is designed to determine if the EZ-Urso combination therapy provides benefit for subjects with NAFLD. Should this combination prove efficacious, the condition of these subjects will improve. Subjects will receive results of clinical labs that are standard of care in NAFLD, but not other labs that are of experimental value. Subjects will receive cash compensation for their time but not enough to be coercive. In addition, volunteers may receive personal satisfaction from participating in a study that is designed to improve a health condition that directly affects them.

The risks to the subject are minimal. The procedures to be performed are limited to blood collection, MRI and the administration of two well-tolerated therapeutics. All procedures will be performed in the CCTS CSC using skilled nurses, a hospital environment, and sterile procedures. MRIs will be performed by Dr. Peter Hardy, PhD and Dr. James Lee, MD. To protect privacy, all data will only be identified by the assigned unique study number, and no identifying information will be collected.

STATISTICAL ANALYSIS

Statistical Methods

Clinical and biochemical measures in pre and post-treatment samples will be analyzed using a paired t-test. Linear regression will be used to determine relationships between changes in indices of cholesterol synthesis and absorption (plasma lathosterol, campesterol, & campesterol/lathosterol ratio) and changes in clinical and biochemical measures (e.g. Δ lathosterol vs. Δ ALT). Differences will be considered significant at $p < 0.05$.

A reduction in plasma ALT to within 50% of the normal range ($<50\text{IU/L}$) will be considered as clinically relevant (i.e. reduced to 75IU/L). Using previously published data from the chief physician's studies, ALT levels in subjects with NASH are expected to be $\sim 106 \pm 65$ [227]. Using a type 1 error rate of 5% and a sample size of 9, the type 2 error rate will be 50%

Any deviation from the planned analyses will be done in consult with the biostatistics core within the UK CCTS and reported to the IRB.

Primary Endpoints

The primary endpoints of this study will include the reduction in ALT and reduction in ALT/AST ratio.

Secondary Endpoints

Secondary endpoints will include reduction in hepatic fat fraction, changes in GGT, total cholesterol, LDL, HDL, triglycerides, fasting glucose, fasting insulin, HbA1c, IL-8, IL-6, CK18, and differences in plasma lipids.

STUDY MANAGEMENT

IRB Approval

This study must have initial and at least annual approval from an Institutional Review Board (IRB) responsible for approving human subject research. Furthermore, screening and enrollment of subjects into the trial will not commence until Investigator receives the IRB approval letter. In addition, a copy of the IRB approval letter must be filed on-site in the investigator's study binder. When appropriate, amendments to the protocol must be submitted for IRB review and approval before being implemented.

Informed Consent

- Study enrollment should not begin until the Investigator has received an approved and validated informed consent from the IRB.
- All subjects enrolling in the study:
 1. Will be informed of the investigational nature of the study
 2. Must be given a copy of the Informed Consent Form
 3. Must be given the opportunity to ask any questions regarding the study treatment
 4. Will have voluntarily and willingly signed the Informed Consent Form prior to initiation of any study related test/procedure.

Protocol Adherence

The Investigator agrees to conduct the study in accordance with this protocol. Prior to beginning the study, the Investigator(s) must sign both the Investigator Agreement and the protocol signature page.

An Investigator must not make any changes to the study without first receiving written approval from the Principal Investigator and IRB, except when necessary to eliminate apparent immediate hazard to a subject.

Study Monitoring and Auditing

Study monitoring will be carried out in compliance with FDA regulation (21 CFR 812) and all GCP guidelines.

Data Recording and Record Retention

1. All data will be recorded on electronic Case Report Forms for each subject enrolled in the study as well as in the subject records.
2. The Investigator will ensure that the medical records are made available for review by the study monitor or governmental regulatory bodies as required.
3. All subject study records are to be maintained in a secure storage facility until notified by the Principal Investigator that the forms may be discarded. This includes the following:
 - a) Case Report Forms, source documentation, signed informed consents and enrollment logs
 - b) Drug Accountability Records and shipment receipts of all drug shipped to the study site
 - c) Correspondence with the IRB or Ethics Committee, Principal Investigator, FDA, monitor, or other investigators
 - d) Study protocol and any amendments issued
 - e) Protocol and informed consent approvals from the IRB
 - f) Investigator agreements and curricula vitae of Investigator(s), and the site personnel signature form
 - g) Laboratory certificates, if applicable

Data from the analyses of human samples will be managed using Research Electronic Data Capture (REDCap), which is provided through the UK CCTS. REDCap is a secure web-based application for building and managing online databases. The application is trademarked by the Vanderbilt CTSA. Vanderbilt developed a Consortium of institutions to share this research and data capture tool. Users are engaged in a Regulatory and Software Validation Committee, which includes compliance with 21 CFR Part 11, HIPAA, and other regulations. The University of Kentucky REDCap software was installed in the Institute for Pharmaceutical Outcomes & Policy in 2008 and is located in 180 BioPharm Complex (BPC). The web server and the database server are located on separate servers behind a firewall with in-house control with UK's campus network. In addition, in order to maintain secure communications, the web server has a secured security license (SSL) and is located on <https://redcap.rdmc.org/redcap/>. Research data is stored locally and is backed up daily using MySQL Administrator software using the Windows Server 2008 R2 edition. Accounts are created using domain accounts generated by UK used for authentication purposes. This login process requires individual password protection for investigators. Dr. Graf will assign users to the REDCap project and define permissions for each user. User rights that may be issued include the ability to create calendar events, import or export data, build reports, lock or unlock records when entry is completed, create records, rename records, edit or delete records, and determine if an electronic signature is required for certain events. In addition, each user can be given an expiration date which will remove access to that individual user. REDCap maintains a built-in audit trail that logs all user activity and pages viewed. The logging record can be viewed by those with proper user rights. When investigators are logged onto REDCap to enter data, a vulnerability to hacking the account while open is of concern; however, all data is encrypted when transmitted to the REDCap server. Portable devices

are not at risk because nothing is downloaded onto the device. A secure web based connection is used for all data collection. Data storage on portable devices is not a security concern for REDCap administration, but appropriate measures will be taken when exporting data from REDCap. To assist investigators, REDCap has an email function that offers greater security for large attachments that contain sensitive data. Each recipient receives an email containing a unique downloaded URL, along with a second follow up email with the password for downloading the files. The file is stored securely and removed from the server upon the specified expiration date.

Data and Safety Monitoring

Monitoring for adverse events will be conducted in real-time by the study investigators and study coordinators. Risks involved with this study are considered greater than minimal risk. For this reason, we will utilize the standing independent Data Safety Monitoring Board (DSMB) as chartered by the Center for Clinical and Translational Science (CCTS). The DSMB will meet semiannually or as needed, and will review subject recruitment, AE's, side effects, laboratory results, dropouts, protocol violations, and inclusion/exclusion criteria. More frequent meetings will take place if side effects or other problems are prevalent.

All procedures will be conducted by well-trained nursing staff or physicians. Once subjects begin the pharmacotherapy phase of the trial, patient safety will be monitored through routine phone calls by the clinical research coordinator. Incidental significant MRI findings or reported unexpected and known side effects will be recorded and regularly reported to Drs. Grigorian and Graf at monthly research staff meetings. Any serious side effects or adverse events will be immediately reported to the chief physician who will take appropriate actions to ensure there is no compromise of patient care or safety. These subjects may be removed from the study depending on the nature of the event.

Interim reviews

The PI will ensure that the IRB is notified within the timeframe set by the IRB of any AEs and SAEs, protocol deviation/violation notification. The PI will ensure that the IRB is immediately made aware of any protocol amendments, study suspension/termination, safety reporting by the sponsor.

This protocol will be continuously monitored in real-time by the principal investigator and study coordinator for adverse events (AEs).

AEs will be graded according to intensity. Mild: Discomfort noticed but no disruption of normal daily activity. Moderate: Discomfort sufficient to reduce or affect normal daily activity. Severe: Incapacitating with inability to work or perform normal daily activity.

The attribution scale for AE reporting will be as follows. Probable: AE is related to the procedure or drug (e.g. infection from a fat biopsy). Possible: AE follows the procedure or drug within a reasonable period (within 7 days), but may have been produced by the subject's clinical state or other factors (e.g. rash 3 days following the FSIGT). Remote: AE does not follow the procedure or drug within a reasonable period and could readily have been produced by the subject's clinical state or other factors. Unrelated: AE is judged to be clearly due to extraneous causes and does not meet the above criteria.

Plan for unexpected adverse event (AE) reporting

Serious AEs will be reported to Human Subjects/IRB within 48 hr, and will also be reported to Merck, within 24 hours of the Investigator becoming aware of the event. Unanticipated events will be reported to the IRB no later than 15 days after the event. Annual reporting of adverse events will be reported to the University of Kentucky Institutional Review Board, and Merck.

Monitoring of adverse events

As described in the research plan, subjects who are treated with EZ-Urso combination therapy

will have a total of two clinical visits and 5 telephone contacts. Adverse events will be monitored via exams, vital signs, review of subject's medical chart, phone interviews and documented. Each visit will be documented with a progress note in the research chart.

SUBJECT CONFIDENTIALITY

The Investigator and the Principal Investigator affirm a subject's right to protection against invasion of privacy. In compliance with United States federal regulations, the Principal Investigator requires the Investigator(s) to permit, when necessary, representatives from the FDA or other regulatory authorities to review and/or copy any medical records relevant to the study in accordance with local laws. Should direct access to medical records require a waiver or authorization separate from the subject's statement of informed consent, it is the responsibility of the Investigator to obtain such permission in writing from the appropriate individual.

Appendix 2

Abbreviations

4S: Scandinavian simvastatin survival study
ABCA1: ATP binding cassette subfamily A, member 1
ABCB11: ATP binding cassette, subfamily B, member 11
ABCB4: ATP binding cassette, subfamily B, member 4
ABCD2: ATP binding cassette, subfamily D, member 2
ABCG5: ATP binding cassette subfamily G, member 5
ABCG8: ATP binding cassette subfamily G, member 8
ABKO: adipose-Bmal1 knockout mice
ACAT2: acetyl-CoA acyltransferase 2
Ad-Cre: adenoviral vectors contained Cre recombinase
Ad-Empty: adenoviral vectors containing no insert
ALT: alanine aminotransferase
APOA1: apolipoprotein A1
APOB: apolipoprotein B
APOCIII: apolipoprotein CIII
APOE: apolipoprotein E
ASBT: apical sodium-dependent bile acid transporter
ASO: antisense oligonucleotide
AST: aspartate aminotransferase
ATGL: adipose triglyceride lipase
BMAL1: aryl hydrocarbon receptor nuclear translocator-like protein 1
BMI: body mass index
CA: cholic acid
cAMP: cyclic adenosine monophosphate
CD: control diet
CDCA: chenodeoxycholic acid
CETP: cholesteryl ester transfer protein
ChREBP: carbohydrate responsive element binding protein
CLOCK: circadian locomotor output cycles kaput
CRY: cryptochrome
CSI: cholesterol saturation index
CVD: cardiovascular disease
CYP27A1: sterol 27-hydroxylase
CYP7A1: cholesterol 7 α -hydroxylase
CYP7B1: 25-hydroxycholesterol 7 α -hydroxylase
CYP8B1: sterol 12 α -hydroxylase
DAVID: Database for Annotation, Visualization and Integrate Discovery
Db/db: leptin receptor-deficient mice
DBP: d site albumin promotor binding protein
DD: diabetogenic diet
EE: energy expenditure
ER: endoplasmic reticulum
EZ: ezetimibe
FAA: food anticipatory activity
FABP-4: fatty acid binding protein
FFA: free fatty acid
FGF15: fibroblast growth factor 15
FGF15/19: FGF15 and FGF19

FGFR4: fibroblast growth factor receptor 4
 FLINT: Farnesoid X Receptor Ligand Obeticholic Acid in NASH Treatment
 FOXO1: forkhead box protein O1
 FPLC: fast protein liquid chromatography
 FXR: farnesoid X receptor
 FXRE: FXR response element
 G5G8: ABCG5 ABCG8
 GTT: glucose tolerance test
 HDL: high density lipoprotein
 HLF: hepatic leukemia factor
 HMG-CoA: 3-hydroxy-3-methylglutary CoA
 HMGCR: HMG-CoA reductase
 HSL: hormone sensitive lipase
 IL-1 α : interleukin 1 alpha
 IL-10: interleukin 10
 IL-6: interleukin 6
 IMPROVE-IT: Vytorin efficacy international trial
 INSIG1: insulin-induced protein 1
 INSIG2: insulin-induced protein 2
 IR: insulin resistant
 IRS-1: insulin receptor substrate
 IS: insulin sensitive
 IST: insulin sensitivity test
 KO: knockout
 LABKO: liver- and adipose-Bmal1 knockout mice
 LCAT: lecithin:cholesterol acyltransferase
 LDL: low density lipoprotein
 LDLR: low density lipoprotein receptor
 LPL: lipoprotein lipase
 LXR α : liver X receptor alpha
 MetS: metabolic syndrome
 MTP: microsomal triglyceride transfer protein
 NAFLD: nonalcoholic fatty liver disease
 NASH: nonalcoholic steatohepatitis
 NEFA: non-esterified fatty acid
 NF- κ B: nuclear factor kappa-light-chain-enhancer of activated B cells
 NPC1L1: Niemann-Pick C1-like 1
 Ob/ob: leptin-deficient mice
 OCA: obeticholic acid
 OST α/β : organic solute transporter alpha/beta
 PAR bZip: proline- and acid-rich basic region leucine zipper
 PEPCK: phosphoenolpyruvate carboxykinase
 PER: period
 PGC1 α : PPARG coactivator 1 alpha
 PPAR α : peroxisome proliferator activated receptor alpha
 PPAR γ : peroxisome proliferator activated receptor gamma
 RCT: reverse cholesterol transport
 REE: resting energy expenditure
 RER: respiratory exchange ratio
 REV-ERB α : nuclear receptor subfamily 1, group D, member 1
 ROR α : Retinoic acid receptor-related orphan receptor alpha

RORE: retinoic acid-related orphan receptor response element
RXR: retinoid X receptor
SCAP: SREBP cleavage-activating protein
SCN: suprachiasmatic nucleus
SHP: small heterodimer partner
SR-B1: scavenger receptor B1
SREBP-1c: sterol regulatory element binding protein 1c
SREBP-2: sterol regulatory element binding protein 2
T2DM: type 2 diabetes mellitus
 τ : tau or period
TEF: thyrotroph embryonic factor
TLR2: toll like receptor 2
TLR4: toll like receptor 4
TNF- α : tumor necrosis factor alpha
TUDCA: tauroursodeoxycholic acid
Urso: ursodiol
VLDL: very low density lipoprotein
WAT: white adipose tissue
WT: wildtype
ZO-1: zona occludens-1

REFERENCES

1. Pais, R., et al., *Fatty liver is an independent predictor of early carotid atherosclerosis*. J Hepatol, 2016. **65**(1): p. 95-102.
2. Karlsson, B., A. Knutsson, and B. Lindahl, *Is there an association between shift work and having a metabolic syndrome? Results from a population based study of 27,485 people*. Occup Environ Med, 2001. **58**(11): p. 747-52.
3. Mohebbi, I., K. Shateri, and M. Seyedmohammadzad, *The relationship between working schedule patterns and the markers of the metabolic syndrome: comparison of shift workers with day workers*. Int J Occup Med Environ Health, 2012. **25**(4): p. 383-91.
4. Aguilar, M., et al., *Prevalence of the metabolic syndrome in the United States, 2003-2012*. Jama, 2015. **313**(19): p. 1973-4.
5. Kolovou, G.D., et al., *The prevalence of metabolic syndrome in various populations*. Am J Med Sci, 2007. **333**(6): p. 362-71.
6. Park, Y.W., et al., *The metabolic syndrome: prevalence and associated risk factor findings in the US population from the Third National Health and Nutrition Examination Survey, 1988-1994*. Arch Intern Med, 2003. **163**(4): p. 427-36.
7. Sarafidis, P.A. and P.M. Nilsson, *The metabolic syndrome: a glance at its history*. J Hypertens, 2006. **24**(4): p. 621-6.
8. Reaven, G.M., *Banting lecture 1988. Role of insulin resistance in human disease*. Diabetes, 1988. **37**(12): p. 1595-607.
9. Haffner, S.M., et al., *Prospective analysis of the insulin-resistance syndrome (syndrome X)*. Diabetes, 1992. **41**(6): p. 715-22.
10. Lam, T.K., et al., *Mechanisms of the free fatty acid-induced increase in hepatic glucose production*. Am J Physiol Endocrinol Metab, 2003. **284**(5): p. E863-73.
11. Dusserre, E., P. Moulin, and H. Vidal, *Differences in mRNA expression of the proteins secreted by the adipocytes in human subcutaneous and visceral adipose tissues*. Biochim Biophys Acta, 2000. **1500**(1): p. 88-96.
12. Fontana, L., et al., *Visceral fat adipokine secretion is associated with systemic inflammation in obese humans*. Diabetes, 2007. **56**(4): p. 1010-3.
13. Alberti, K.G., et al., *Harmonizing the metabolic syndrome: a joint interim statement of the International Diabetes Federation Task Force on Epidemiology and Prevention; National Heart, Lung, and Blood Institute; American Heart Association; World Heart Federation; International Atherosclerosis Society; and International Association for the Study of Obesity*. Circulation, 2009. **120**(16): p. 1640-5.
14. Marchesini, G., et al., *Association of nonalcoholic fatty liver disease with insulin resistance*. Am J Med, 1999. **107**(5): p. 450-5.
15. Lin, C.H., et al., *Systematic review of impact of lifestyle-modification programs on metabolic risks and patient-reported outcomes in adults with metabolic syndrome*. Worldviews Evid Based Nurs, 2014. **11**(6): p. 361-8.
16. Pi-Sunyer, X., *The medical risks of obesity*. Postgrad Med, 2009. **121**(6): p. 21-33.
17. Otto, T.C. and M.D. Lane, *Adipose development: from stem cell to adipocyte*. Crit Rev Biochem Mol Biol, 2005. **40**(4): p. 229-42.
18. Cheung, C.C., D.K. Clifton, and R.A. Steiner, *Proopiomelanocortin neurons are direct targets for leptin in the hypothalamus*. Endocrinology, 1997. **138**(10): p. 4489-92.
19. Considine, R.V., et al., *Serum immunoreactive-leptin concentrations in normal-weight and obese humans*. N Engl J Med, 1996. **334**(5): p. 292-5.
20. Long, Y.C. and J.R. Zierath, *AMP-activated protein kinase signaling in metabolic regulation*. J Clin Invest, 2006. **116**(7): p. 1776-83.
21. Hummel, K.P., M.M. Dickie, and D.L. Coleman, *Diabetes, a new mutation in the mouse*. Science, 1966. **153**(3740): p. 1127-8.

22. Ingalls, A.M., M.M. Dickie, and G.D. Snell, *Obese, a new mutation in the house mouse*. J Hered, 1950. **41**(12): p. 317-8.
23. Hajer, G.R., et al., *Low plasma levels of adiponectin are associated with low risk for future cardiovascular events in patients with clinical evident vascular disease*. Am Heart J, 2007. **154**(4): p. 750.e1-7.
24. Lindsay, R.S., et al., *Adiponectin and development of type 2 diabetes in the Pima Indian population*. Lancet, 2002. **360**(9326): p. 57-8.
25. Combs, T.P., et al., *Endogenous glucose production is inhibited by the adipose-derived protein Acrp30*. J Clin Invest, 2001. **108**(12): p. 1875-81.
26. Yamauchi, T., et al., *The fat-derived hormone adiponectin reverses insulin resistance associated with both lipoatrophy and obesity*. Nat Med, 2001. **7**(8): p. 941-6.
27. Hu, E., P. Liang, and B.M. Spiegelman, *AdipoQ is a novel adipose-specific gene dysregulated in obesity*. J Biol Chem, 1996. **271**(18): p. 10697-703.
28. Trujillo, M.E. and P.E. Scherer, *Adiponectin--journey from an adipocyte secretory protein to biomarker of the metabolic syndrome*. J Intern Med, 2005. **257**(2): p. 167-75.
29. Surmi, B.K. and A.H. Hasty, *Macrophage infiltration into adipose tissue: initiation, propagation and remodeling*. Future Lipidol, 2008. **3**(5): p. 545-556.
30. Nieto-Vazquez, I., et al., *Insulin resistance associated to obesity: the link TNF-alpha*. Arch Physiol Biochem, 2008. **114**(3): p. 183-94.
31. Tsigos, C., et al., *Dose-dependent effects of recombinant human interleukin-6 on glucose regulation*. J Clin Endocrinol Metab, 1997. **82**(12): p. 4167-70.
32. Wallenius, V., et al., *Interleukin-6-deficient mice develop mature-onset obesity*. Nat Med, 2002. **8**(1): p. 75-9.
33. Nielsen, S., et al., *Splanchnic lipolysis in human obesity*. J Clin Invest, 2004. **113**(11): p. 1582-8.
34. Himsworth, H.P., *Diabetes mellitus: its differentiation into insulin-sensitive and insulin-insensitive types*. Diabet Med, 2011. **28**(12): p. 1440-4.
35. Olefsky, J., J.W. Farquhar, and G. Reaven, *Relationship between fasting plasma insulin level and resistance to insulin-mediated glucose uptake in normal and diabetic subjects*. Diabetes, 1973. **22**(7): p. 507-13.
36. Yalow, R.S. and S.A. Berson, *Plasma insulin concentrations in nondiabetic and early diabetic subjects. Determinations by a new sensitive immuno-assay technic*. Diabetes, 1960. **9**: p. 254-60.
37. Opie, L.H. and P.G. Walfish, *Plasma free fatty acid concentrations in obesity*. N Engl J Med, 1963. **268**: p. 757-60.
38. Nguyen, M.T., et al., *A subpopulation of macrophages infiltrates hypertrophic adipose tissue and is activated by free fatty acids via Toll-like receptors 2 and 4 and JNK-dependent pathways*. J Biol Chem, 2007. **282**(48): p. 35279-92.
39. Hotamisligil, G.S., et al., *Reduced tyrosine kinase activity of the insulin receptor in obesity-diabetes. Central role of tumor necrosis factor-alpha*. J Clin Invest, 1994. **94**(4): p. 1543-9.
40. He, J., et al., *Interleukin-1alpha inhibits insulin signaling with phosphorylating insulin receptor substrate-1 on serine residues in 3T3-L1 adipocytes*. Mol Endocrinol, 2006. **20**(1): p. 114-24.
41. Schottelius, A.J., et al., *Interleukin-10 signaling blocks inhibitor of kappaB kinase activity and nuclear factor kappaB DNA binding*. J Biol Chem, 1999. **274**(45): p. 31868-74.
42. Foretz, M., et al., *Sterol regulatory element binding protein-1c is a major mediator of insulin action on the hepatic expression of glucokinase and lipogenesis-related genes*. Proc Natl Acad Sci U S A, 1999. **96**(22): p. 12737-42.

43. Shimomura, I., et al., *Insulin selectively increases SREBP-1c mRNA in the livers of rats with streptozotocin-induced diabetes*. Proc Natl Acad Sci U S A, 1999. **96**(24): p. 13656-61.
44. Yamashita, H., et al., *A glucose-responsive transcription factor that regulates carbohydrate metabolism in the liver*. Proc Natl Acad Sci U S A, 2001. **98**(16): p. 9116-21.
45. Stoeckman, A.K. and H.C. Towle, *The role of SREBP-1c in nutritional regulation of lipogenic enzyme gene expression*. J Biol Chem, 2002. **277**(30): p. 27029-35.
46. Lambert, J.E., et al., *Increased de novo lipogenesis is a distinct characteristic of individuals with nonalcoholic fatty liver disease*. Gastroenterology, 2014. **146**(3): p. 726-35.
47. Schwarz, J.M., et al., *Hepatic de novo lipogenesis in normoinsulinemic and hyperinsulinemic subjects consuming high-fat, low-carbohydrate and low-fat, high-carbohydrate isoenergetic diets*. Am J Clin Nutr, 2003. **77**(1): p. 43-50.
48. Qatanani, M. and M.A. Lazar, *Mechanisms of obesity-associated insulin resistance: many choices on the menu*. Genes Dev, 2007. **21**(12): p. 1443-55.
49. Martins, A.R., et al., *Mechanisms underlying skeletal muscle insulin resistance induced by fatty acids: importance of the mitochondrial function*. Lipids Health Dis, 2012. **11**: p. 30.
50. Adams, J.M., 2nd, et al., *Ceramide content is increased in skeletal muscle from obese insulin-resistant humans*. Diabetes, 2004. **53**(1): p. 25-31.
51. Itani, S.I., et al., *Lipid-induced insulin resistance in human muscle is associated with changes in diacylglycerol, protein kinase C, and IkappaB-alpha*. Diabetes, 2002. **51**(7): p. 2005-11.
52. Younossi, Z.M., et al., *Changes in the prevalence of the most common causes of chronic liver diseases in the United States from 1988 to 2008*. Clin Gastroenterol Hepatol, 2011. **9**(6): p. 524-530.e1; quiz e60.
53. Younossi, Z.M., et al., *Global epidemiology of nonalcoholic fatty liver disease-Meta-analytic assessment of prevalence, incidence, and outcomes*. Hepatology, 2016. **64**(1): p. 73-84.
54. Browning, J.D., et al., *Prevalence of hepatic steatosis in an urban population in the United States: impact of ethnicity*. Hepatology, 2004. **40**(6): p. 1387-95.
55. Byrne, C.D. and G. Targher, *NAFLD: a multisystem disease*. J Hepatol, 2015. **62**(1 Suppl): p. S47-64.
56. Targher, G., et al., *Prevalence of nonalcoholic fatty liver disease and its association with cardiovascular disease among type 2 diabetic patients*. Diabetes Care, 2007. **30**(5): p. 1212-8.
57. Portillo-Sanchez, P., et al., *High Prevalence of Nonalcoholic Fatty Liver Disease in Patients With Type 2 Diabetes Mellitus and Normal Plasma Aminotransferase Levels*. J Clin Endocrinol Metab, 2015. **100**(6): p. 2231-8.
58. Sookoian, S. and C.J. Pirola, *Non-alcoholic fatty liver disease is strongly associated with carotid atherosclerosis: a systematic review*. J Hepatol, 2008. **49**(4): p. 600-7.
59. Anstee, Q.M., G. Targher, and C.P. Day, *Progression of NAFLD to diabetes mellitus, cardiovascular disease or cirrhosis*. Nat Rev Gastroenterol Hepatol, 2013. **10**(6): p. 330-44.
60. Byrne, C.D. and G. Targher, *Ectopic fat, insulin resistance, and nonalcoholic fatty liver disease: implications for cardiovascular disease*. Arterioscler Thromb Vasc Biol, 2014. **34**(6): p. 1155-61.
61. Stepanova, M. and Z.M. Younossi, *Independent association between nonalcoholic fatty liver disease and cardiovascular disease in the US population*. Clin Gastroenterol Hepatol, 2012. **10**(6): p. 646-50.

62. Chalasani, N., et al., *The diagnosis and management of non-alcoholic fatty liver disease: practice guideline by the American Gastroenterological Association, American Association for the Study of Liver Diseases, and American College of Gastroenterology*. Gastroenterology, 2012. **142**(7): p. 1592-609.
63. Feldstein, A.E., et al., *Free fatty acids promote hepatic lipotoxicity by stimulating TNF- α expression via a lysosomal pathway*. Hepatology, 2004. **40**(1): p. 185-94.
64. Liu, J., et al., *Free fatty acids, not triglycerides, are associated with non-alcoholic liver injury progression in high fat diet induced obese rats*. Lipids in Health and Disease, 2016. **15**(1): p. 27.
65. DeFilippis, A.P., et al., *Nonalcoholic fatty liver disease and serum lipoproteins: the Multi-Ethnic Study of Atherosclerosis*. Atherosclerosis, 2013. **227**(2): p. 429-36.
66. Cohen, D.E. and E.A. Fisher, *Lipoprotein metabolism, dyslipidemia, and nonalcoholic fatty liver disease*. Semin Liver Dis, 2013. **33**(4): p. 380-8.
67. Altomonte, J., et al., *Foxo1 mediates insulin action on apoC-III and triglyceride metabolism*. J Clin Invest, 2004. **114**(10): p. 1493-503.
68. Kamagate, A., et al., *FoxO1 mediates insulin-dependent regulation of hepatic VLDL production in mice*. J Clin Invest, 2008. **118**(6): p. 2347-64.
69. Foger, B., et al., *Relationship of plasma cholesteryl ester transfer protein to HDL cholesterol. Studies in normotriglyceridemia and moderate hypertriglyceridemia*. Arterioscler Thromb Vasc Biol, 1996. **16**(12): p. 1430-6.
70. Lucero, D., et al., *Does non-alcoholic fatty liver impair alterations of plasma lipoproteins and associated factors in metabolic syndrome?* Clin Chim Acta, 2011. **412**(7-8): p. 587-92.
71. Puri, P., et al., *A lipidomic analysis of nonalcoholic fatty liver disease*. Hepatology, 2007. **46**(4): p. 1081-90.
72. Caballero, F., et al., *Enhanced free cholesterol, SREBP-2 and StAR expression in human NASH*. J Hepatol, 2009. **50**(4): p. 789-96.
73. Min, H.K., et al., *Increased hepatic synthesis and dysregulation of cholesterol metabolism is associated with the severity of nonalcoholic fatty liver disease*. Cell Metab, 2012. **15**(5): p. 665-74.
74. Subramanian, S., et al., *Dietary cholesterol exacerbates hepatic steatosis and inflammation in obese LDL receptor-deficient mice*. J Lipid Res, 2011. **52**(9): p. 1626-35.
75. Ioannou, G.N., et al., *Association between dietary nutrient composition and the incidence of cirrhosis or liver cancer in the United States population*. Hepatology, 2009. **50**(1): p. 175-84.
76. Ioannou, G.N., et al., *Hepatic cholesterol crystals and crown-like structures distinguish NASH from simple steatosis*. J Lipid Res, 2013. **54**(5): p. 1326-34.
77. Bungler, M.K., et al., *Mop3 is an essential component of the master circadian pacemaker in mammals*. Cell, 2000. **103**(7): p. 1009-17.
78. van der Horst, G.T., et al., *Mammalian Cry1 and Cry2 are essential for maintenance of circadian rhythms*. Nature, 1999. **398**(6728): p. 627-30.
79. Vitaterna, M.H., et al., *Mutagenesis and mapping of a mouse gene, Clock, essential for circadian behavior*. Science, 1994. **264**(5159): p. 719-25.
80. Kondratov, R.V., et al., *Early aging and age-related pathologies in mice deficient in BMAL1, the core component of the circadian clock*. Genes Dev, 2006. **20**(14): p. 1868-73.
81. Miller, B.H., et al., *Circadian clock mutation disrupts estrous cyclicity and maintenance of pregnancy*. Curr Biol, 2004. **14**(15): p. 1367-73.
82. Rudic, R.D., et al., *BMAL1 and CLOCK, two essential components of the circadian clock, are involved in glucose homeostasis*. PLoS Biol, 2004. **2**(11): p. e377.
83. Franken, P., et al., *The transcription factor DBP affects circadian sleep consolidation and rhythmic EEG activity*. J Neurosci, 2000. **20**(2): p. 617-25.

84. Gachon, F., et al., *The loss of circadian PAR bZip transcription factors results in epilepsy*. Genes Dev, 2004. **18**(12): p. 1397-412.
85. Lopez-Molina, L., et al., *The DBP gene is expressed according to a circadian rhythm in the suprachiasmatic nucleus and influences circadian behavior*. Embo j, 1997. **16**(22): p. 6762-71.
86. Gachon, F., et al., *The circadian PAR-domain basic leucine zipper transcription factors DBP, TEF, and HLF modulate basal and inducible xenobiotic detoxification*. Cell Metab, 2006. **4**(1): p. 25-36.
87. Moore, R.Y. and V.B. Eichler, *Loss of a circadian adrenal corticosterone rhythm following suprachiasmatic lesions in the rat*. Brain Res, 1972. **42**(1): p. 201-6.
88. Stephan, F.K. and I. Zucker, *Circadian rhythms in drinking behavior and locomotor activity of rats are eliminated by hypothalamic lesions*. Proc Natl Acad Sci U S A, 1972. **69**(6): p. 1583-6.
89. Dibner, C., U. Schibler, and U. Albrecht, *The mammalian circadian timing system: organization and coordination of central and peripheral clocks*. Annu Rev Physiol, 2010. **72**: p. 517-49.
90. Johnson, R.F., L.P. Morin, and R.Y. Moore, *Retinohypothalamic projections in the hamster and rat demonstrated using cholera toxin*. Brain Res, 1988. **462**(2): p. 301-12.
91. Sujino, M., et al., *Suprachiasmatic nucleus grafts restore circadian behavioral rhythms of genetically arrhythmic mice*. Curr Biol, 2003. **13**(8): p. 664-8.
92. Damiola, F., et al., *Restricted feeding uncouples circadian oscillators in peripheral tissues from the central pacemaker in the suprachiasmatic nucleus*. Genes Dev, 2000. **14**(23): p. 2950-61.
93. Schwartz, M.W., et al., *Central nervous system control of food intake*. Nature, 2000. **404**(6778): p. 661-71.
94. Storch, K.F. and C.J. Weitz, *Daily rhythms of food-anticipatory behavioral activity do not require the known circadian clock*. Proc Natl Acad Sci U S A, 2009. **106**(16): p. 6808-13.
95. Stephan, F.K., J.M. Swann, and C.L. Sisk, *Anticipation of 24-hr feeding schedules in rats with lesions of the suprachiasmatic nucleus*. Behav Neural Biol, 1979. **25**(3): p. 346-63.
96. Akerstedt, T., *Shift work and disturbed sleep/wakefulness*. Occup Med (Lond), 2003. **53**(2): p. 89-94.
97. Vyas, M.V., et al., *Shift work and vascular events: systematic review and meta-analysis*. Bmj, 2012. **345**: p. e4800.
98. Thomas, C. and C. Power, *Shift work and risk factors for cardiovascular disease: a study at age 45 years in the 1958 British birth cohort*. Eur J Epidemiol, 2010. **25**(5): p. 305-14.
99. Pan, A., et al., *Rotating night shift work and risk of type 2 diabetes: two prospective cohort studies in women*. PLoS Med, 2011. **8**(12): p. e1001141.
100. O'Reardon, J.P., et al., *Circadian eating and sleeping patterns in the night eating syndrome*. Obes Res, 2004. **12**(11): p. 1789-96.
101. Rogers, N.L., et al., *Assessment of sleep in women with night eating syndrome*. Sleep, 2006. **29**(6): p. 814-9.
102. Shimba, S., et al., *Deficient of a clock gene, brain and muscle Arnt-like protein-1 (BMAL1), induces dyslipidemia and ectopic fat formation*. PLoS One, 2011. **6**(9): p. e25231.
103. Lamia, K.A., K.F. Storch, and C.J. Weitz, *Physiological significance of a peripheral tissue circadian clock*. Proc Natl Acad Sci U S A, 2008. **105**(39): p. 15172-7.
104. Paschos, G.K., et al., *Obesity in mice with adipocyte-specific deletion of clock component Arntl*. Nat Med, 2012. **18**(12): p. 1768-77.
105. Turek, F.W., et al., *Obesity and metabolic syndrome in circadian Clock mutant mice*. Science, 2005. **308**(5724): p. 1043-5.

106. Grimaldi, B., et al., *PER2 controls lipid metabolism by direct regulation of PPARgamma*. Cell Metab, 2010. **12**(5): p. 509-20.
107. Yang, S., et al., *The role of mPer2 clock gene in glucocorticoid and feeding rhythms*. Endocrinology, 2009. **150**(5): p. 2153-60.
108. Bur, I.M., et al., *The circadian clock components CRY1 and CRY2 are necessary to sustain sex dimorphism in mouse liver metabolism*. J Biol Chem, 2009. **284**(14): p. 9066-73.
109. Lamia, K.A., et al., *Cryptochromes mediate rhythmic repression of the glucocorticoid receptor*. Nature, 2011. **480**(7378): p. 552-6.
110. Delezie, J., et al., *The nuclear receptor REV-ERBalpha is required for the daily balance of carbohydrate and lipid metabolism*. Faseb j, 2012. **26**(8): p. 3321-35.
111. Mamontova, A., et al., *Severe atherosclerosis and hypoalphalipoproteinemia in the staggerer mouse, a mutant of the nuclear receptor RORalpha*. Circulation, 1998. **98**(24): p. 2738-43.
112. Chua, E.C., et al., *Extensive diversity in circadian regulation of plasma lipids and evidence for different circadian metabolic phenotypes in humans*. Proc Natl Acad Sci U S A, 2013. **110**(35): p. 14468-73.
113. Gooley, J.J. and E.C. Chua, *Diurnal regulation of lipid metabolism and applications of circadian lipidomics*. J Genet Genomics, 2014. **41**(5): p. 231-50.
114. Krieger, D.T., et al., *Characterization of the normal temporal pattern of plasma corticosteroid levels*. J Clin Endocrinol Metab, 1971. **32**(2): p. 266-84.
115. la Fleur, S.E., et al., *A daily rhythm in glucose tolerance: a role for the suprachiasmatic nucleus*. Diabetes, 2001. **50**(6): p. 1237-43.
116. Morgan, L., et al., *Effects of the endogenous clock and sleep time on melatonin, insulin, glucose and lipid metabolism*. J Endocrinol, 1998. **157**(3): p. 443-51.
117. Shea, S.A., et al., *Independent circadian and sleep/wake regulation of adipokines and glucose in humans*. J Clin Endocrinol Metab, 2005. **90**(5): p. 2537-44.
118. Xu, B., et al., *Daily changes in hypothalamic gene expression of neuropeptide Y, galanin, proopiomelanocortin, and adipocyte leptin gene expression and secretion: effects of food restriction*. Endocrinology, 1999. **140**(6): p. 2868-75.
119. Akhtar, R.A., et al., *Circadian cycling of the mouse liver transcriptome, as revealed by cDNA microarray, is driven by the suprachiasmatic nucleus*. Curr Biol, 2002. **12**(7): p. 540-50.
120. Eckel-Mahan, K.L., et al., *Coordination of the transcriptome and metabolome by the circadian clock*. Proc Natl Acad Sci U S A, 2012. **109**(14): p. 5541-6.
121. Panda, S., et al., *Coordinated transcription of key pathways in the mouse by the circadian clock*. Cell, 2002. **109**(3): p. 307-20.
122. Pan, X., C.A. Bradfield, and M.M. Hussain, *Global and hepatocyte-specific ablation of Bmal1 induces hyperlipidaemia and enhances atherosclerosis*. Nat Commun, 2016. **7**: p. 13011.
123. Duez, H., et al., *Regulation of bile acid synthesis by the nuclear receptor Rev-erbalpha*. Gastroenterology, 2008. **135**(2): p. 689-98.
124. Lavery, D.J. and U. Schibler, *Circadian transcription of the cholesterol 7 alpha hydroxylase gene may involve the liver-enriched bZIP protein DBP*. Genes Dev, 1993. **7**(10): p. 1871-84.
125. Roesler, W.J., P.J. McFie, and C. Dauvin, *The liver-enriched transcription factor D-site-binding protein activates the promoter of the phosphoenolpyruvate carboxykinase gene in hepatoma cells*. J Biol Chem, 1992. **267**(29): p. 21235-43.
126. Arble, D.M., et al., *Circadian timing of food intake contributes to weight gain*. Obesity (Silver Spring), 2009. **17**(11): p. 2100-2.

127. Bray, M.S., et al., *Time-of-day-dependent dietary fat consumption influences multiple cardiometabolic syndrome parameters in mice*. Int J Obes (Lond), 2010. **34**(11): p. 1589-98.
128. Fonken, L.K., et al., *Light at night increases body mass by shifting the time of food intake*. Proc Natl Acad Sci U S A, 2010. **107**(43): p. 18664-9.
129. Hatori, M., et al., *Time-restricted feeding without reducing caloric intake prevents metabolic diseases in mice fed a high-fat diet*. Cell Metab, 2012. **15**(6): p. 848-60.
130. Salgado-Delgado, R., et al., *Food intake during the normal activity phase prevents obesity and circadian desynchrony in a rat model of night work*. Endocrinology, 2010. **151**(3): p. 1019-29.
131. Garaulet, M., et al., *Timing of food intake predicts weight loss effectiveness*. Int J Obes (Lond), 2013. **37**(4): p. 604-11.
132. Stone, N.J., et al., *2013 ACC/AHA guideline on the treatment of blood cholesterol to reduce atherosclerotic cardiovascular risk in adults: a report of the American College of Cardiology/American Heart Association Task Force on Practice Guidelines*. J Am Coll Cardiol, 2014. **63**(25 Pt B): p. 2889-934.
133. Altmann, S.W., et al., *Niemann-Pick C1 Like 1 protein is critical for intestinal cholesterol absorption*. Science, 2004. **303**(5661): p. 1201-4.
134. Bays, H.E., et al., *Effectiveness and tolerability of ezetimibe in patients with primary hypercholesterolemia: pooled analysis of two phase II studies*. Clin Ther, 2001. **23**(8): p. 1209-30.
135. Assmann, G., et al., *Effects of ezetimibe, simvastatin, atorvastatin, and ezetimibe-statin therapies on non-cholesterol sterols in patients with primary hypercholesterolemia*. Curr Med Res Opin, 2008. **24**(1): p. 249-59.
136. Lakoski, S.G., et al., *Indices of cholesterol metabolism and relative responsiveness to ezetimibe and simvastatin*. J Clin Endocrinol Metab, 2010. **95**(2): p. 800-9.
137. Miettinen, T.A., T.E. Strandberg, and H. Gylling, *Noncholesterol sterols and cholesterol lowering by long-term simvastatin treatment in coronary patients: relation to basal serum cholestanol*. Arterioscler Thromb Vasc Biol, 2000. **20**(5): p. 1340-6.
138. van Himbergen, T.M., et al., *Comparison of the effects of maximal dose atorvastatin and rosuvastatin therapy on cholesterol synthesis and absorption markers*. J Lipid Res, 2009. **50**(4): p. 730-9.
139. Miettinen, T.A., et al., *Baseline serum cholestanol as predictor of recurrent coronary events in subgroup of Scandinavian simvastatin survival study*. Finnish 4S Investigators. Bmj, 1998. **316**(7138): p. 1127-30.
140. Cannon, C.P., et al., *Ezetimibe Added to Statin Therapy after Acute Coronary Syndromes*. N Engl J Med, 2015. **372**(25): p. 2387-97.
141. Repa, J.J., et al., *Regulation of ATP-binding cassette sterol transporters ABCG5 and ABCG8 by the liver X receptors alpha and beta*. J Biol Chem, 2002. **277**(21): p. 18793-800.
142. Yu, L., et al., *Stimulation of cholesterol excretion by the liver X receptor agonist requires ATP-binding cassette transporters G5 and G8*. J Biol Chem, 2003. **278**(18): p. 15565-70.
143. Yu, L., et al., *Disruption of Abcg5 and Abcg8 in mice reveals their crucial role in biliary cholesterol secretion*. Proc Natl Acad Sci U S A, 2002. **99**(25): p. 16237-42.
144. Yu, L., et al., *Overexpression of ABCG5 and ABCG8 promotes biliary cholesterol secretion and reduces fractional absorption of dietary cholesterol*. J Clin Invest, 2002. **110**(5): p. 671-80.
145. Wilund, K.R., et al., *High-level expression of ABCG5 and ABCG8 attenuates diet-induced hypercholesterolemia and atherosclerosis in Ldlr^{-/-} mice*. J Lipid Res, 2004. **45**(8): p. 1429-36.

146. Basso, F., et al., *Hepatic ABCG5/G8 overexpression reduces apoB-lipoproteins and atherosclerosis when cholesterol absorption is inhibited*. J Lipid Res, 2007. **48**(1): p. 114-26.
147. Su, K., et al., *Acceleration of biliary cholesterol secretion restores glycemic control and alleviates hypertriglyceridemia in obese db/db mice*. Arterioscler Thromb Vasc Biol, 2014. **34**(1): p. 26-33.
148. Sabeva, N.S., E.J. Rouse, and G.A. Graf, *Defects in the leptin axis reduce abundance of the ABCG5-ABCG8 sterol transporter in liver*. J Biol Chem, 2007. **282**(31): p. 22397-405.
149. Su, K., et al., *The ABCG5 ABCG8 Sterol Transporter Opposes the Development of Fatty Liver Disease and Loss of Glycemic Control Independently of Phytosterol Accumulation*. J Biol Chem, 2012. **287**(34): p. 28564-75.
150. Wang, Y., et al., *The combination of ezetimibe and ursodiol promotes fecal sterol excretion and reveals a G5G8-independent pathway for cholesterol elimination*. J Lipid Res, 2015. **56**(4): p. 810-20.
151. Beuers, U., *Drug insight: Mechanisms and sites of action of ursodeoxycholic acid in cholestasis*. Nat Clin Pract Gastroenterol Hepatol, 2006. **3**(6): p. 318-28.
152. Graf, G.A., et al., *Coexpression of ATP-binding cassette proteins ABCG5 and ABCG8 permits their transport to the apical surface*. J Clin Invest, 2002. **110**(5): p. 659-69.
153. Graf, G.A., et al., *ABCG5 and ABCG8 are obligate heterodimers for protein trafficking and biliary cholesterol excretion*. J Biol Chem, 2003. **278**(48): p. 48275-82.
154. Okiyonedo, T., et al., *Calreticulin facilitates the cell surface expression of ABCG5/G8*. Biochem Biophys Res Commun, 2006. **347**(1): p. 67-75.
155. Insull, W., Jr., *Clinical utility of bile acid sequestrants in the treatment of dyslipidemia: a scientific review*. South Med J, 2006. **99**(3): p. 257-73.
156. Lefebvre, P., et al., *Role of bile acids and bile acid receptors in metabolic regulation*. Physiol Rev, 2009. **89**(1): p. 147-91.
157. Staels, B. and V.A. Fonseca, *Bile acids and metabolic regulation: mechanisms and clinical responses to bile acid sequestration*. Diabetes Care, 2009. **32 Suppl 2**: p. S237-45.
158. Ballatori, N., et al., *OSTalpha-OSTbeta: a major basolateral bile acid and steroid transporter in human intestinal, renal, and biliary epithelia*. Hepatology, 2005. **42**(6): p. 1270-9.
159. Dawson, P.A., et al., *Targeted deletion of the ileal bile acid transporter eliminates enterohepatic cycling of bile acids in mice*. J Biol Chem, 2003. **278**(36): p. 33920-7.
160. Dawson, P.A., et al., *The heteromeric organic solute transporter alpha-beta, Ostalpha-Ostbeta, is an ileal basolateral bile acid transporter*. J Biol Chem, 2005. **280**(8): p. 6960-8.
161. Weinberg, S.L., G. Burckhardt, and F.A. Wilson, *Taurocholate transport by rat intestinal basolateral membrane vesicles. Evidence for the presence of an anion exchange transport system*. J Clin Invest, 1986. **78**(1): p. 44-50.
162. Makishima, M., et al., *Identification of a nuclear receptor for bile acids*. Science, 1999. **284**(5418): p. 1362-5.
163. Inagaki, T., et al., *Fibroblast growth factor 15 functions as an enterohepatic signal to regulate bile acid homeostasis*. Cell Metab, 2005. **2**(4): p. 217-25.
164. McWhirter, J.R., et al., *A novel fibroblast growth factor gene expressed in the developing nervous system is a downstream target of the chimeric homeodomain oncoprotein E2A-Pbx1*. Development, 1997. **124**(17): p. 3221-32.
165. Brensike, J.F., et al., *Effects of therapy with cholestyramine on progression of coronary arteriosclerosis: results of the NHLBI Type II Coronary Intervention Study*. Circulation, 1984. **69**(2): p. 313-24.

166. Levy, R.I., et al., *The influence of changes in lipid values induced by cholestyramine and diet on progression of coronary artery disease: results of NHLBI Type II Coronary Intervention Study*. *Circulation*, 1984. **69**(2): p. 325-37.
167. Cariou, B., et al., *The farnesoid X receptor modulates adiposity and peripheral insulin sensitivity in mice*. *J Biol Chem*, 2006. **281**(16): p. 11039-49.
168. Ma, K., et al., *Farnesoid X receptor is essential for normal glucose homeostasis*. *J Clin Invest*, 2006. **116**(4): p. 1102-9.
169. Zhang, Y., et al., *Activation of the nuclear receptor FXR improves hyperglycemia and hyperlipidemia in diabetic mice*. *Proc Natl Acad Sci U S A*, 2006. **103**(4): p. 1006-11.
170. Mudaliar, S., et al., *Efficacy and safety of the farnesoid X receptor agonist obeticholic acid in patients with type 2 diabetes and nonalcoholic fatty liver disease*. *Gastroenterology*, 2013. **145**(3): p. 574-82.e1.
171. Neuschwander-Tetri, B.A., et al., *Farnesoid X nuclear receptor ligand obeticholic acid for non-cirrhotic, non-alcoholic steatohepatitis (FLINT): a multicentre, randomised, placebo-controlled trial*. *Lancet*, 2015. **385**(9972): p. 956-65.
172. Choi, M., et al., *Identification of a hormonal basis for gallbladder filling*. *Nat Med*, 2006. **12**(11): p. 1253-5.
173. Fu, L., et al., *Fibroblast growth factor 19 increases metabolic rate and reverses dietary and leptin-deficient diabetes*. *Endocrinology*, 2004. **145**(6): p. 2594-603.
174. Tomlinson, E., et al., *Transgenic mice expressing human fibroblast growth factor-19 display increased metabolic rate and decreased adiposity*. *Endocrinology*, 2002. **143**(5): p. 1741-7.
175. Kir, S., et al., *FGF19 as a postprandial, insulin-independent activator of hepatic protein and glycogen synthesis*. *Science*, 2011. **331**(6024): p. 1621-4.
176. Potthoff, M.J., et al., *FGF15/19 regulates hepatic glucose metabolism by inhibiting the CREB-PGC-1alpha pathway*. *Cell Metab*, 2011. **13**(6): p. 729-38.
177. Edwards, P.A., H. Muroya, and R.G. Gould, *In vivo demonstration of the circadian rhythm of cholesterol biosynthesis in the liver and intestine of the rat*. *J Lipid Res*, 1972. **13**(3): p. 396-401.
178. Hamprecht, B., C. Nussler, and F. Lynen, *Rhythmic changes of hydroxymethylglutaryl coenzyme a reductase activity in livers of fed and fasted rats*. *FEBS Lett*, 1969. **4**(2): p. 117-121.
179. Shapiro, D.J. and V.W. Rodwell, *Diurnal variation and cholesterol regulation of hepatic HMG-CoA reductase activity*. *Biochem Biophys Res Commun*, 1969. **37**(5): p. 867-72.
180. Noshiro, M., M. Nishimoto, and K. Okuda, *Rat liver cholesterol 7 alpha-hydroxylase. Pretranslational regulation for circadian rhythm*. *J Biol Chem*, 1990. **265**(17): p. 10036-41.
181. Sundseth, S.S. and D.J. Waxman, *Hepatic P-450 cholesterol 7 alpha-hydroxylase. Regulation in vivo at the protein and mRNA level in response to mevalonate, diurnal rhythm, and bile acid feedback*. *J Biol Chem*, 1990. **265**(25): p. 15090-5.
182. Kudo, T., et al., *Clock mutation facilitates accumulation of cholesterol in the liver of mice fed a cholesterol and/or cholic acid diet*. *Am J Physiol Endocrinol Metab*, 2008. **294**(1): p. E120-30.
183. Pijut, S.S., et al., *Effect of peripheral circadian dysfunction on metabolic disease in response to a diabetogenic diet*. *Am J Physiol Endocrinol Metab*, 2016. **310**(11): p. E900-11.
184. Gachon, F., et al., *Proline- and acidic amino acid-rich basic leucine zipper proteins modulate peroxisome proliferator-activated receptor alpha (PPARalpha) activity*. *Proc Natl Acad Sci U S A*, 2011. **108**(12): p. 4794-9.
185. Takahashi, S., et al., *A promoter in the novel exon of hPPARgamma directs the circadian expression of PPARgamma*. *J Atheroscler Thromb*, 2010. **17**(1): p. 73-83.

186. Wu, X., et al., *Expression profile of mRNAs encoding core circadian regulatory proteins in human subcutaneous adipose tissue: correlation with age and body mass index*. *Int J Obes (Lond)*, 2009. **33**(9): p. 971-7.
187. Liu, J., et al., *The absence of ABCD2 sensitizes mice to disruptions in lipid metabolism by dietary erucic acid*. *J Lipid Res*, 2012. **53**(6): p. 1071-9.
188. Liu, J., et al., *ABCD2 is abundant in adipose tissue and opposes the accumulation of dietary erucic acid (C22:1) in fat*. *J Lipid Res*, 2010. **51**(1): p. 162-8.
189. van Roermund, C.W., et al., *Differential substrate specificities of human ABCD1 and ABCD2 in peroxisomal fatty acid beta-oxidation*. *Biochim Biophys Acta*, 2011. **1811**(3): p. 148-52.
190. Huang da, W., B.T. Sherman, and R.A. Lempicki, *Bioinformatics enrichment tools: paths toward the comprehensive functional analysis of large gene lists*. *Nucleic Acids Res*, 2009. **37**(1): p. 1-13.
191. Huang da, W., B.T. Sherman, and R.A. Lempicki, *Systematic and integrative analysis of large gene lists using DAVID bioinformatics resources*. *Nat Protoc*, 2009. **4**(1): p. 44-57.
192. Shimba, S., et al., *Brain and muscle Arnt-like protein-1 (BMAL1), a component of the molecular clock, regulates adipogenesis*. *Proc Natl Acad Sci U S A*, 2005. **102**(34): p. 12071-6.
193. Shostak, A., J. Meyer-Kovac, and H. Oster, *Circadian regulation of lipid mobilization in white adipose tissues*. *Diabetes*, 2013. **62**(7): p. 2195-203.
194. Cain, S.W., et al., *Sex differences in phase angle of entrainment and melatonin amplitude in humans*. *J Biol Rhythms*, 2010. **25**(4): p. 288-96.
195. Duffy, J.F., et al., *Sex difference in the near-24-hour intrinsic period of the human circadian timing system*. *Proc Natl Acad Sci U S A*, 2011. **108 Suppl 3**: p. 15602-8.
196. Lim, A.S., et al., *Sex difference in daily rhythms of clock gene expression in the aged human cerebral cortex*. *J Biol Rhythms*, 2013. **28**(2): p. 117-29.
197. Schneider, J.E., *Metabolic and hormonal control of the desire for food and sex: implications for obesity and eating disorders*. *Horm Behav*, 2006. **50**(4): p. 562-71.
198. Valenstein, E.S., V.C. Cox, and J.W. Kakolewski, *Sex differences in hyperphagia and body weight following hypothalamic damage*. *Ann N Y Acad Sci*, 1969. **157**(2): p. 1030-48.
199. Gomez-Abellan, P., et al., *Sexual dimorphism in clock genes expression in human adipose tissue*. *Obes Surg*, 2012. **22**(1): p. 105-12.
200. Zheng, B., et al., *The mPer2 gene encodes a functional component of the mammalian circadian clock*. *Nature*, 1999. **400**(6740): p. 169-73.
201. Wakamatsu, H., et al., *Restricted-feeding-induced anticipatory activity rhythm is associated with a phase-shift of the expression of mPer1 and mPer2 mRNA in the cerebral cortex and hippocampus but not in the suprachiasmatic nucleus of mice*. *Eur J Neurosci*, 2001. **13**(6): p. 1190-6.
202. Hara, R., et al., *Restricted feeding entrains liver clock without participation of the suprachiasmatic nucleus*. *Genes Cells*, 2001. **6**(3): p. 269-78.
203. Urs, S., et al., *Selective expression of an aP2/Fatty Acid Binding Protein 4-Cre transgene in non-adipogenic tissues during embryonic development*. *Transgenic Res*, 2006. **15**(5): p. 647-53.
204. Lee, K.Y., et al., *Lessons on conditional gene targeting in mouse adipose tissue*. *Diabetes*, 2013. **62**(3): p. 864-74.
205. Kohsaka, A., et al., *High-fat diet disrupts behavioral and molecular circadian rhythms in mice*. *Cell Metab*, 2007. **6**(5): p. 414-21.
206. Eckel-Mahan, K.L., et al., *Reprogramming of the circadian clock by nutritional challenge*. *Cell*, 2013. **155**(7): p. 1464-78.

207. Pan, X., X.C. Jiang, and M.M. Hussain, *Impaired cholesterol metabolism and enhanced atherosclerosis in clock mutant mice*. *Circulation*, 2013. **128**(16): p. 1758-69.
208. Hughes, M.E., et al., *Harmonics of circadian gene transcription in mammals*. *PLoS Genet*, 2009. **5**(4): p. e1000442.
209. Cai, W., et al., *Expression levels of estrogen receptor beta are modulated by components of the molecular clock*. *Mol Cell Biol*, 2008. **28**(2): p. 784-93.
210. Brockman, R., D. Bunick, and M.M. Mahoney, *Estradiol deficiency during development modulates the expression of circadian and daily rhythms in male and female aromatase knockout mice*. *Horm Behav*, 2011. **60**(4): p. 439-47.
211. Mendoza, J., et al., *Dimorphic effects of leptin on the circadian and hypocretinergic systems of mice*. *J Neuroendocrinol*, 2011. **23**(1): p. 28-38.
212. Chatrath, H., R. Vuppalaanchi, and N. Chalasani, *Dyslipidemia in patients with nonalcoholic fatty liver disease*. *Semin Liver Dis*, 2012. **32**(1): p. 22-9.
213. Zhang, Q.Q. and L.G. Lu, *Nonalcoholic Fatty Liver Disease: Dyslipidemia, Risk for Cardiovascular Complications, and Treatment Strategy*. *J Clin Transl Hepatol*, 2015. **3**(1): p. 78-84.
214. Savard, C., et al., *Synergistic interaction of dietary cholesterol and dietary fat in inducing experimental steatohepatitis*. *Hepatology*, 2013. **57**(1): p. 81-92.
215. Klett, E.L., et al., *A mouse model of sitosterolemia: absence of Abcg8/sterolin-2 results in failure to secrete biliary cholesterol*. *BMC Med*, 2004. **2**: p. 5.
216. Plosch, T., et al., *Sitosterolemia in ABC-transporter G5-deficient mice is aggravated on activation of the liver-X receptor*. *Gastroenterology*, 2004. **126**(1): p. 290-300.
217. Potthoff, M.J., S.A. Kliewer, and D.J. Mangelsdorf, *Endocrine fibroblast growth factors 15/19 and 21: from feast to famine*. *Genes Dev*, 2012. **26**(4): p. 312-24.
218. Holt, J.A., et al., *Definition of a novel growth factor-dependent signal cascade for the suppression of bile acid biosynthesis*. *Genes Dev*, 2003. **17**(13): p. 1581-91.
219. Bhatnagar, S., H.A. Damron, and F.B. Hillgartner, *Fibroblast growth factor-19, a novel factor that inhibits hepatic fatty acid synthesis*. *J Biol Chem*, 2009. **284**(15): p. 10023-33.
220. Talalay, P., *Enzymic analysis of steroid hormones*. *Methods Biochem Anal*, 1960. **8**: p. 119-43.
221. Goodwin, B., et al., *A regulatory cascade of the nuclear receptors FXR, SHP-1, and LRH-1 represses bile acid biosynthesis*. *Mol Cell*, 2000. **6**(3): p. 517-26.
222. Shaffer, E.A. and D.M. Small, *Biliary lipid secretion in cholesterol gallstone disease. The effect of cholecystectomy and obesity*. *J Clin Invest*, 1977. **59**(5): p. 828-40.
223. Buch, S., et al., *A genome-wide association scan identifies the hepatic cholesterol transporter ABCG8 as a susceptibility factor for human gallstone disease*. *Nat Genet*, 2007. **39**(8): p. 995-9.
224. Wang, Y., et al., *ATP binding cassette G8 T400K polymorphism may affect the risk of gallstone disease among Chinese males*. *Clin Chim Acta*, 2007. **384**(1-2): p. 80-5.
225. Yamazaki, Y., et al., *Involvement of a cyclic adenosine monophosphate-dependent signal in the diet-induced canalicular trafficking of adenosine triphosphate-binding cassette transporter g5/g8*. *Hepatology*, 2015. **62**(4): p. 1215-26.
226. Dufour, J.F., et al., *Randomized placebo-controlled trial of ursodeoxycholic acid with vitamin e in nonalcoholic steatohepatitis*. *Clin Gastroenterol Hepatol*, 2006. **4**(12): p. 1537-43.
227. Lindor, K.D., et al., *Ursodeoxycholic acid for treatment of nonalcoholic steatohepatitis: results of a randomized trial*. *Hepatology*, 2004. **39**(3): p. 770-8.
228. Kiyici, M., et al., *Ursodeoxycholic acid and atorvastatin in the treatment of nonalcoholic steatohepatitis*. *Can J Gastroenterol*, 2003. **17**(12): p. 713-8.
229. Laurin, J., et al., *Ursodeoxycholic acid or clofibrate in the treatment of non-alcohol-induced steatohepatitis: a pilot study*. *Hepatology*, 1996. **23**(6): p. 1464-7.

230. Adams, L.A., et al., *A pilot trial of high-dose ursodeoxycholic acid in nonalcoholic steatohepatitis*. *Hepatol Int*, 2010. **4**(3): p. 628-33.
231. Ratziu, V., et al., *A randomized controlled trial of high-dose ursodesoxycholic acid for nonalcoholic steatohepatitis*. *J Hepatol*, 2011. **54**(5): p. 1011-9.
232. Ozcan, U., et al., *Chemical chaperones reduce ER stress and restore glucose homeostasis in a mouse model of type 2 diabetes*. *Science*, 2006. **313**(5790): p. 1137-40.
233. Xie, Q., et al., *Effect of tauroursodeoxycholic acid on endoplasmic reticulum stress-induced caspase-12 activation*. *Hepatology*, 2002. **36**(3): p. 592-601.
234. Alnouti, Y., I.L. Csanaky, and C.D. Klaassen, *Quantitative-profiling of bile acids and their conjugates in mouse liver, bile, plasma, and urine using LC-MS/MS*. *J Chromatogr B Analyt Technol Biomed Life Sci*, 2008. **873**(2): p. 209-17.
235. Chiang, J.Y., *Bile acid metabolism and signaling*. *Compr Physiol*, 2013. **3**(3): p. 1191-212.
236. Yoneda, M., et al., *Efficacy of ezetimibe for the treatment of non-alcoholic steatohepatitis: An open-label, pilot study*. *Hepatol Res*, 2010. **40**(6): p. 566-73.
237. Chan, D.C., et al., *Effect of ezetimibe on hepatic fat, inflammatory markers, and apolipoprotein B-100 kinetics in insulin-resistant obese subjects on a weight loss diet*. *Diabetes Care*, 2010. **33**(5): p. 1134-9.
238. Ezzet, F., et al., *The plasma concentration and LDL-C relationship in patients receiving ezetimibe*. *J Clin Pharmacol*, 2001. **41**(9): p. 943-9.
239. Knopp, R.H., et al., *Effects of ezetimibe, a new cholesterol absorption inhibitor, on plasma lipids in patients with primary hypercholesterolemia*. *Eur Heart J*, 2003. **24**(8): p. 729-41.
240. Sudhop, T., et al., *Inhibition of intestinal cholesterol absorption by ezetimibe in humans*. *Circulation*, 2002. **106**(15): p. 1943-8.
241. van Heek, M., et al., *Ezetimibe selectively inhibits intestinal cholesterol absorption in rodents in the presence and absence of exocrine pancreatic function*. *Br J Pharmacol*, 2001. **134**(2): p. 409-17.
242. Wang, H., et al., *Endogenous bile acids are ligands for the nuclear receptor FXR/BAR*. *Mol Cell*, 1999. **3**(5): p. 543-53.
243. Lew, J.L., et al., *The farnesoid X receptor controls gene expression in a ligand- and promoter-selective fashion*. *J Biol Chem*, 2004. **279**(10): p. 8856-61.
244. Mueller, M., et al., *Ursodeoxycholic acid exerts farnesoid X receptor-antagonistic effects on bile acid and lipid metabolism in morbid obesity*. *J Hepatol*, 2015. **62**(6): p. 1398-404.
245. Davis, H.R., Jr., et al., *The synergistic hypocholesterolemic activity of the potent cholesterol absorption inhibitor, ezetimibe, in combination with 3-hydroxy-3-methylglutaryl coenzyme a reductase inhibitors in dogs*. *Metabolism*, 2001. **50**(10): p. 1234-41.
246. Adorini, L., M. Pruzanski, and D. Shapiro, *Farnesoid X receptor targeting to treat nonalcoholic steatohepatitis*. *Drug Discov Today*, 2012. **17**(17-18): p. 988-97.
247. Makri, E., E. Cholongitas, and K. Tziomalos, *Emerging role of obeticholic acid in the management of nonalcoholic fatty liver disease*. *World J Gastroenterol*, 2016. **22**(41): p. 9039-9043.
248. Paumgartner, G. and U. Beuers, *Ursodeoxycholic acid in cholestatic liver disease: mechanisms of action and therapeutic use revisited*. *Hepatology*, 2002. **36**(3): p. 525-31.
249. Carey, M.C. and D.M. Small, *The physical chemistry of cholesterol solubility in bile. Relationship to gallstone formation and dissolution in man*. *J Clin Invest*, 1978. **61**(4): p. 998-1026.
250. Small, D.M., *Role of ABC transporters in secretion of cholesterol from liver into bile*. *Proc Natl Acad Sci U S A*, 2003. **100**(1): p. 4-6.

251. Moschetta, A., A.L. Bookout, and D.J. Mangelsdorf, *Prevention of cholesterol gallstone disease by FXR agonists in a mouse model*. Nat Med, 2004. **10**(12): p. 1352-8.
252. Xu, Y., et al., *Farnesoid X receptor activation increases reverse cholesterol transport by modulating bile acid composition and cholesterol absorption in mice*. Hepatology, 2016. **64**(4): p. 1072-85.
253. Zhang, Y., et al., *Identification of novel pathways that control farnesoid X receptor-mediated hypocholesterolemia*. J Biol Chem, 2010. **285**(5): p. 3035-43.
254. Wang, H.H., et al., *Effect of ezetimibe on the prevention and dissolution of cholesterol gallstones*. Gastroenterology, 2008. **134**(7): p. 2101-10.
255. CDC, *Obesity: Halting The Epidemic by Making Health Easier-At A Glance*. 2011.
256. McCullough, A.J., *Epidemiology of the metabolic syndrome in the USA*. J Dig Dis, 2011. **12**(5): p. 333-40.
257. Farrell, G.C. and C.Z. Larter, *Nonalcoholic fatty liver disease: from steatosis to cirrhosis*. Hepatology, 2006. **43**(2 Suppl 1): p. S99-s112.
258. Cohen, J.C., J.D. Horton, and H.H. Hobbs, *Human fatty liver disease: old questions and new insights*. Science, 2011. **332**(6037): p. 1519-23.
259. Malhi, H. and R.J. Kaufman, *Endoplasmic reticulum stress in liver disease*. J Hepatol, 2011. **54**(4): p. 795-809.
260. de Bari, O., et al., *Ezetimibe: its novel effects on the prevention and the treatment of cholesterol gallstones and nonalcoholic Fatty liver disease*. J Lipids, 2012. **2012**: p. 302847.
261. Ushio, M., et al., *Ezetimibe prevents hepatic steatosis induced by a high-fat but not a high-fructose diet*. Am J Physiol Endocrinol Metab, 2013. **305**(2): p. E293-304.
262. Zheng, S., et al., *Ezetimibe improves high fat and cholesterol diet-induced non-alcoholic fatty liver disease in mice*. Eur J Pharmacol, 2008. **584**(1): p. 118-24.
263. Deushi, M., et al., *Ezetimibe improves liver steatosis and insulin resistance in obese rat model of metabolic syndrome*. FEBS Lett, 2007. **581**(29): p. 5664-70.
264. Ozcan, U., et al., *Endoplasmic reticulum stress links obesity, insulin action, and type 2 diabetes*. Science, 2004. **306**(5695): p. 457-61.
265. Van Rooyen, D.M., et al., *Hepatic free cholesterol accumulates in obese, diabetic mice and causes nonalcoholic steatohepatitis*. Gastroenterology, 2011. **141**(4): p. 1393-403, 1403.e1-5.
266. Davis, H.R., Jr., et al., *Niemann-Pick C1 Like 1 (NPC1L1) is the intestinal phytosterol and cholesterol transporter and a key modulator of whole-body cholesterol homeostasis*. J Biol Chem, 2004. **279**(32): p. 33586-92.
267. Fukuda, M., et al., *Ezetimibe Ameliorates Cardiovascular Complications and Hepatic Steatosis in Obese and Type 2 Diabetic db/db Mice*. Journal of Pharmacology and Experimental Therapeutics, 2010. **335**(1): p. 70-75.
268. Jakulj, L., et al., *Ezetimibe stimulates faecal neutral sterol excretion depending on abcg8 function in mice*. FEBS Letters, 2010. **584**(16): p. 3625-3628.
269. Kammoun, H.L., et al., *GRP78 expression inhibits insulin and ER stress-induced SREBP-1c activation and reduces hepatic steatosis in mice*. J Clin Invest, 2009. **119**(5): p. 1201-15.
270. Du, K., et al., *TRB3: a tribbles homolog that inhibits Akt/PKB activation by insulin in liver*. Science, 2003. **300**(5625): p. 1574-7.
271. Kilberg, M.S., J. Shan, and N. Su, *ATF4-dependent transcription mediates signaling of amino acid limitation*. Trends Endocrinol Metab, 2009. **20**(9): p. 436-43.
272. Wilund, K.R., et al., *High-level expression of ABCG5 and ABCG8 attenuates diet-induced hypercholesterolemia and atherosclerosis in Ldlr^{-/-} mice*. J Lipid Res, 2004. **45**(8): p. 1429-1436.

273. Yoneda, M., et al., *Efficacy of ezetimibe for the treatment of non-alcoholic steatohepatitis: An open-label, pilot study*. Hepatol Res, 2010. **40**(6): p. 613-21.
274. Enjoji, M., et al., *NPC1L1 inhibitor ezetimibe is a reliable therapeutic agent for non-obese patients with nonalcoholic fatty liver disease*. Lipids Health Dis, 2010. **9**: p. 29.
275. Park, H., et al., *Efficacy of long-term ezetimibe therapy in patients with nonalcoholic fatty liver disease*. J Gastroenterol, 2011. **46**(1): p. 101-7.
276. Ratziu, V., et al., *A randomized controlled trial of high-dose ursodesoxycholic acid for nonalcoholic steatohepatitis*. Journal of Hepatology, 2011. **54**(5): p. 1011-1019.

VITA

NAME

Sonja Sheena Pijut

EDUCATION

PharmD August 2007-May 2011
University of Kentucky College of Pharmacy; Lexington, KY
magna cum laude

Pre-pharmacy coursework August 2005-May 2007
University of Kentucky College of Pharmacy; Lexington, KY

PROFESSIONAL POSITIONS

Clinical Staff Pharmacist, Internal Medicine October 2013-present
University of Kentucky Chandler Medical Center, Lexington,
KY

Clinical Staff Pharmacist May 2011-October 2013
University of Kentucky Chandler Medical Center; Lexington,
KY

HONORS

Manuscript highlighted in APSselect June 2016
American Physiological Society

T32 Interdisciplinary Cardiovascular Training Program July 2013-June 2014
University of Kentucky
Predoctoral Fellow

Rho Chi Research Day Poster Presentation 2nd Place Award April 2012
University of Kentucky

PUBLICATIONS

Pijut SS, Corbett DE, Wang Y, Li J, Charnigo RJ, Graf GA. Effect of peripheral circadian dysfunction on metabolic disease in response to a diabetogenic diet. *Am J Physiol Endocrinol Metab.* 2016;310(11):E900-911. PMID: 27048996.

Wang Y, Liu X, **Pijut SS**, Li J, Horn J, Bradford EM, Leggas M, Barrett TA, Graf GA. The combination of ezetimibe and ursodiol promotes fecal sterol excretion and reveals a G5G8-independent pathway for cholesterol elimination. *J Lipid Res.* 2015;56(4):810-820. PMID: 25635125.

Liu X, Liu J, Lester JD, **Pijut SS**, Graf GA. ABCD2 identifies a subclass of peroxisomes in mouse adipose tissue. *Biochem Biophys Res Commun*. 2015;456(1):129-134. PMID: 25446110.

Rhee S, Walsh K, Lewis D, Davis G, Smith KM. Pharmacogenomic considerations for customizing warfarin therapy in the orthopedic patient. *Orthopedics*. 2010;33(11): 828-831. PMID: 21053849.